52/1/2020
ISSN 1338-3523
ISSN 0369-2086

# Mineralia Slovaca

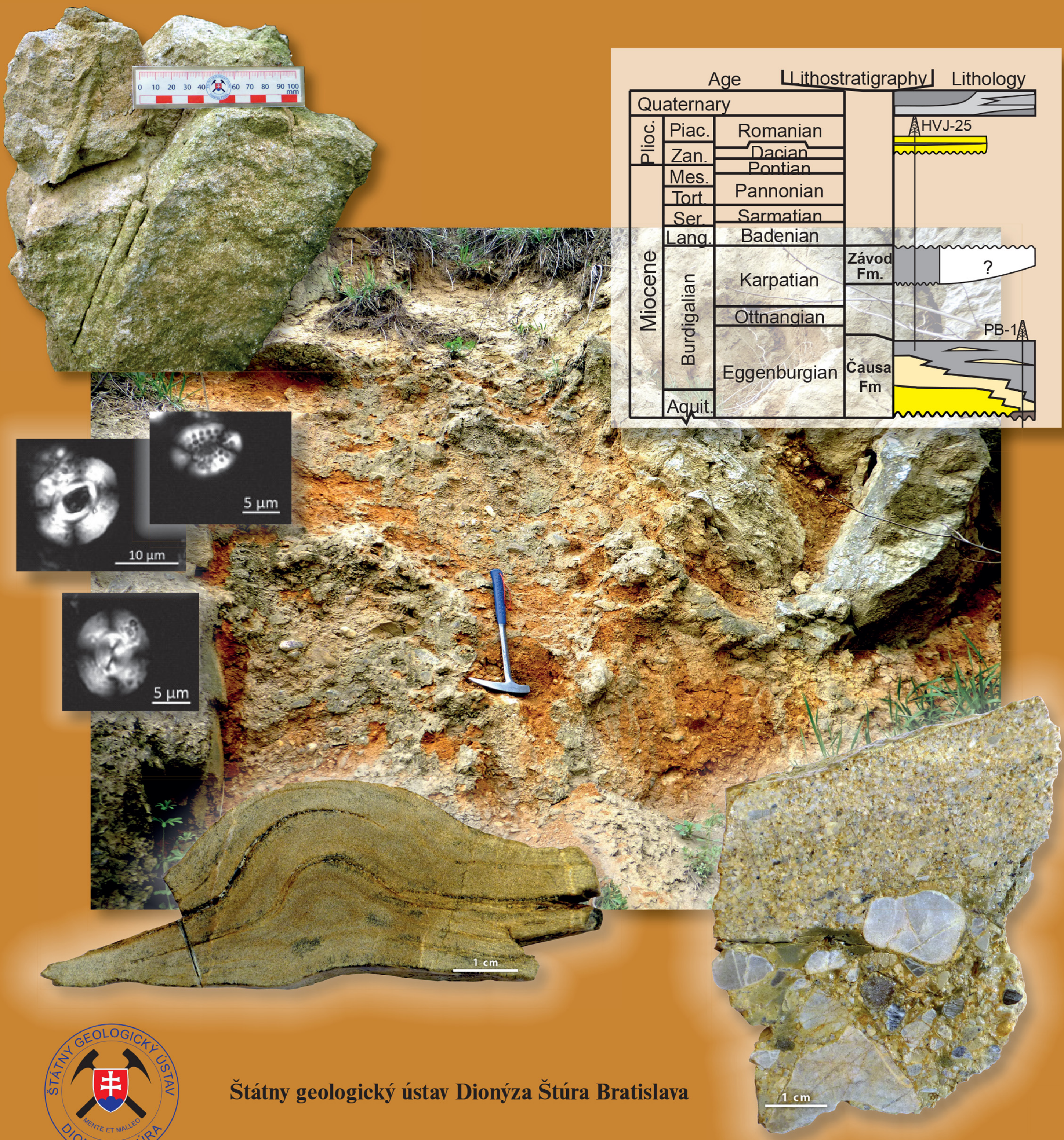


Štátny geologický ústav Dionýza Štúra Bratislava

**Mineralia Slovaca**

Časopis pre regionálnu a environmentálnu geológiu
a aktivity Slovenskej geologickej spoločnosti a geologických asociácií



Mineralia Slovaca (Web ISSN 1338-3523, ISSN 0369-2086), EV 3534/09, vychádza dvakrát ročne. Vydavateľ a tlač: Štátny geologický ústav Dionýza Štúra, Mlynská dolina 1, 817 04 Bratislava, IČO 31 753 604. Dátum vydania čísla 52/1/2020: august 2020. Predplatné v roku 2020 vrátane DPH, poštovného a balného pre jednotlivcov 22,00 €, pre členov SGS a geologických asociácií 20,90 €, pre organizácie v SR 31,90 €, pre organizácie v ČR 55,00 €. Cena jednotlivého čísla pri osobnom nákupe v predajniach ŠGÚDŠ v Bratislave a v Košiciach je 6,05 € vrátane DPH. Časopis možno objednať v redakcii a v knižnici regionálneho centra v Košiciach. Adresa redakcie: Štátny geologický ústav D. Štúra – RC Košice (Mineralia Slovaca), Jesenského 8, 040 01 Košice. Telefón: 055/625 00 43; fax: 055/625 00 44, e-mail: mineralia.slovaca@geology.sk, e-mail knižnica: secretary.ke@geology.sk

Mineralia Slovaca (Web ISSN 1338-3523, ISSN 0369-2086) is published twice a year by the State Geological Institute of Dionýz Štúr Bratislava, Slovak Republic. The date of issuing of the number 52/1/2020: August 2020.
Subscription for the whole 2020 calendar year (two numbers of the journal): 66.00 € (Europe), 77.00 € (besides Europe), including VAT, postage and packing cost. Claims for nonreceipt of any issue will be filled gratis.
Order of the Editorial Office: Štátny geologický ústav D. Štúra – RC Košice (Library), Jesenského 8, SK-040 01 Košice, Slovak Republic. Phone: +421/55/625 00 43; fax: +421/55/625 00 44, e-mail: mineralia.slovaca@geology.sk, library: secretary.ke@geology.sk



**www.geology.sk/mineralia**

Mineralia Slovaca 52 (2020) • 1

# Obsah – Content

PÔVODNÉ ČLÁNKY – ORIGINAL PAPERS

*Pelech, O., Žecová, K., Jamrich, M., Littva, J., Demko, R., Zlinská, A. & Olšavský, M.*
**Trenčianska kotlina and Ilavská kotlina basins – Remnants of an inverted Early Miocene wedge top basin (Western Carpathians, Slovakia)**
Trenčianska kotlina a Ilavská kotlina – zvyšky invertovanej nesenej spodnomiocénnej panvy ........ 1

*Quintana, J. R., Melgar, G. A. O., Peña, A. C. & Cambra, K. E. N.*
**Main geological and mineralogical characteristics of the Cajálbana lateritic deposit, Pinar del Río, Cuba**
Hlavné geologické a mineralogické charakteristiky lateritického ložiska Cajálbana v provincii Pinar del Río, Kuba........ 23

*Ščerbáková, B., Gawlick, H.-J. & Németh, Z.*
**Differential stresses estimated from calcite veins in HP-LT Triassic Hallstatt Limestones (Northern Calcareous Alps, Austria)**
Diferenciálne napätia z deformovaných kalcitových žíl vo vysokotlakovo-nízkoteplotne deformovaných triasových hallstattských vápencoch (Severné Vápencové Alpy, Rakúsko) ........ 33

*Stercz, M., Grega, D., Pačajová, K. & Petro, Ľ.*
**Hydrogeological parameters trend analysis in the the Slanec village landslide area (Slovakia), crossed by transit gas pipeline of European imporance**
Trendová analýza hydrogeologických parametrov zosuvného územia v trase tranzitného plynovodu európskeho významu pri obci Slanec........ 45

*Turnovec, I. & Illášová, Ľ.*
**Calculating minor constituents in synthetic corundum abrasives**
Výpočet zastúpenia sprievodných zložiek v umelom korundovom brúsive........ 57

**OBÁLKA:**

Obrázok v pozadí: rozsadlina v mraznickom súvrství (staršia krieda) fatrika vyplnená pliocénnymi štrkmi s nálezmi pozostatkov stavovcov, Ivanovská skalka.

Obrázok vľavo hore: egenburský hrubozrnný vápnitý pieskovec čausianskeho súvrstvia so stopami po hrabavej činnosti – *Ophiomorpha*, Skalka nad Váhom.

Obrázok vľavo v strede: nanoplanktón z egenburských vápnitých ílovcov: *Pontosphaera multipora* (Kamptner) Roth (hore), *Cyclicargolithus abisectus* (Muller) Wise (v strede), *Reticulofenestra bisecta* (Hay, Mohler & Wade) Roth (dole).

Obrázok vľavo dole: sklzová vrása z tenkodoskovitých egenburských pieskovcov, Soblahov.

Obrázok vpravo hore: litostratigrafická schéma Trenčianskej kotliny a Ilavskej kotliny, korelácia mediteránnych a centrálnoparatetýdnych stupňov podľa práce Kováča et al. (2017).

Obrázok vpravo dole: zlepencová medzivrstva v egenburských hrubozrnných pieskovcoch, Soblahov.

**COVER**

Figure in the background: Extensional cleft in the Mraznica Formation (Early Cretaceous), Fatricum, filled by the Pliocene gravel with mammal remains, Ivanovská skalka hill.

Figure top left: Eggenburgian coarse-grained calcareous sandstone of the Čausa Formation with burrowing activity – *Ophiomorpha*, Skalka nad Váhom.

Figure left center: Nannoplankton species from the Eggenburgian calcareous claystones: *Pontosphaera multipora* (Kamptner) Roth (top), *Cyclicargolithus abisectus* (Muller) Wise (middle), *Reticulofenestra bisecta* (Hay, Mohler & Wade) Roth (bottom).

Figure bottom left: Slump fold from thin-bedded Eggenburgian sandstones, Soblahov.

Figure top right: Schematic lithostratigraphy of the Trenčianska kotlina and Ilavská kotlina basins. Mediterranean and Central Paratethys stages correlation according to Kováč et al. (2017).

Figure bottom right: Conglomerate interbed in the Eggenburgian coarse-grained sandstone, Soblahov.

*Mineralia Slovaca, Web ISSN 1338-3523, ISSN 0369-2086*
*52, 1 (2020), 1 – 22,* 

# Trenčianska kotlina and Ilavská kotlina basins – Remnants of an inverted Early Miocene wedge top basin (Western Carpathians, Slovakia)

ONDREJ PELECH[1], KATARÍNA ŽECOVÁ[2], MICHAL JAMRICH[3], JURAJ LITTVA[4], RASTISLAV DEMKO[1], ADRIENA ZLINSKÁ[1] and MÁRIO OLŠAVSKÝ[5]

[1] State Geological Institute of Dionýz Štúr, Mlynská dolina 1, SK-817 04, Bratislava 11, Slovakia, e-mail: ondrej.pelech@geology.sk
[2] State Geological Institute of Dionýz Štúr, Regional centre Košice, Jesenského 8, SK-040 01 Košice, Slovakia
[3] Department of Geology and Paleontology, Faculty of Natural Sciences, Comenius University in Bratislava, Mlynská dolina, Ilkovičova 6, SK-842 15 Bratislava, Slovakia
[4] State Nature Conservancy of the Slovak Republic, Slovak Caves Administration, Hodžova 11, SK-031 01 Liptovský Mikuláš, Slovakia
[5] State Geological Institute of Dionýz Štúr, Zelená 5, SK-974 04 Banská Bystrica, Slovakia

**Abstract:** The paper summarizes the latest knowledge about the Early Miocene Trenčianska kotlina and Ilavská kotlina basins, Slovakia. The studied basins are located at the boundary between the Internal and External Western Carpathians and overlie the Pieniny Klippen Belt and Internal Carpathian Mesozoic nappes (Tatricum, Fatricum and Hronicum). This research is based on the results of geological mapping in the northwestern Trenčianska kotlina Basin and westernmost part of the Ilavská kotlina Basin and summarizes all previous (bio)stratigraphic, sedimentological, geophysical and borehole (PB-1, HVJ-25) data. Sedimentary fill of the basins is represented by the transgressive Eggenburgian Čausa and Karpatian Závod formations. Sedimentary record is fragmentary since the Lower Miocene formations are reduced. Youngest sediments are represented by the Pliocene gravels and Quaternary fluvial and eolian deposits. Both Trenčianska kotlina and Ilavská kotlina basins formerly represented one Early Miocene wedge top basin connected with nearby Vienna Basin, Blatné depression, Bánovská kotlina, Hornonitrianska kotlina and Turčianska kotlina basins. The present shape of the Trenčianska kotlina and Ilavská kotlina basins is a result of inversion, rotation, and backthrusting occurring since the Karpatian-Badenian with additional inversion during Pliocene–Quaternary. There are no strong arguments for interpretation of the pull-apart nature of the basins as it was considered in the past.

**Key words:** Central Paratethys, Early Miocene, Middle Váh Valley, Pieniny Klippen Belt, Internal Western Carpathians

**Graphical abstract**

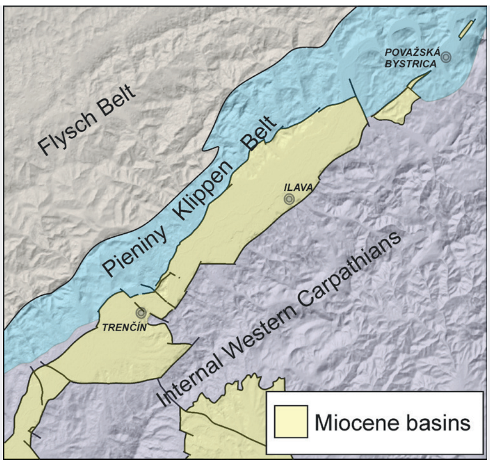


**Highlights**

- Trenčianska kotlina and Ilavská kotlina basins overlie the Pieniny Klippen Belt and Internal Western Carpathian units (Tatricum, Fatricum and Hronicum)
- Three tectonic phases can be recognized: (1) Wedge-top basin represented by Early Miocene (Eggenburgian to Ottnangian) sediments of the Čausa Fm.; (2) latest Early Miocene (Karpatian) to Middle Miocene extrusion, CCW rotation, backthrusting, and disintegration of pre-existing basin into horst and graben structure, during which the Závod Fm. (Karpatian) was deposited; (3) continuing tectonic inversion coeval with deposition of Pliocene fluvial gravels and Quaternary fluvial and eolian sediments

## Introduction

The Western Carpathians represent the northern segment of the Alpine (Tethyan) collision zone formed by the Mesozoic to Paleogene northward-propagating nappe pile (Rakús et al., 1988; Vozár et al., 1999; Plašienka, 2018a; Schmid et al., 2020). The Carpathian nappes are traditionally divided into Outer (or External) and Inner (Internal) Carpathians (Uhlig, 1903; Mišík, 1997a; Lexa et al., 2000). The Outer Western Carpathians are represented by the Flysch Belt, composed of thin-skinned nappes (from north to south: Silesian-Krosno and Magura nappes) formed during the Cretaceous and Paleogene thrusting and Neogene collision (Poprawa & Nemčok, 1988; Ślączka et al., 2006). The Carpathian Flysch Belt is composed mainly of submarine mass wasting siliciclastic deposits alternating with pelagic claystones, the so-called “flysch”. On contrary, the Internal Western Carpathians (IWECA) are represented by thick-skinned nappes including the pre-Alpine crystalline basement (from north to south Tatricum, Veporicum, and Gemericum) with mostly Mesozoic sedimentary cover and Mesozoic thin-skinned nappes (from north to south: Fatricum, Hronicum, Meliaticum, Turnaicum, and Silicicum, Hók et al., 2019). The dividing line between the External and Internal Western Carpathians is represented by the narrow Pieniny Klippen Belt (PKB), composed of “sub-autochthonous” Oravicum and overlying non-Oravic units, derived probably from the IWECA. The internal structure of the Pieniny Klippen Belt is very complicated and controversial. It is characterized by the presence of rigid Jurassic to Early Cretaceous limestone “klippen” surrounded by rheologically softer Late Cretaceous claystone and sandstone formations (Mišík, 1997b; Plašienka, 2018b).

The Late Cretaceous to Paleogene and Neogene to Quaternary sedimentary and volcanic formations in the IWECA are usually considered to post-date the nappe stacking. Especially the Late Cretaceous to Eocene Gosau type basins locally bear signs of post-depositional deformation, including folding and north-vergent thrusting, due to their wedge-top structural setting (Plašienka & Soták, 2015). The younger Eocene – Oligocene formations of the Central Carpathian Paleogene Basin, deposited between the Pieniny Klippen Belt and the outer edge of IWECA, are interpreted as forearc basin (Kováč et al., 1995; Soták et al., 2001; Plašienka & Soták, 2015; Kováč et al., 2016). The Early Miocene basins represented relic foreland and hinterland (retro-arc) basins. The Middle Miocene to Quaternary basins are largely connected to the back-arc Pannonian Basin system (Kováč, 2000; Vass, 2002, Kováč et al., 2017). The northwestern part of the Pannonian Basin is termed Danube Basin on the Slovak territory (or Kisalföld in Hungary). The Western Carpathian Middle Miocene volcanism is mostly calc-alkaline and related to the subduction rollback of the former basement of the Flysch Belt (Lexa & Konečný, 1998; Harangi & Lenkey, 2007).

The investigated Trenčianska kotlina and Ilavská kotlina basins (Fig. 1) are located within the outer edge of the IWECA and are partly overlying the Pieniny Klippen Belt units.

The Early Miocene (Eggenburgian to Karpatian; = late Aquitanian – Burdigalian according to the international time scale, e.g. Kováč et al., 2017, 2018), was a period of an ongoing collision in the western segment of the Carpathian Flysch Belt, where thrusting of the Waschberg-Ždánice (Silesian-Krosno nappe) units onto Carpathian foredeep occurred (Jiříček, 1979; Picha et al.; 2006, Stráník et al., 2007). The Lower Miocene sediments present in the IWECA are usually transgressively overlapping various Mesozoic and Paleogene tectonic units and formations (Kováč et al. 1988; Baráth & Kováč, 1989; Mello et al.,

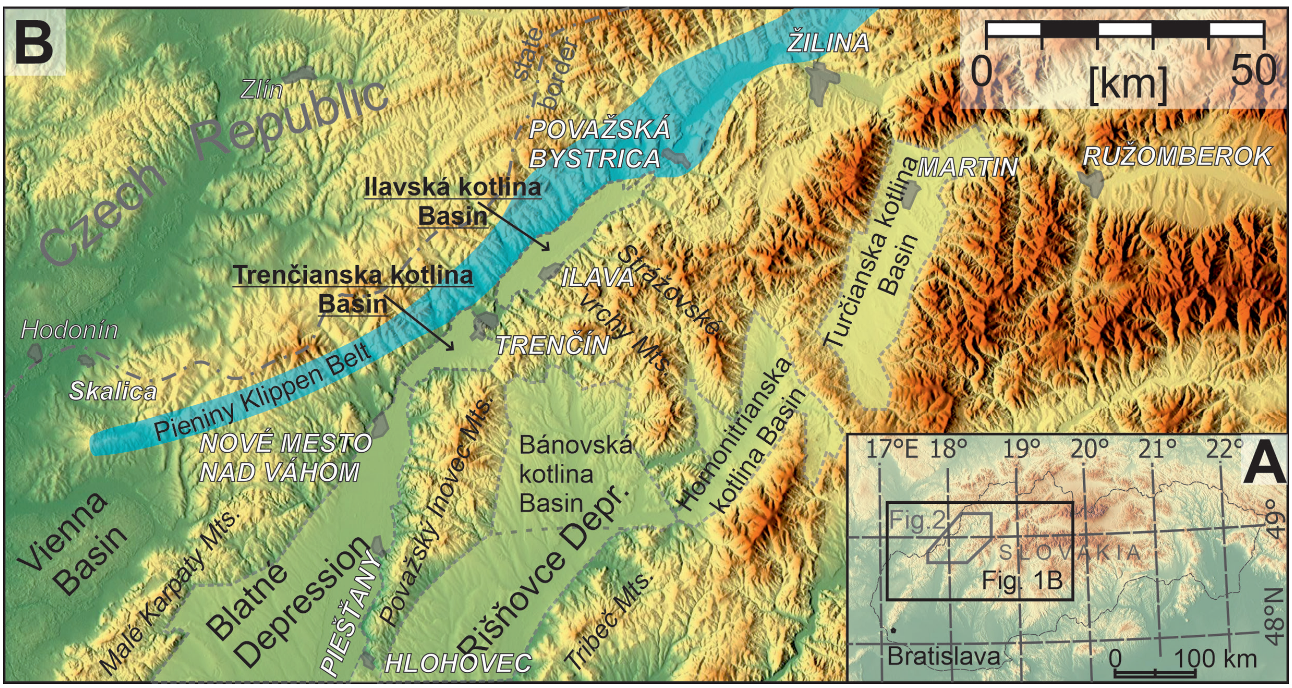


**Fig. 1.** Location of the studied area. A – Location within the Western Carpathians (Slovakia). B – Detailed view showing main basins/depressions and other important orographic features. Pieniny Klippen Belt marked in blue.

2005, 2011; Teťák, 2017). The Eggenburgian sediments in the western part of the Western Carpathians are particularly known only in the Turčianska kotlina Basin (Gašparik et al., 1993; Hók et al., 1998), Hornonitrianska kotlina Basin (Čechovič, 1959; Čechovič & Šínaly, 1962), Bánovská kotlina Basin (Fordinál et al., 2001a, 2001b), the northern part of Blatné Depression (Biela, 1978; Vrana et al., 2009), Trenčianska kotlina, Ilavská kotlina and Vienna basins – thus generally in the northern part of the Danube and Vienna basins and basins connected with Carpathian foredeep (Vass, 2002). The Eggenburgian sediments from the East Slovakian Basin have similar structural position, however, are present in laterally different segment of the thrust belt (Kováč et al., 1995). The Rožňava and Turňa basins (= South Slovakian Basin) have different paleogeographical provenance (Vass, 2002; Nagymarosy, 2013). Another type of Lower Miocene sediments is found in the Kremna Formation of the Carpathian Flysch Belt (Oszczypko-Clowes et al., 2018). The Kremna Formation represents more or less continuous sedimentation from the Oligocene and is located in clearly wedge-top setting between the thrust-sheets of the accretionary prism.

In the present shape, the Trenčianska kotlina and Ilavská kotlina basins represent relict or erosional remnants of larger Early Miocene basin system situated between the Vienna Basin and the northern margins of the Danube Basin (Blatné Depression, Bánovská kotlina Basin), and Hornonitrianska kotlina and Turčianska kotlina basins (Fig. 1). In today's form, however, both are modified by the Middle Miocene and Pliocene horst and graben structure and Pliocene-Quaternary erosion and deposition of the Váh River.

The Neogene sediments in the studied area were for the first time cartographically visualized on the Austrian--Hungarian geological map sheet Trentschin at scale 1 : 75,000 as "*Congerien Schichten*"). The presence of the Neogene sediments was shown as well in the other maps (Uhlig, 1903; Jahn & Beck, 1911; and Lóczy et al., 1922) and post-war general geological maps at scale 1 : 200,000 (sheets Gottwaldov and Žilina, Buday et al., 1963; Maheľ et al., 1964). Mapping was accompanied by biostratigraphic study of macro- and microfauna (Čtyroký, 1957, 1960; Seneš, 1960) and borehole PB-1 (Gabčo et al., 1963). Part of the sedimentary fill of the Trenčianska kotlina and Ilavská kotlina basins was partly incorrectly considered as Central Carpathian Paleogene sediments (a strip south of Trenčín castle ridge). The strip north of Trenčín castle ridge between the Trenčín, Skalka nad Váhom, and Visolaje was properly reported as lower Burdigalian (Maheľ et al., 1964). The fill of the Trenčianska kotlina and Ilavská kotlina basins was at this time mostly considered as Pontian (Late Miocene, Buday et al., 1963; Maheľ et al., 1964). This was later refined as Ruscinian (MN15) due to findings of mammalian macrofauna near Ivanovce (Fejfar & Heinrich, 1985; Fejfar & Sabol, 2004). Later maps of surrounding regions (Biele Karpaty Mts. and Strážovské vrchy Mts., Maheľ et al., 1982; Maheľ, 1985; Began et al., 1993) at scale 1 : 50,000 paid only minor attention to the research of the Neogene fill of the Trenčianska kotlina and Ilavská kotlina basins. Latest partial knowledge about the Trenčianska kotlina and Ilavská kotlina basins was published in maps and explanatory notes of the Middle Váh Valley, Považský Inovec Mts. and Biele Karpaty Mts. geological maps (Mello et al., 2005, 2011; Ivanička et al., 2007, 2011; Pešková et al., 2020). Studied region includes auxiliary stratotype of the Eggenburgian near Sverepec (Steininger & Seneš, 1971).

Both Trenčianska kotlina and Ilavská kotlina basins are considered underexplored due to lack of deep boreholes penetrating the greater thickness of the Miocene sediments or reaching the pre-Cenozoic basement. Only a few boreholes are known, located on the opposite side of the investigated area (Fig. 2). In the northeastern tip of the Ilavská kotlina Basin, such a borehole is located near Sverepec (borehole PB-1, Gabčo et al., 1963). In the southwest Trenčianska kotlina Basin such boreholes/wells are represented by the HVJ-25 and 26 (Pospíšil et al., 1971). The thickness of Miocene sediments in the Trenčianska kotlina Basin was interpreted from vertical electric sounding (Zbořil et al., 1984) and seismic profiles (124, 6HR, Kadlečík et al., 1980; Vozár et al., 1999). In the Trenčianska kotlina Basin, it is reaching 1,000 m (Fig. 3) in the central part and in the Ilavská kotlina Basin approx. 250 m according to geophysical data (Kilény & Šefara, 1989). The pre-Cenozoic basement of Trenčianska kotlina and Ilavská kotlina basins is represented mainly by tectonic units of Pieniny Klippen Belt *sensu lato* (both Oravic and so-called Peri-Klippen or non-Oravic units) in the northwest and Mesozoic rocks of the IWECA units (Tatricum, Fatricum, and Hronicum) in the southeast (Fusán et al., 1987).

Miocene sedimentary fill in the northern part of nearby Blatné depression (so-called Beckov "gate") was drilled by the geothermal well GZV-1 Zelená voda (Fig. 2). Miocene sediments drilled by the well are represented by approx. 300 m of dark grey and sandy clays which directly overlap the pre-Cenozoic basement (Vrana et al., 2009). The core cuttings from the GZV-1, however, lack adequate biostratigraphic processing and are not entirely reliable, as the Karpatian age was gathered only from sediments at the depth 20–24 m. In the southern parts of the Blatné depression continuous Early Miocene sequence to the Pannonian can be observed (Biela, 1978; Rybár et al., 2015). The thickness of the Závod Fm. (Karpatian) in the borehole HVJ-25, located slightly northward, is only 70 m, and below it, 130 m thick Eggenburgian sandstones, claystones, and conglomerates of the Čausa Fm. are present directly above the pre-Cenozoic basement (Pospíšil et al., 1971).

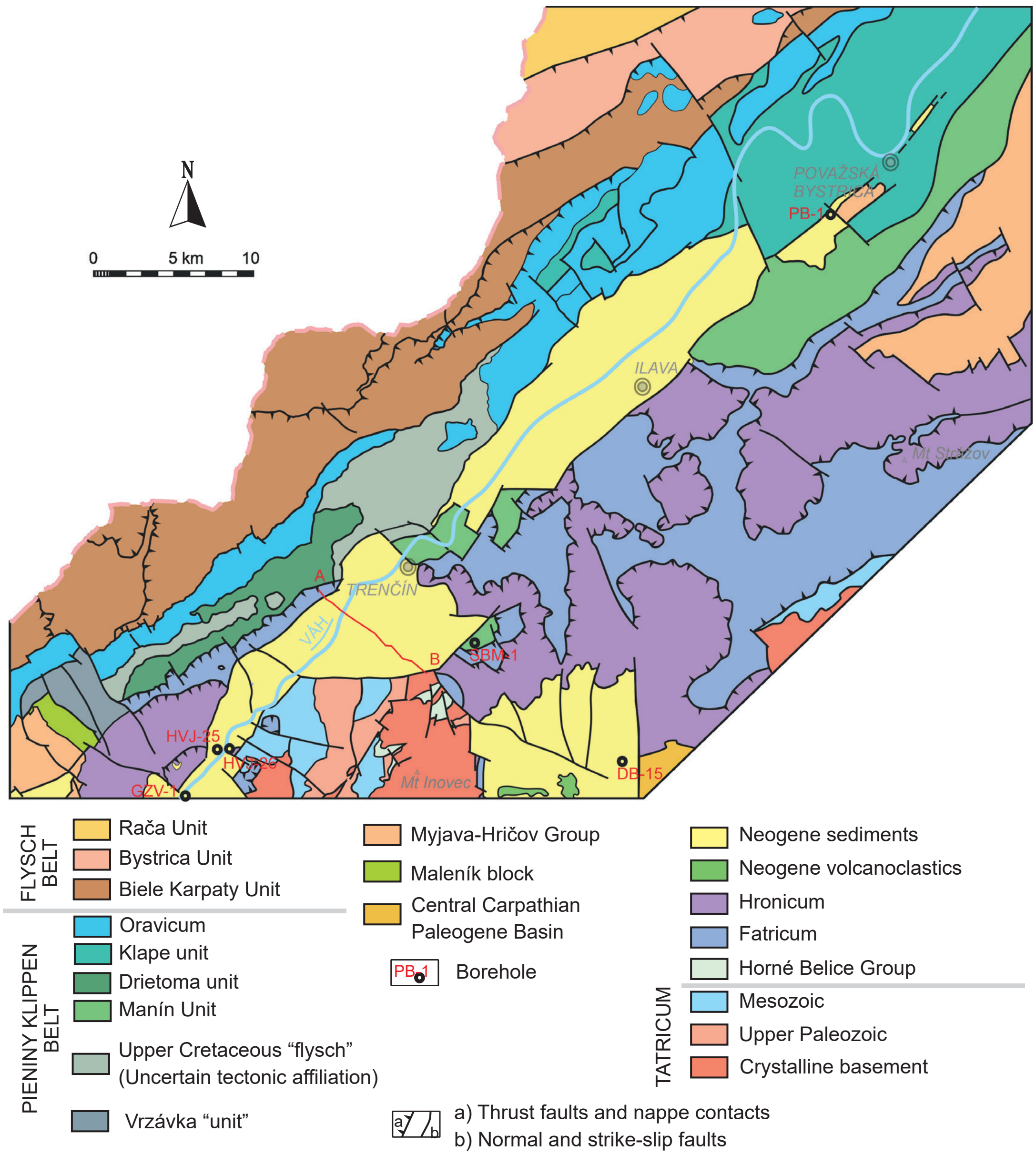


**Fig. 2.** Tectonic map of the wider region of the Trenčianska kotlina and Ilavská kotlina basins (compiled according to Mahel' et al., 1982; Mello et al., 2005; Ivanička et al., 2007; Bezák et al., 2008; Potfaj et al., 2014; Pešková et al., 2020). Cross-section A–B in Fig. 3.

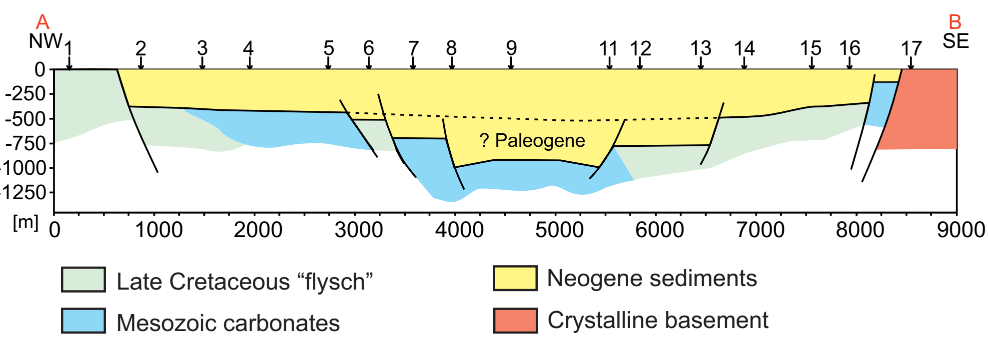


**Fig. 3.** Schematic cross-section A–B of the Trenčianska kotlina Basin based on vertical electric sounding data (Zbořil et al., 1984), partly modified according to recent knowledge of surface geology (Ivanička et al., 2007; Pešková et al., 2020).

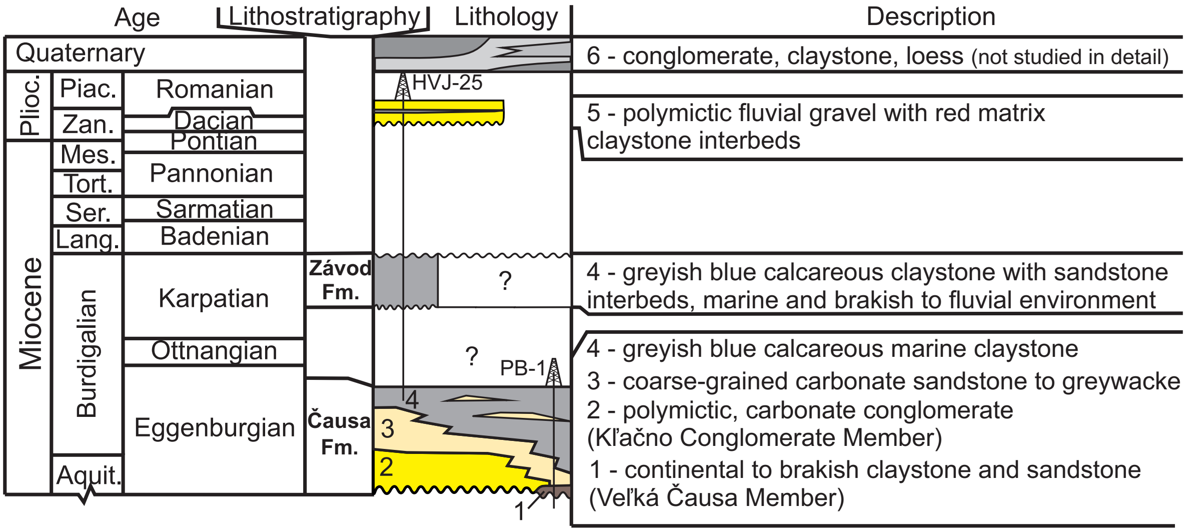


**Fig. 4.** Schematic lithostratigraphy of the Trenčianska kotlina and Ilavská kotlina basins. Mediterranean and Central Paratethys stages correlation according to Kováč et al. (2017).

Different depositional and tectonic history is seen from the borehole data in the nearby Bánovská kotlina Basin (Figs. 1 and 2). The whole basin contains Lower Miocene sediments (Čausa, Bánovce and Lakšárska formations), however, NE part was eroded and SW part subsided during Badenian (Brestenská et al., 1975; Fordinál et al., 2001a, 2001b).

## Objectives and methods

The main aim of this paper is to summarize recent knowledge about geology and tectonics of the Early Miocene sedimentary fill of the Trenčianska kotlina and Ilavská kotlina basins, which are rather poorly covered in the present geological literature.

The research is largely based on the review and reinterpretation of the older sedimentological, structural, geophysical, and paleontological data. New field data were gathered during the geological mapping in the area of the Biele Karpaty Mts. in 2016–2019. Important studied sites and boreholes/wells are listed in Tab. 1. New results are supported by additional sedimentological and petrographic analyses as well as biostratigraphy (nannoplankton and foraminifera). Foraminifera and nannoplankton samples were treated with standard methods. Heavy minerals

**Tab. 1**
Table of important studied outcrops and boreholes/wells described in the text.

| No. | Name | X (Long, E) ° | Y (Lat., N) ° | Lithology | Note | Reference |
|---|---|---|---|---|---|---|
| 1 | Soblahov | 18.062132 | 48.867448 | claystone, sandstone, conglomerate | material from well drilling (OP1TN/Ch1D) | |
| 2 | Trenčianska Turná, Hámre | 18.037836 | 48.844728 | claystone | Engineering geology borehole, depth 5 m (OP3TN) | |
| 3 | Chocholná-Velčice | 17.946382 | 48.854646 | claystone | Engineering geology borehole, depth 5m (OP556BKs) | |
| 4 | Skalka nad Váhom, Starý háj | 18.061907 | 48.919941 | sandstone, conglomerate | outcrop (OP397BKs) | |
| 5 | Skalka nad Váhom, Skalská Nová Ves | 18.071691 | 48.929303 | conglomerate | outcrop (OP492BKs) | |
| 6 | Kobela, Nové Mesto nad Váhom | 17.831240 | 48.780534 | conglomerate, calcarenite | outcrop (OP555BKs) | |
| 7 | Trenčín, Brezina | 18.050383 | 48.879332 | calcarenite, sandstone | outcrop (OP2TN) | |
| 8 | Ivanovská skalka | 17.904632 | 48.824779 | gravel | Railroad cut, caverns filled by gravel with mammal macrofauna | Fejfar & Heinrich (1985) |
| 9 | PB-1 | 17.857543 | 48.763418 | - | Borehole | Gabčo et al. (1963) |
| 10 | HVJ-25 | 17.875758 | 48.788937 | - | Borehole/Well | Pospíšil et al. (1971) |
| 11 | GZV-1 | 17.857543 | 48.763418 | - | Well | Vrana et al. (2009) |

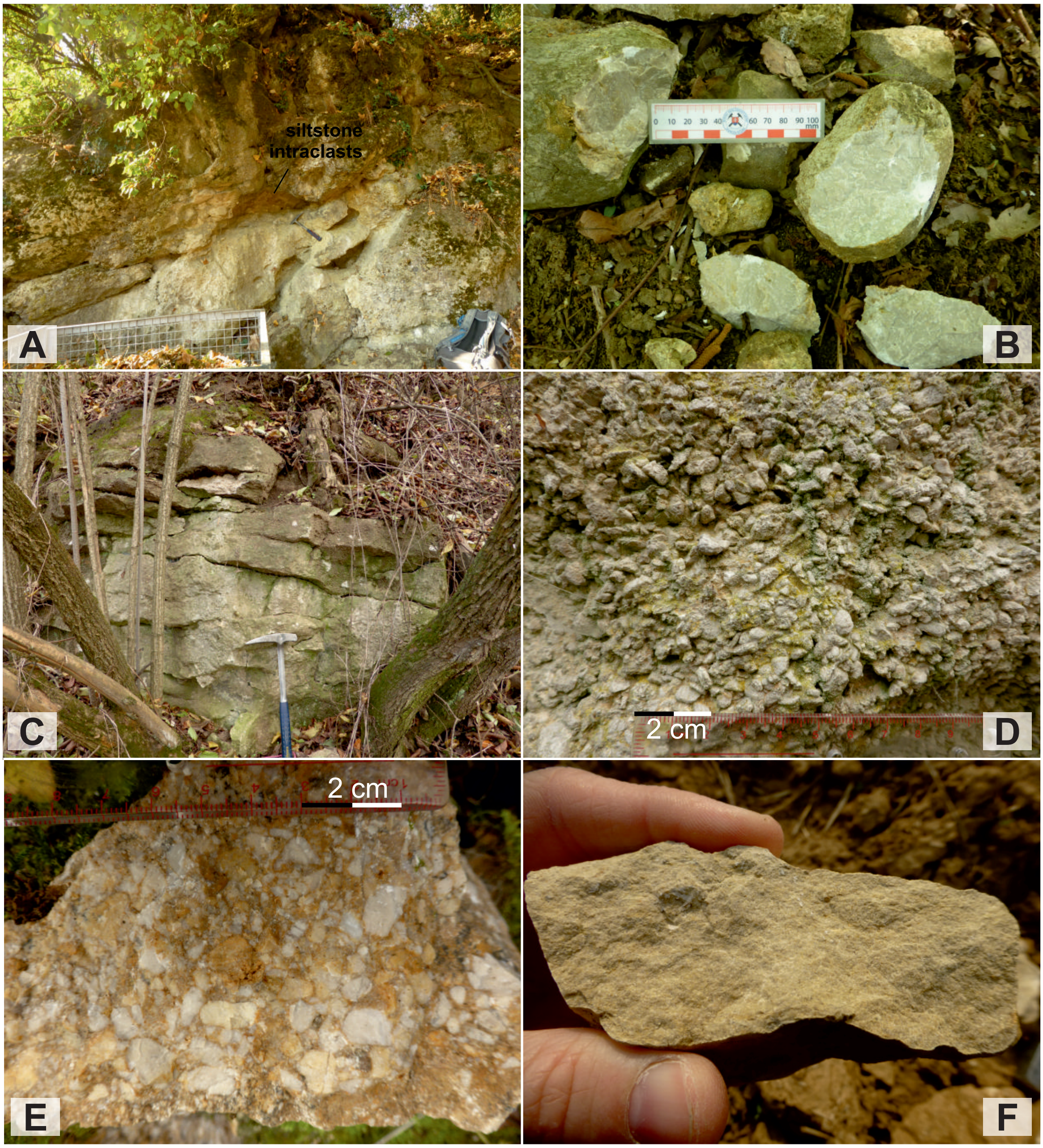


**Fig. 5.** A – Outcrop of thick-bedded conglomerates with siltstone intraclasts containing Cretaceous and Paleogene (redeposited) nanoplankton, Skalka nad Váhom, site 5. B – Boulders of the Wetterstein Limestone eroded from the conglomerates found in loose debris near the Skalka nad Váhom, site 4. C – Medium-bedded monomictic conglomerate, Kobela, N of Nové Mesto nad Váhom, site 6. D – Detail on the weathered surface from the previous figure. E – Fresh surface of monomictic conglomerate from the previous figure. F – Calcarenite with abundant echinoderm detritus, Kobela, N of Nové Mesto nad Váhom, site 6.

were studied by CAMECA SX 100 microprobe at the Department of special laboratories State geological institute of Dionýz Štúr.

## Results

The Eggenburgian sediments of the Trenčianska kotlina and Ilavská kotlina basins are represented by the Čausa Formation (originally defined in the Hornonitrianska kotlina Basin, see Samuel et al., 1988; Vass, 2002). The Čausa Formation is traditionally divided into (1) Basal continental, freshwater to brackish sandstones and claystones (the Veľká Čausa Member); (2) Upward-fining grey-brown to yellow alluvial to littoral conglomerates (the Kľačno Conglomerate Member) that pass into calcareous

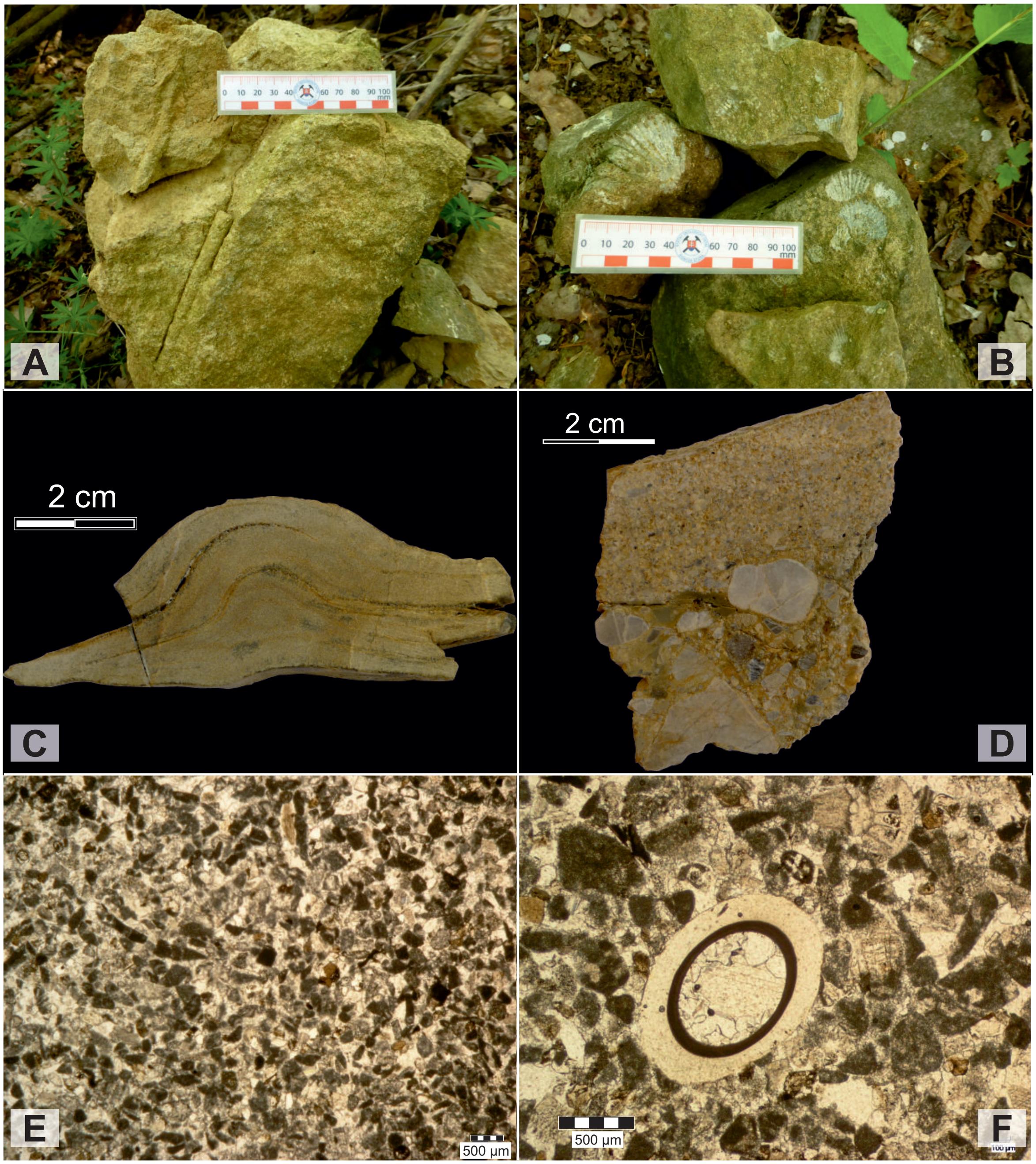


**Fig. 6.** A – Coarse-grained sandstones with *Ophiomorpha* burrows, site 4. B – Sandstones with fragments of thick-walled bivalvia, site 4. C – Slump fold from thin-bedded sandstones, site 1. D – Conglomerate interbed in the coarse-grained sandstone, site 6. E – Thin-section of calcarenite, site 6. F – Section of serpulid worm *Ditrupa cornea*, site 6.

littoral sandstones, calcarenites, or greywackes (3). The greyish calcareous sub-littoral to bathyal claystone ("schlier") sediments (4; Fig. 4) are traditionally included into the Čausa Formation (Mello et al., 2011; Ivanička et al., 2011). This lithofacies can be correlated with the lower part of the Lužice Formation (defined in Vienna Basin).

(1) Basal non-marine Eggenburgian sediments – so-called Veľká Čausa Member are described only from the PB-1 borehole (depth 80–60 m, Gabčo et al., 1963; Began et al., 1963). They are represented by the varicoloured sandstones and claystones lacking any faunistic remains and rich in siderite, probably of pedogenic origin. The sediments were deposited in continental or freshwater environment. The following 6 m thick dark grey sandy clays with sandy intercalations, probably of brackish, lagoonal origin, contain mollusc macrofauna of *Tympanotonus*

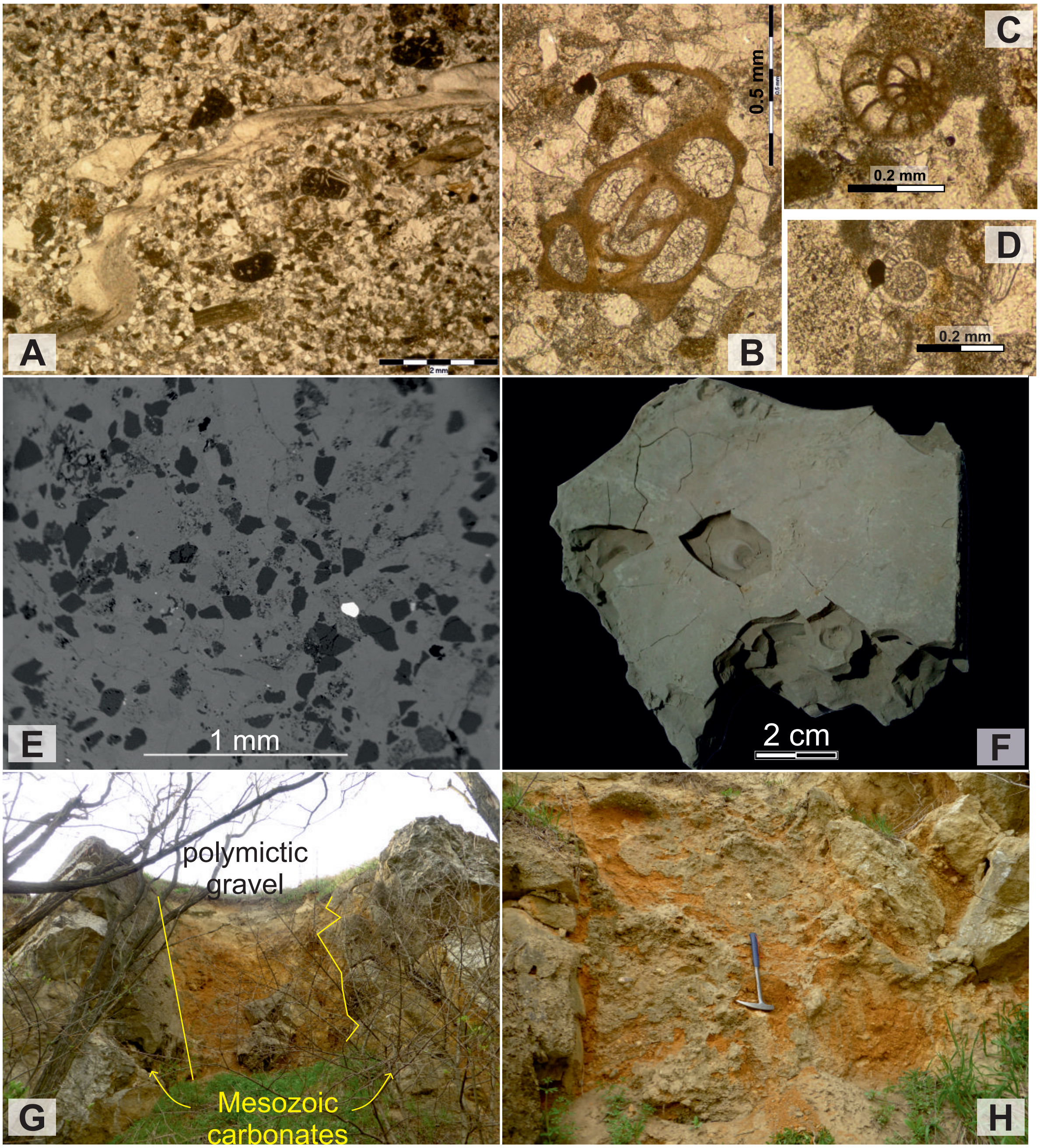


**Fig. 7.** A – Thin-section of sandstone with the thick-walled bivalve, site 1. B – Cross-section of *Quinqueloculina* cf. *buchiana* (d'Orbigny). C – Foraminifer *Ammonia* cf. *beccari* (Linnaeus). D – Foraminifer *Elphidium* sp. E – BSE image of sandstone, site 1. Dominating lithoclastic carbonate (pale grey) and angular clasts of quartz (dark grey) with homogenous grain size. Carbonate is present as well as cement. White mineral in the center, identified as monazite with marked oscillating zones, indicates its magmatic origin. F – Grey calcareous claystone representing typical pelitic lithofacies of the Čausa Fm. from the engineering borehole near Trenčianska Turná, site 2. G – Karst fillings with polymictic gravel of Pliocene age in the railroad cut near Ivanovce, site 8. H – Detail on the gravel from the previous image.

*margaritaceus moniliformis* (Grat.), *Tympanotonus margaritaceus grateloupi* (d'Orb.), *Melanopsis hantkeni* Hofm., *Clithon (Vittoclithon) pictus* Fér. and *Meretrix* sp.; foraminifera *Rotalia beccarii* (Linnaeus); sporadic radiolarians, *Characeae;* and pollen assemblage indicating humid subtropical climate (Began et al., 1963; Planderová, 1990). The overall thickness of the continental and brackish sediments is 40–50 m (Salaj, 1995).

(2) The conglomerate lithofacies, i.e. the Kľačno Conglomerate Member represents a continual transition

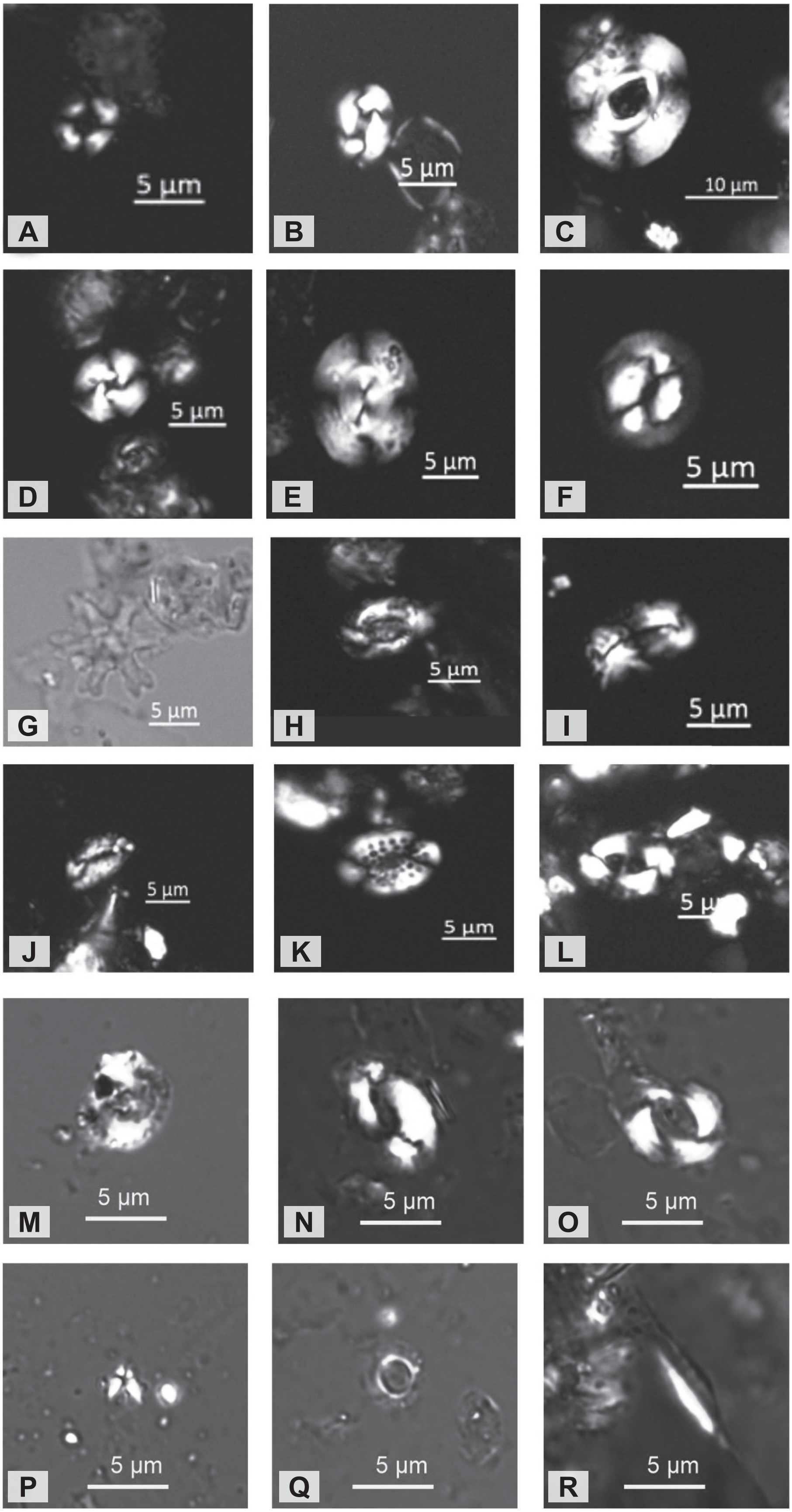


**Fig. 8.** Documented nannoplankton species (for location of samples see Tab. 1). A – *Reticulofenestra ornata* Müller, XN, site 1. B – *Reticulofenestra lockeri* Müller, XN, site 2. C – *Cyclicargolithus abisectus* (Muller) Wise, XN, site 2. D – *Cyclicargolithus floridanus* (Roth & Hay) Bukry, XN, site 2. E – *Reticulofenestra bisecta* (Hay, Mohler & Wade) Roth, XN, site 2. F – *Coccolithus pelagicus* (Wallich) Schiller, XN, site 2. G – *Discoster deflandrei* Bramlette & Riedel, XN, site 2. H – *Helicosphaera* cf. *ampliaperta* Bramlette & Wilcoxon, XN, site 2. I – *Helicosphaera scissura* Miller, XN, site 2. J – *Helicosphaera carteri* (Wallich) Kamptner, XN, site 1. K – *Pontosphaera multipora* (Kamptner) Roth, XN, site 2. L – *Helicosphaera recta* (Haq) Jafar & Martini, XN, site 2. M – *Calcidiscus leptoporus* (Murray & Blackman) Loeblich & Tappan, site 3. N – *Helicosphaera ampliaperta* Bramlette & Wilcoxon, site 3. O – *Reticulofenestra excavata* Lehotayová, site 3. P – *Sphenolithus* aff. *belemnos* Bramlette & Wilcoxon, site 3. Q – *Umbilicosphaera rotula* (Kamptner) Varol, site 3. R – *Triquetrorhabdulus carinatus* Martini, site 3.

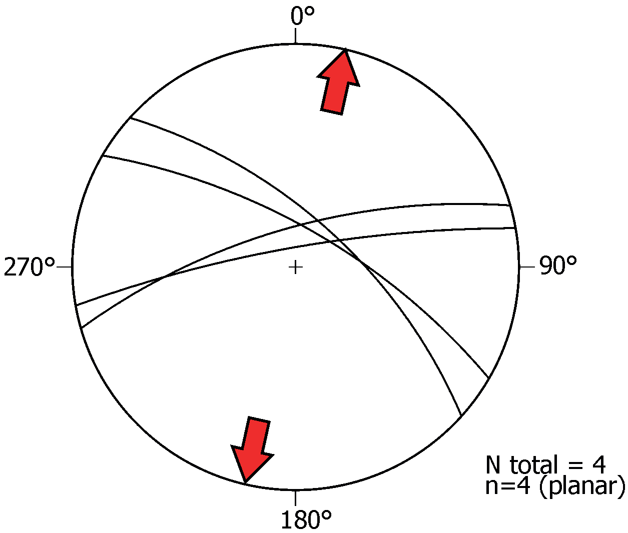


**Fig. 9.** Orientation of caverns in the Ivanovecká skalka elevation (site 8, for location see Tab. 1).

between the coarse-grained sandstone/fine-grained conglomerate to cobble conglomerate with clasts up to 10 cm in diameter (Fig. 6 A-B). The clasts are mostly represented by the Middle Triassic carbonates (Wetterstein limestone and dolomite), but also quartzites, radiolarites, sandstones, or siltstones, and clayey limestones with calpionellids. The conglomerates contain a mixed material, a large volume of which comes from the Hronicum and other Inner Carpathian nappes. Crystalline basement rocks were observed in negligible amount (for a more detailed analysis see Kováč et al., 1988; Baráth & Kováč, 1989). The matrix of conglomerates is calcareous and sandy. Since the conglomerates onlap the Pieniny Klippen Belt rocks as well, it can be assumed that deposition took place on the tectonically disintegrated basement, which, however, was not eroded up to the base of the Tatric sedimentary cover. Locally 5–10 cm beds of cross-bedded sandstones intercalate with conglomerates (Salaj, 1995). The overall thickness of the conglomerates is 80–100 m (Salaj, 1995).

The conglomerate and overlying calcarenites differ in the western tip of the Trenčianska kotlina Basin, north of Nové Mesto nad Váhom (site 6; Tab. 1), where the basal carbonate conglomerates are structurally immature (Figs. 5 C–E). Clasts – granules to small pebbles are poorly rounded, often angular, monomictic, mostly represented by Wetterstein Limestone and Wetterstein Dolomite, which are located in their basement. The conglomerates and calcarenites could possibly represent erosional remnant of the Planinka Formation (Ottnangian, Kováč et al., 1992). Due to the missing features which would allow precise stratigraphic assignment, we conditionally include the sediments into the Čausa Fm.

(3) The sandstone lithofacies is represented by the medium- to thick-bedded fine-grained to coarse-grained calcareous sandstone or calcarenites, locally with conglomerate interbeds, usually of greyish to yellow colour on weathered surfaces and grey-brown on a fresh surface (Figs. 5 F and 6 A–B). Apart from quartz and/or carbonate grains, also feldspars and muscovite are common. Matrix is mostly calcareous, however, silicification was locally observed as well. Sandstones are mostly structureless, however, may contain abundant fucoids (*Ophiomorpha*, Fig. 6 B) and fragments of thick-walled bivalves (Fig. 6 B). Locally, also minor slump folds were recorded (Fig. 6 C). Lithic detritus is mostly represented by clasts of carbonates. It is possible to identify clasts of calpionellid, radiolarian and Saccocoma limestones, clasts with thin-walled bivalves or rare *Globotruncanidae* fragments (Mesozoic redeposits). Heavy minerals from sandstones both from Trenčianska kotlina and Ilavská kotlina basins are characterized by the presence of apatite, leucoxene, zircon, rutile, garnet, tourmaline, epidote, spinel, staurolite, and monazite (Fig. 7 E). The chemical composition of 9 garnet grains analysed by electron microprobe in one thin section suggests presence of mixed populations, where composition (in mol %) varied as:

- almandine (59–46) – grossular (27–16) – pyrope (26–23) – spessartine (2–1)
- almandine (72–63) – grossular (26–3) – pyrope (11–7) – spessartine (25–2)
- almandine (64) – grossular (26) – pyrope (4) – spessartine (15)

The composition of analysed spinel grains (four grains per one thin section) responds to magnesiochromite and spinel, where Cr/(Cr+Al) = 0.28–0.55 and FeII/(FeII+Mg) = 0.3–0.47. Spinels and garnets chemically does not diverge from composition of samples from External Carpathian Flysch Belt sandstones.

Sandstones and calcarenites contain also *in situ* fossil remains. Apart of common fragments of thick-walled bivalves (Figs. 6 B and 7 A; described by Čtyroký, 1960), bryozoa, echinoderm spines, and foraminifers *Ammonia* cf. *beccarii* (Linnaeus), *Quinqueloculina* cf. *buchiana* (d'Orbigny), *Elphidium* sp. (Figs. 7 B-D) were identified from a thin section. Other foraminifers found in the sandstone are listed in Tab. 3. Eggenburgian age of the sandstones is based on the occurrence of the bivalves *Chlamys gigas* (Schlotheim) described from the Skalka nad Váhom (part Skala) and Horovce villages (Čtyroký, 1957; 1960). The yellow calcarenites occurring above the carbonate conglomerates north of the Nové Mesto nad Váhom are characterized by remains of serpulid *Ditrupa cornea* (Figs. 6 F). Similar as the underlying conglomerates they could possibly represent erosional remnant of the Planinka Fm. For now the calcarenites are included into the Čausa Fm.

The sandstones of the Čausa Formation pass gradually and laterally into siltstones, calcareous claystones, and

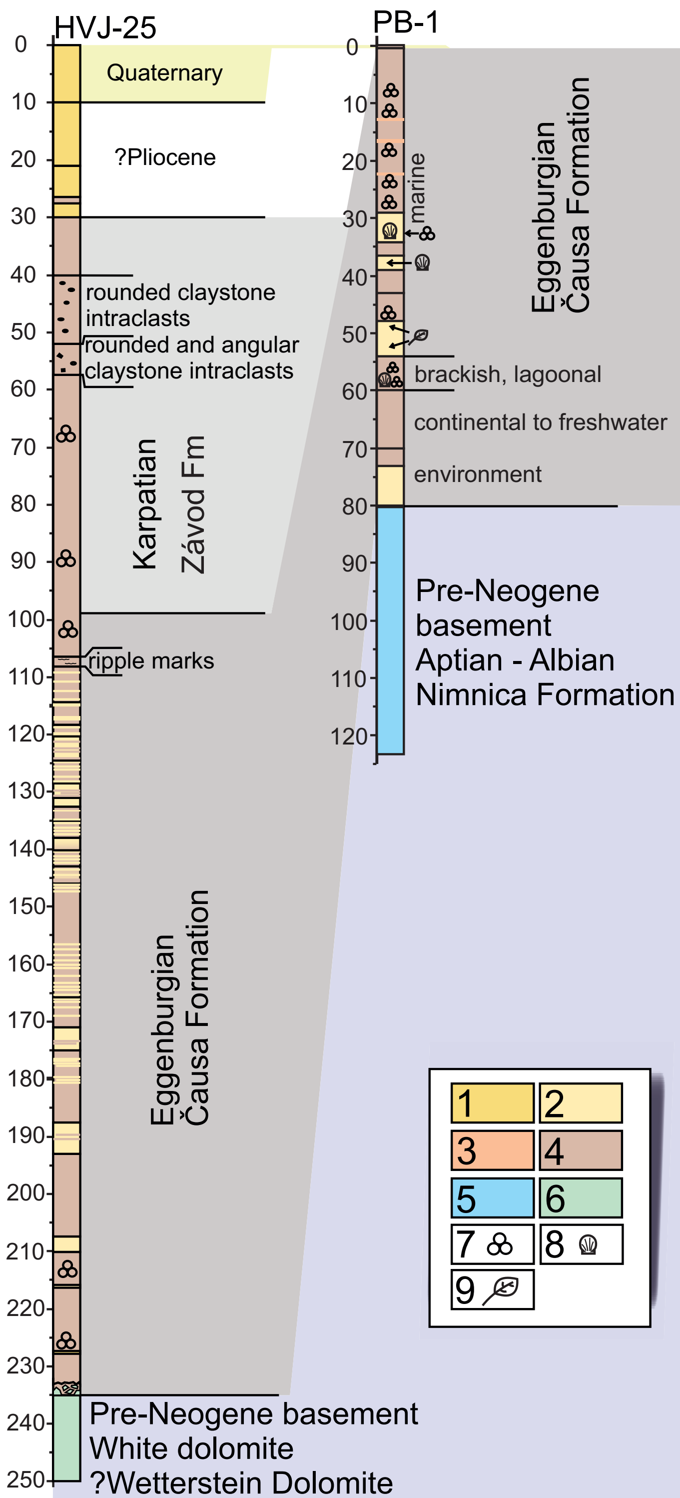


**Fig. 10.** Correlation profile across the boreholes HVJ-25 and PB-1 (based on Pospíšil et al., 1971; Gabčo et al., 1963). For the boreholes location see Fig. 3 and Tab. 1. 1 – conglomerate or gravel; 2 – sandstone; 3 – siltstone; 4 – claystone or clay; 5 – limestone; 6 – dolomite; 7 – microfauna; 8 – macrofauna; 9 – macroflora.

"schlier" sediments, that represent pelitic lithofacies. The overall thickness of the conglomerate and sandstone lithofacies is according to field observation maximum 80–150 m in the Trenčianska kotlina and Ilavská kotlina basins.

(4) Pelitic lithofacies is dominated by blueish, grey, and grey-green sandy calcareous claystones, siltstones, and "schlier" sediments (Fig. 7 F). Sediments are mostly massive, irregular lamination is usually observed only in the interbeds with higher sandy admixture. Fine-grained sediments form only sporadic outcrops and are mostly covered by Quaternary deposits. The wider occurrence of this facies in the larger area of Trenčianska kotlina Basin was confirmed by several shallow engineering geology boreholes, and hydrogeologic wells (Tab. 1; other localities are reported by Kysela, 1978).

Thickness of the pelagic claystones in the Trenčianska kotlina and Ilavská kotlina basins varies between 54 m in the borehole PB-1 (Sverepec) (Gabčo et al., 1963) and 136.5 m in the well HVJ-25 (Pospíšil et al., 1971). The borehole data for the region are, however, sparse. Outside the studied region, the DB-15 (Horňany) in the northern Bánovská kotlina Basin contains 204 m of the Eggenburgian pelagic claystones (Brestenská et al., 1975; Biela, 1978; Fordinál et al., 2001b). Not even such thickness would, however, explain the occurrence of pelagic claystones in various places under the Quaternary sediments in the central part of the Trenčianska kotlina Basin. The presence of the Ottnangian Bánovce Formation, possibly occurring above the Čausa Fm. could not be confirmed.

The age of the pelitic lithofacies was based on nannoplankton and foraminifers. Samples from pelagic claystones from sites 1 (Soblahov), 3 (Chocholná-Velčice), and 2 (Trenčianska Turná-Hámre) yielded Early Miocene nannoplankton assemblage of NN2 Zone based on the occurrence of *Helicosphaera scissura* Miller, *Helicosphaera recta* (Haq) Jafar & Martini, *Helicosphaera ampliaperta* Bramlette & Wilcoxon (Perch-Nielsen, 1985), and *Helicosphaera carteri* (Wallich) Kamptner (Figs. 8 A-R; Tab. 2). Studied foraminifera samples were poorer and did not contain index species (Tab. 3), however, planktonic zones N5 and N6 were described by previous research (Salaj & Zlinská, 1991).

The Závod Formation (Figs. 4 and 10) consists of grey sandy calcareous claystones, with yellow calcareous claystone and lignite interbeds containing brackish and freshwater microfauna of the Karpatian age. Sediments are not present on the surface in the Trenčianska kotlina and Ilavská kotlina basins,

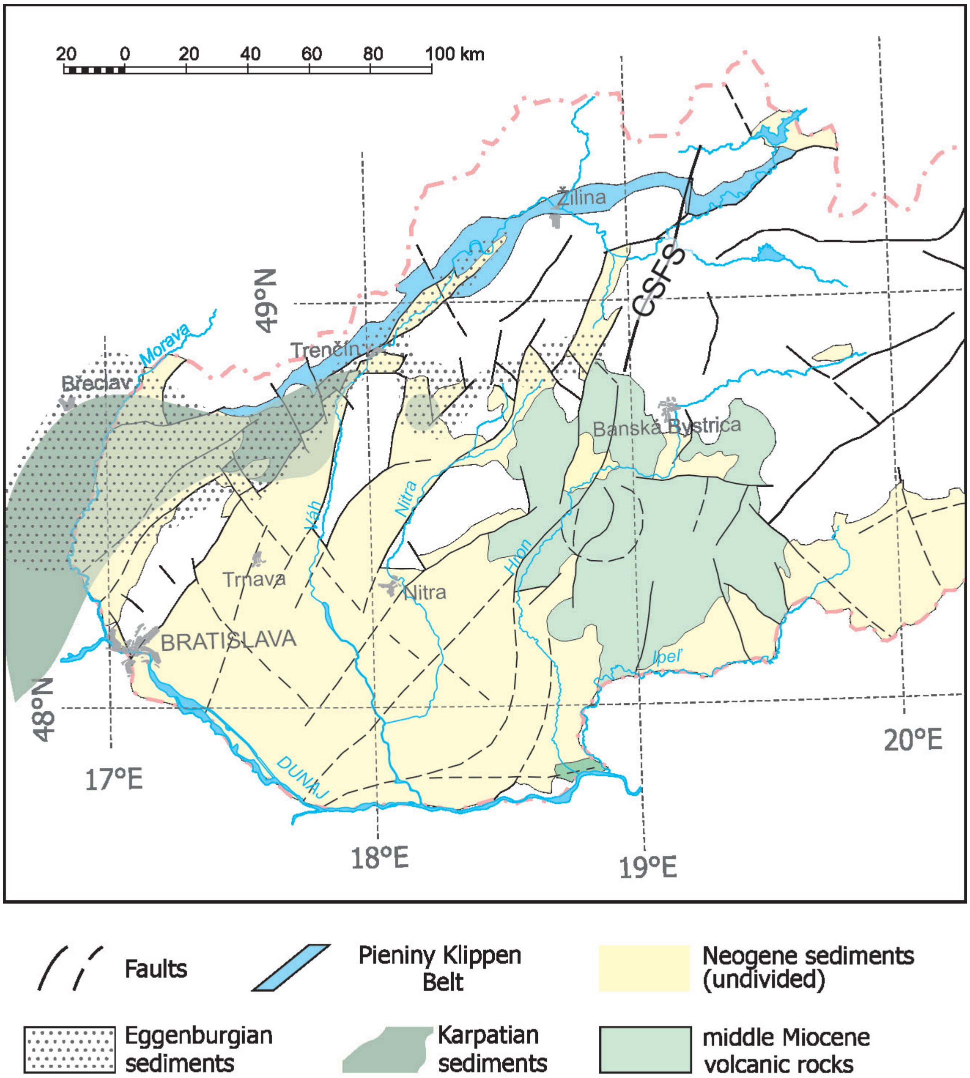


**Fig. 11.** Schematic map showing the distribution of Eggenburgian (dotted) and Karpatian (transparent grey-green) sediments in the Western Slovakia and surrounding regions (compiled according to Biela, 1978; Kováč et al., 1988; Kováč & Baráth, 1989; Gašparik et al., 1993; Pristaš et al., 2000; Ivanička et al., 2007; Potfaj et al., 2014; Pešková et al., 2020). Occurrences the Early Miocene sediments and in the South Slovakian Basin and the Flysch Belt are not shown. Background map based on Hók et al. (2019). CSFS = Central Slovak Fault System.

however, were revealed by the borehole HVJ-25 (Pospíšil et al., 1971). It overlies the basinal clays of the Čausa Formation and is characterized by sediments of similar lithology as the upper portion of the Čausa Formation. Their mutual contact suggests gradual transition; however, it includes hiatus and transgression that lacks basal clastics which are absent in the distal part of the basin. The Závod Formation was identified in the depth of 30–99 m in the HVJ-25 borehole (Pospíšil et al., 1971).

Sediments of the Pliocene age in the region are usually not sufficiently exposed, therefore most of the information came only from the boreholes. We include here medium-grained grey, yellow gravel with well-rounded quartzite and conglomerate pebbles reported from the upper portion of the borehole HVJ-25 (depth 10–37 m). Direct paleontological evidence is not given, however, possible redeposition of Karpatian microfauna in the clay interbed from depth 27.6–28.5 m was stated (Pospíšil et al., 1971). The post-Miocene sediments are represented as well by the red-brown fine- to medium-grained gravel observed in the railroad cut near Ivanovce village (site 8, Figs. 7 E–F). Mammal terrestrial macrofauna remains from this site indicate late Pliocene age (Ruscinian, MN15, Fejfar & Heinrich, 1985; Fejfar & Sabol, 2004). The gravel is present as cavern fill in the Mesozoic carbonates (Fatric Mraznica Fm.). The caverns have ESE-WNW and NW-SE strike and dip generally to the north (Fig. 9), suggesting NNW-SSE extension during the late Pliocene. Older reports also suggest the presence of greenish or brown clay interbeds considered as Pliocene in age (e.g. Salaj, 1988). The varicoloured gravel can be potentially correlated with the Kolárovo Formation.

Quaternary sediments of the Trenčianska kotlina and Ilavská kotlina basins were not studied in detail. The Quaternary fluvial terraces and alluvial fans of the wider area were studied for almost a hundred years (e.g. Hromádka, 1931; Andrusov, 1932), with some of the studies paying particular attention to the Trenčianska kotlina and/or Ilavská kotlina basins (e.g. Lukniš, 1946; Ložek & Tyráček, 1960; Mazúr & Kalaš, 1963a, b; Mazúrová, 1972; Beták, 2002). The Quaternary terraces and fans were also studied by mapping (e.g. Salaj, et al., 1989; Began et al., 1990; Potfaj, 2005; Ivanička et al., 2007, 2011; Mello et al., 2005, 2011; Pešková et al., 2020) and technical works (Zaťko et al., 1988; Mlynarčík, 1998; Šalagová et al., 1990). In the studied region, their overall thickness is usually 5–13 m, locally up to 20 m. The fluvial and alluvial accumulations (channel fill sand and gravel and floodplain clays) of the Váh River and alluvial fans of smaller tributary streams (notably Vlára and Drietomica) dominate NW part of the Trenčianska kotlina Basin and central part of Ilavská kotlina Basin. The eolian deposits are mostly grey and yellow loess and resedimented loess, often up to 10 m thick.

Several notable general patterns can be discerned in the Plio-Quaternary features of the Trenčianska kotlina and Ilavská kotlina basins. (1) The presence of NE–SW trend in both basins (albeit more pronounced in the Ilavská kotlina Basin) caused by the likewise-oriented faults. (2) Strong morphological contrasts between the flat and wide fluvial plains of the basins and the narrow, entrenched valleys, with steeper topography (so-called “gates”) separating the basins. These are in all likelihood related to the faults running perpendicular to the basins. Differences between relative height in corresponding river terraces were observed between the basins and the “gates”, implicating some degree of activity of these faults. (3) Gradual straightening of the Váh River channel, as well as narrowing of its alluvial plain during the Quaternary. The spatial distribution of terrace remnants demonstrates that the alluvial plain was much wider during the Pleistocene. Significantly greater river curvature in the entrenched “gates” presumably reflects the original watercourse preserved due to the more erosion-resistant bedrock. (4) Terrace and fan system dominated by the deposits of tributary streams. When compared to the upstream basins, the terrace remnants of the Váh River in the study area are characterized by a lesser extent, more fragmentary nature, and more material admixture from the tributary streams. The prevalence of the terraces diminishes further downstream, with little to almost none Váh River river terraces identified in the Trenčianska kotlina Basin. However, the increasing dominance of the tributary depositional landforms does not have an apparent effect on the erosive capability of the main river, as it laterally eroded distal parts of several fans. The older fans are dissected by their streams and, given enough space, basinward propagation of the younger fans can be observed within both basins, most prominently in the southeastern part of the Trenčianska kotlina Basin. The implications resulting from the presence of these features are debated in the discussion.

## Interpretation and discussion

Despite the basic features of the Trenčianska kotlina and Ilavská kotlina basins sedimentary fill was already known since the 1960s, the information was fragmented, mostly available only in unpublished manuscripts and technical reports (Gabčo et al., 1963; Pospíšil et al., 1971; Kysela, 1978; Zbořil et al., 1984; Kováč et al., 1988), and later partly summarized in explanation notes to 3 different geological maps 1:50 000, covering various parts of the studied region (Mello et al., 2011; Ivanička et al., 2011; Pešková et al., 2020).

In the larger picture, the sedimentary fill of the Trenčianska kotlina and Ilavská kotlina basins (Figs. 1 and 2) was formerly an integral part of the larger Early Miocene sedimentary basin occurring on the outer margin of the IWECA, from the west located Vienna Basin to Blatné Depression and Bánovská kotlina, Hornonitrianska kotlina, and Turčianska kotlina basins in the eastern side (Fig. 11; Lexa et al., 2000; Kováč, 2000; Vass, 2002, Kováč et al., 2017). The deposition started in the early Eggenburgian with continental (limnic) and brackish clays and sands, locally also coarser clastics, known in the Brezovské Karpaty Mts. (Potfaj et al., 2014; Teťák et al., 2015), north-east located Ilavská kotlina Basin (borehole PB-1, Gabčo et al., 1963) and further south located Hornonitrianska kotlina Basin (Čechovič, 1959; Čechovič & Šinály, 1962). Much more widespread are the onshore (marginal) coarse clastics with different names and source areas in different basins – e.g. Chropov, Winterberg, Podbranč conglomerates in the Vienna Basin; Kľačno Conglomerate in Hornonitrianska kotlina, Bánovská kotlina, Trenčianska kotlina, and Ilavská kotlina basins, and Rakša and Slovany conglomerates in Turčianska kotlina Basin (Teťák, 2017; Ivanička et al., 2007; Pristaš et al., 2000; Mello et al., 2005; Gašparik et al., 1993; Vass, 2002). The coarse clastic sediments represent the onset of marine transgression affecting region along the western segment of the PKB – IWECA contact zone. The conglomerates were gradually replaced by finer clastics, mostly littoral sandstones, and finally, open marine calcareous claystones (Čechovič, 1959; Salaj & Zlinská, 1991), representing the maximum Early Miocene flooding. The Ottnangian Bánovce Formation was formerly described near the Soblahov village above the Eggenburgian Čausa Formation, however, without biostratigraphic verification (site 1, Tab. 1; see Maheľ et al., 1982; Ivanička et al., 2007). This study contradicts such interpretation, as the biostratigraphic analysis did not confirm the presence of Ottnangian sediments NW of Soblahov. The Ottnangian sediments among the western part of the Western Carpathian Neogene basins are represented by the Bánovce Fm. reported from the Bánovská kotlina Basin (Brestenská et al., 1975; Fordinál et al., 2001b) and the upper portion of the Lužice Fm. in the Vienna Basin. The absence of Ottnangian sediments is similar to the Hornonitrianska kotlina and Turčianska kotlina basins (Vass, 2002). It cannot be, however, excluded that the Ottnangian sediments were deposited and later eroded in the Trenčianska kotlina and Ilavská kotlina basins (as was stated by Salaj & Zlinská, 1991; Salaj, 1995). The more-or-less continuous marine sedimentation throughout the entire Early Miocene until the Karpatian was confirmed only in the Vienna Basin, northern Blatné Depression (e.g. borehole K-1 and possibly also GZV-1, Biela, 1978; Vrana et al., 2009), southwestern portion of the Trenčianska kotlina Basin (borehole HVJ-25, Pospíšil et al., 1971), and northern Bánovská kotlina Basin (Brestenská et al., 1975; Biela, 1978; Baráth & Kováč, 2000; Fordinál et al., 2001a, 2001b).

The Early Miocene stress regime was characterized by the NW-SE principal compressive stress ($\sigma_1$) in the Eggenburgian and was later accompanied by SW-NE tension ($\sigma_3$) in the Ottnangian and Karpatian in the western portion of the Western Carpathians (Hók et al., 1995; Nemcok et al., 1998; Fodor et al., 1999; Marko, 2012).

The following Middle Miocene rifting phase, starting in the Badenian, affected a large portion of the Pannonian Basin. Thick sequences of Badenian sediments accumulated in the northern Danube Basin, including Blatné and Rišňovce depressions (Biela, 1978; Baráth & Kováč, 2000; Hók et al., 2016). Simultaneously horst blocks of the Malé Karpaty, Považský Inovec, and Strážovské vrchy Mts. were elevated (Kováč et al., 1994; Danišík et al., 2004, Králiková et al., 2016; Marko et al., 2017), completely disrupting the existing Early Miocene basins configuration (Vass et al., 2002; Marko, 2012). The Badenian stress regime was characterized by the N-S to NNE-SSW principal compressive stress ($\sigma_1$) and E-W to ESE-WNW tension ($\sigma_3$) (Hók et al., 1995; Nemcok et al., 1998; Fodor et al., 1999; Marko, 2012)

Different mechanisms were proposed for the tectonic setting of the Early Miocene basins of the west portion of the IWECA. Formerly the model of strike-slip/wrench furrow basins was proposed (Vass et al., 1988; Kováč, 2000) and persists in the literature until today (Ivanička et al., 2011; Mello et al., 2011; Ludwiniak et al., 2019; Plašienka et al., 2020). The main arguments for a such model are: (1) the structural position on the outer margin of the IWECA at the contact with PKB which is usually interpreted as major oblique-slip plate boundary (Kováč & Hók, 1997); (2) elongate shape of the Ilavská kotlina Basin; and (3) signs of the compressional to strike-slip tectonic regime in the surrounding regions (Kováč & Hók, 1997; Šimonová & Plašienka, 2011). Such interpretation, however, lacks more solid arguments. The pull-apart nature of Trenčianska kotlina and Ilavská kotlina basins was never proved by structural (e.g. fault slip) or seismic data. There is lack of other strike-slip basin features including (Miall, 2000, p. 518): fault-flank conglomeratic wedges; strata with numerous facies changes; sediments with different stratigraphy; ample evidence of syndepositional tectonics (including intraformational folds and unconformities); offset of basin fill from their source area etc.

The Early Miocene basin was situated above the contact of the upper (continental) ALCAPA (IWECA) microplate and internally of accretionary prism represented by the Flysch Belt (EWECA). The basin represented continuous WSW-ENE oriented (in present coordinates) depositional area from the Vienna Basin, northern Blatné Depression and Bánovská kotlina, Trenčianska kotlina, Ilavská kotlina, Hornonitrianska kotlina, and Turčianska kotlina basins (approx. 100 km long and 40 km wide). It should be noted, that the Lower Miocene sediments are not present in the central part of Western Carpathians east of the Central Slovak fault system and west of the Hornád fault system. Their absence is probably the result of Ottnangian or later erosion (as was proposed in East Slovakian Basin, e.g. Kováč et al., 1995; Baráth & Kováč, 2000). The nature of microfauna and nannoplankton from the studied region confirms earlier assumptions of Salaj & Zlinská (1991) that the Trenčianska kotlina and Ilavská kotlina basins represented uniform open marine basin and not a restricted embayment during the late Eggenburgian. The tectonic classification of this basin is not entirely straightforward as the Lower Miocene sediments between the Vienna and Turčianska kotlina basins overlap various parts of the Western Carpathian orogenic wedge. The large-scale thrusting in the western segment of the Pieniny Klippen Belt gradually ceased during the Early Miocene. The Eggenburgian sediments seemingly seal and overlap the Pieniny Klippen Belt units without any signs of north-vergent thrusting in the studied region. However, the leading edge of the fore-thrusts propagated northward into the Waschberg-Ždánice units of the outer Silesian--Krosno nappes (Jiříček, 1979; Picha et al., 2006; Stráník et al., 2007). The basin was therefore still in the wedge top setting. The Early Miocene subsidence affecting relatively wide region was triggered by orogenic wedge collapse and had only minor strike-slip (transtensional) component. The fault deformation of the Lower Miocene sediments is not well documented, mostly due to poor outcrops, however, occurrences supporting such interpretation are known, e.g. near the Krásna Ves in the Bánovská kotlina Basin (Marko, 2012).

The present shape of Early Miocene basins is a result of disintegration and inversion during the Middle Miocene and later rearrangement of basins and changes in stress regime due to CCW rotation of ALCAPA (Márton et al., 2016). It is thought that the Middle Váh valley formed due to the activity of the NE-SW-striking faults, and was subsequently divided into an array of smaller basins by activity of perpendicular NW-SE-striking faults (e.g. Began et al., 1993; Mello et al., 2011; Ivanička et al., 2011; Pešková et al., 2020). The observed Pliocene–Quaternary features are consistent with the model, as they point out to the preexistence of a wide, NE-SW-trending basin bounded by the faults with the same orientation. The narrowing of the alluvial plain, as well as the increasing dominance of the tributary alluvial fans, and their progradation towards the basin axes, point to the diminishing activity of the marginal faults. Moreover, the subsequent activity of perpendicular faults with NW-SE orientation likely followed, which segmented the primary basin into an array of smaller basins. The perpendicular faults were likely active throughout the Quaternary, as indicated by the relative height perturbations of river terrace levels (Mazúr & Kalaš, 1963a, b; Began et al., 1993; Pešková et al., 2020) The neotectonic map of Maglay et al. (1999) interprets Trenčianska kotlina and Ilavská kotlina basins as Pliocene–Quaternary subsiding regions resulting from the ongoing orogenic collapse. Despite other models, e.g. the Quaternary strike-slip faulting (most recently by Ludwiniak et al., 2019) was proposed, there is no strong evidence to support such an interpretation. Although some streams at the basin margins could be interpreted as deflected or offset streams, no other geomorphological features associated with the strike-slip faults (such as fault-parallel linear throughs, benches, pressure ridges, shutter ridges, or alluvial fan offset) were observed. Also, the marginal faults lack distinct linearity that is typical for an active strike-slip fault. Moreover, the map of the Quaternary sediment thickness (Maglay et al., 2009) reveals a pattern that is not consistent with the typical depocentre distribution in the pull-apart basins. Therefore, in our opinion, there is insufficient evidence to warrant the interpretation of the Trenčianska kotlina and Ilavská kotlina basins as the Quaternary pull-apart basins. Despite some strike-slip component cannot be ruled out, the available evidence points out to the marginal faults with a predominant dip-slip component. In addition, the prevalence of the dissected and propagating alluvial fans, combined with the irregular nature of the basin margins, supports the notion of marginal faults with a diminishing degree of activity, that were later dissected by the younger perpendicular faults.

The problem and gap in our knowledge that persist are the absence of deeper (more than 300 m) borehole which would clarify the sedimentary fill nature of Trenčianska kotlina and Ilavská kotlina basins. Another difficulty that needs to be solved, is the abnormally thick Early Miocene sequence in the central part of the Trenčianska kotlina Basin indicated by the geophysical data (Fig. 4), which could be explained by the presence of Paleogene sediments or other kinds of low resistivity rocks.

## Conclusions

The Neogene sedimentary fill of the Trenčianska kotlina and Ilavská kotlina basins is mostly represented by the following formations (Fig. 4): (a) The Eggenburgian Čausa Formation, divided into 4 lithofacies. (1) The locally preserved continental to brackish claystones and sandstones at the base of the formation. (2) Kľačno Conglomerate Member represented by the continental to littoral carbonate conglomerates with carbonate matrix. (3) Littoral calcareous sandstones to calcarenites often with thick-walled bivalves, *Ophiomorpha* burrows, and conglomerate and claystone interbeds. (4) Pelagic, open marine calcareous claystones with benthic and planktonic foraminiferal fauna and nannoplankton; (b) The Karpatian Závod Formation represented by the marine, brackish and fluvial calcareous silty claystones, present only in the southwest (borehole HVJ-25). (c) The varicoloured polymict gravel with mammal macrofauna indicating late Pliocene (MN15) age.

The Lower Miocene sediments seal the Pieniny Klippen Belt nappe structure. Northwestward thrusting was, however, still active in the Waschberg-Ždánice Unit of the Silesian-Krosno nappes. Minor horizontal and oblique slip deformation was still ongoing at the contact of ALCAPA (IWECA) with its foreland (EWECA) until the final docking with the Bohemian Massif at the Karpatian–early Badenian. The wedge-top basin model is proposed for the Early Miocene (Eggenburgian–Ottnangian) basin subsidence which was triggered by regional orogenic wedge collapse. The wedge top basin represented first evolution stage of the Trenčianska kotlina and Ilavská kotlina basins, which formed one continuous basin with nearby Blatné Depression, Vienna, Bánovská kotlina, Hornonitrianska kotlina and Turčianska kotlina basins.

The second stage is a result of block rotation, inversion, local backthrusting and exhumation of the Považský Inovec Mts., Strážovské vrchy Mts. and Čachtické Karpaty Mts. expressed as disintegration into horst and graben structure of the so-called Core mountains which occurred in multiple phases since the Middle Miocene (mainly Badenian and later). The final (third) stage of inversion occurred in the Pliocene to Quaternary and is responsible for modelling the Trenčianska kotlina and Ilavská kotlina basins in the present shape.

## Acknowledgement

This research was supported by projects of the Ministry of Environment of Slovak Republic no. 11 15-01 Geological map of Biele Karpaty Mts. – northern part at scale 1 : 50 000 and through the Slovak Research and Development Agency under the contracts No. APVV-15-0575, APVV-16-0121, APVV SK-AT-2017-0010. Authors wish to express their gratitude to Assoc. Prof. Jozef Hók and Dr. Alexander Nagy for fruitful discussions and providing the material that improved the manuscript, as well as to reviewers Prof. Michal Kováč and Assoc. Prof. Katarína Holcová for their constructive comments which improved the paper.

## References

Andrusov, D., 1932: O čtvrtohorních terasách Oravy a středního toku Váhu a několik poznámek o geomorfologii západních Karpát slovenských. *Věst. St. geol. Úst. Č. Republ., 8, 244–257.*

Baráth, I. & Kováč, M., 1989: Podmienky sedimentácie a zdrojové oblasti egenburských klastík v západnej časti Západných Karpát. *Miscel. micropaleont., IV., Knih. Zem. Plyn Nafta, 9, 55–86.*

Baráth, I. & Kováč, M., 2000: Miocene sequence stratigraphic key surfaces and depositional system tracts in the Western Carpathian basins (Central Paratethys, Slovakia). *Slovak Geol. Mag., 6, 2–3, 92–94.*

Began, A., Salaj, J., Hanáček, J., Rakús, M., Nemčok, J., Marschalko, R., Gabčo, R., Kalaš, L. & Kullman, E., 1963: Základný geologický výskum a mapovanie v M 1 : 25 000 a 1 : 50 000, spojený s edíciou máp v M – 1 : 50 000 List M-34-97-D Považská Bystrica. *Manuscript. Bratislava, archive SGIDŠ (arch. no. 11454), 1–197.*

Began, A., Hanáček, J., Maglay, J. & Malík, P., 1990: Vysvetlivky ku geologickej mape list 35-142 (Beckov). *Manuscript. Bratislava, archive SGIDŠ (arch. no. 75296), 1–88.*

Began, A., Salaj, J., Horniš, J., Čechová, A. & Szalaiová, V., 1993: Vysvetlivky ku geologickej mape Bielych Karpát 1 : 50 000. Časť bradlové pásmo. Čiastková záverečná správa. Manuscript. *Bratislava, archive SGIDŠ (arch. no. 78506), 1–166.*

Beták, J., 2002: Geomorfologický výskum a mapovanie v oblasti k. ú. Trenčianska Turná. Diploma Thesis. *Manuscript. Bratislava, archive PriF UK.*

Bezák, V., Elečko, M., Fordinál, K., Ivanička, J., Kaličiak, M., Konečný, V., Kováčik, M., Maglay, J., Mello, J., Nagy, A., Polák, M. & Potfaj, M. (eds.), 2008: Prehľadná geologická mapa Slovenskej republiky 1 : 200 000. *Bratislava, Št. Geol. Úst. D. Štúra.*

Biela, A., 1978: Hlboké vrty v zakrytých oblastiach Vnútorných Západných Karpát. *Region. geol. Západ. Karpát, 11, 9–224.*

Buday, T. (ed.), Cicha, I., Paulík, J., Dornič, J., Dvořák, J., Kamenický, J., Maheľ, M., Matějka, A., Salaj, J., Scheibner, E. & Zelman, J., 1963: Geologická mapa ČSSR 1 : 200 000 M-33-XXX Gottwaldov. *Praha, Ústř. Úst. geol.*

Brestenská, E., Marková, M., Franko, O. & Kullmanová, A., 1975: Záverečná správa o vrte DB-15 Horňany v Bánovskej kotline. *Manuscript. Bratislava, archive SGIDŠ (arch. no. 36027), 1–58.*

Čechovič, V., 1959: Geológia treťohorných vrstiev severného okraja Handlovskej uhoľnej panvy. *Geol. Práce, Zoš., 53, 5–58.*

Čechovič, V. & Šínaly, T., 1962: Paleogénne a spodnomiocénne vrstvy vo veľkobani Handlová. *Geol. Práce, Zpr., 25–26, 163–168.*

Čtyroký, P., 1957: Predbežné výsledky makropaleontologického výzkumu sp. miocénu v Považí. *Manuscript. Bratislava, archive SGIDŠ (arch. no. AP 2552), 1–30.*

Čtyroký, P., 1960: Fauna litorálních sedimentů spodního burdigalu z okolí Povážské Bystrice. *Geol. Práce, Zpr., 18, 141–152.*

Danišík, M., Dunkl, I., Putiš, M., Frisch, W. & Kráľ, J., 2004: Tertiary burial and exhumation history of basement highs along the NW margin of the Pannonian basin – an apatite fission track study. *Austrian J. Earth Sci., 95/96, 60–70.*

Fejfar, O. & Heinrich, W. D., 1985: Zur Bedeutung der Wirbeltierfundstätten von Ivanovce und Hajnáčka für die Säugetierpaläontologie in Pliozän und frühen Pleistozän in Europa: Kenntnisstand und Probleme. *Věst. Ústř. Úst. geol., 60, 213–224.*

Fejfar, O. & Sabol, M., 2004: Pliocene Carnivores (Carnivora, Mammalia) from Ivanovce and Hajnáčka (Slovakia). *Cour. Forsch.-Inst. Senckenberg, 246, 15–53.*

Fodor, L., Csontos, L., Bada, G., Györfi, I. & Benkovics, L., 1999: Tertiary tectonic evolution of the Pannonian Basin system and neighbouring orogens: A new synthesis of palaeostress data. In: Durand, B., Jolivet, L., Horváth, F. & Séranne, M. (eds): The Mediterranean Basins: Tertiary Extension within the Alpine Orogen. *London, Geol. Soc., Spec. Publ., 156, 295–334.*

Fordinál, K., Elečko, M., Šimon, L. & Holcová, K., 2001a: Bánovská kotlina Depression (northern part of the Danube Basin); Neogene stratigraphy and geological development. *Slovak Geol. Mag., 7, 3, 289–301.*

Fordinál, K., Šimon, L. & Elečko, M., 2001b: Regionálny geologický výskum neogénnej výplne a podložia Bánovskej kotliny. *Geol. Práce, Spr., 105, 29–37.*

Fusán, O., Biely, A., Ibrmajer, J., Plančár, J. & Rozložník, L., 1987: Podložie terciéru Vnútorných Západných Karpát. *Bratislava, Geol. Úst. D. Štúra, 1–123.*

Gabčo, R., Seneš, J., Lehotayová, R. & Planderová, E., 1963: Zpráva o geologickom mapovaní na liste mapy 1 : 50 000 Považská Bystrica v roku 1962. *Manuscript. Bratislava, archive SGIDŠ (arch. no. AP 4362), 14 p.*

Gašparik, J. (ed.), Halouzka, R., Bujnovský, A., Fojtík, I., Gorek, J., Haško, J., Lexa, J., Miko, O., Polák, M. & Rakús, M., 1993: Geologická mapa Turčianskej kotliny 1 : 50 000. *Bratislava, Geol. Úst. D. Štúra.*

Harangi, S. & Lenkey, L., 2007: Genesis of the Neogene to Quaternary volcanism in the Carpathian-Pannonian region:

Role of subduction, extension, and mantle plume. *Geol. Soc. Amer., 418, 67–90.*

Hók, J., Šimon, L., Kováč, P., Elečko, M., Vass, D., Halmo, J. & Verbich, F., 1995: Tectonics of the Hornonitrianska kotlina depresion in the Neogene. *Geol. Carpath., 46, 4, 191–196.*

Hók, J., Kováč, M., Rakús, M., Kováč, P., Nagy, A., Kováčová--Slamková, M., Sitár, V. & Šujan, M., 1998: Geologic and tectonic evolution of the Turiec depression in the Neogene. *Slovak Geol. Mag., 4, 3, 165–176.*

Hók, J., Kováč, M., Pelech, O., Pešková, I., Vojtko, R. & Králiková, S., 2016: The Alpine tectonic evolution of the Danube Basin and its northern periphery (southwestern Slovakia). *Geol. Carpath., 67, 5, 495–505.*

Hók, J., Pelech, O., Teťák, F., Németh, Z. & Nagy, A., 2019: Outline of the geology of Slovakia (W. Carpathians). *Miner. Slov., 51, 1, 31–60.*

Hromádka, J., 1931: Třídění povrchových tvarů Slovenska na podkladě jejich vývoje. *Sbor. prírodoved. Odb. Slov. vlastived. Muz. (Bratislava), 1924–1931, 4, 28–48.*

Ivanička, J., Havrila, M., Kohút, M. (eds.), Olšavský, M., Hók, J., Kováčik, M., Madarás, J., Polák, M., Rakús, M., Filo, I., Elečko, M., Fordinál, K., Maglay, J., Pristaš, J., Buček, S., Šimon, L., Kubeš, P., Scherer, S. & Zuberec, J., 2007: Geologická mapa Považského Inovca a jv. časti Trenčianskej kotliny, M 1 : 50 000. *Bratislava, Št. Geol. Úst. D. Štúra.*

Ivanička, J., Kohút, M. (eds.), Olšavský, M., Havrila, M., Hók, J., Kováčik, M., Madarás, J., Polák, M., Rakús, M., Filo, I., Elečko, M., Fordinál, K., Maglay, J., Pristaš, J., Buček, S., Šimon, L., Kubeš, P., Scherer, S. & Zuberec, J., 2011: Vysvetlivky ku geologickej mape regiónu Považský Inovec a jv. časť Trenčianskej kotliny, M = 1 : 50 000. *Bratislava, Št. Geol. Úst. D. Štúra, 1–389.*

Jahn, J. J. & Beck, H., 1911: Přehledná geologická a tektonická mapa Moravy a Slezska 1 : 300 000. 1. vyd. *Brno, Komise přírodovědověd. prozk. Moravy.*

Jiříček, R., 1979: Tektogenetický vývoj karpatského oblouku během oligocénu a neogénu. In: Maheľ, M. (ed.): Tektonické profily Západných Karpát. *Bratislava, Geol. Úst. D. Štúra, 203–213.*

Kadlečík, J., Roth, Z. & Stráník, Z., 1980: Hlubinná stavba v oblasti vnějších karpat na Moravě a Západním Slovensku. In: Maheľ, M. (ed.): Vážnejšie problémy geologického vývoja a stavby Československa. Kľúčové územia, metódy a riešenia. *Bratislava, Geol. Úst. D. Štúra, 65–77.*

Kilényi, E. & Šefara, J. (eds.), 1989: Pre-Tertiary basement contour map of the Carpathian Basin beneath Austria, Czechoslovakia and Hungary. *Budapest, ELGI.*

Kováč, M., 2000: Geodynamický, paleogeografický a štruktúrny vývoj karpatsko-panónskeho regiónu v miocéne: nový pohľad na neogénne panvy Slovenska. *Bratislava, Veda, 1–202.*

Kováč, M., Baráth, I. & Holický, I., 1988: Stratigrafická a paleogeografická korelácia vývoja egenburských sedimentov SV časti Malých Karpát, Trnavskej tabule a Považia. Tektonogenéza a paleogeografia Západných Karpát a ich vzťah k ostatným jednotkám. *Manuscript. Bratislava, archive SGIDŠ (arch. no. 69775), 1–227.*

Kováč, M., Šutovská, K., Baráth, I. & Fordinál, K., 1992: Planinské súvrstvie – sedimenty otnansko-spodnokarpatského veku v severnej časti Malých Karpát. *Geol. Práce, Spr., 96, 47–50.*

Kováč, M., Kováč, P., Marko, F., Karoli, S. & Janočko, J., 1995: The East Slovakian Basin – A complex back-arc basin. *Tectonophysics, 252, 453–466.*

Kováč, M., Kráľ, J., Márton, E., Plašienka, D. & Uher, P., 1994: Alpine uplift history of the Central Western Carpathians: geochronological, paleomagnetic, sedimentary and structural data. *Geol. Carpath., 45, 2, 83–96.*

Kováč, M., Plašienka, D., Soták, J., Vojtko, R., Oszczypko, N., Less, G., Ćosović, V., Fügenschuh, B. & Králiková, S., 2016: Paleogene palaeogeography and basin evolution of the Western Carpathians, Northern Pannonian domain and adjoining areas. *Glob. Planet. Change, 140, 9–27.*

Kováč, M., Márton, E., Oszczypko, N., Vojtko, R., Hók, J., Králiková, S., Plašienka, D., Klučiar, T., Hudáčková, N. & Oszczypko-Clowes, M., 2017: Neogene palaeogeography and basin evolution of the Western Carpathians, Northern Pannonian domain and adjoining areas. *Glob. Planet. Change, 155, 133–154.*

Kováč, M., Halásová, E., Hudáčková, N., Holcová, K., Hyžný, M., Jamrich, M. & Ruman, A., 2018: Towards better correlation of the Central Paratethys regional time scale with the standard geological time scale of the Miocene Epoch. *Geol. Carpath., 69, 283–300.*

Kováč, P. & Hók, J., 1996: Tertiary development of the western part of Klippen Belt. *Slovak Geol. Mag., 1, 2, 137–149.*

Králiková, S., Vojtko, R., Hók, J., Fügenschuh, B. & Kováč, M., 2016: Low-temperature constraints on the Alpine thermal evolution of the Western Carpathian basement rock complexes. *J. struct. Geol., 91, 144–160.*

Kysela, J., 1978: Základná inžinierskogeologická mapa 1 : 25 000 list Trenčín. Manuscript. *Bratislava, archive SGIDŠ (arch. no. 41512), 1–55.*

Lexa, J. & Konečný, V., 1998: Geodynamic aspects of the Neogene to Quaternary volcanism. In: Rakús M. (ed.): Geodynamic development of the Western Carpathians. *Bratislava, GS SR, 219–240.*

Lexa, J., Bezák, V., Elečko, M., Mello, J., Polák, M., Potfaj, M. & Vozár, J. (eds.), 2000: Geological map of the Western Carpathians and adjacent areas 1 : 500 000. *Bratislava, Ministry Environ. Slovak Republic, Geol. Surv. Slovak Republic.*

Lóczy, L., Papp, K. & Teleki, P. (eds.), 1922: Geological map of the Hungarian Empire and the adjacent countries. Map, scale: M = 1 : 900 000. *Budapest, Hung. Geograph. Soc.*

Ložek, V. & Tyráček, J., 1960: Příspevek k poznání vývoje údolí Váhu medzi Trenčínem a Piešťany. *Sbor. Čs. Společ. zeměp., 61, 1, 6–14.*

Ludwiniak, M., Śmigielski, M., Kowalczyk, S., Łoziński, M., Czarniecka, U. & Lewińska, L., 2019: The intramontane Orava Basin – evidence of large-scale Miocene to Quaternary sinistral wrenching in the Alpine-Carpathian-Pannonian area. *Acta geol. pol., 69, 339–386.*

Lukniš, M., 1946: Poznámky ku geomorfológii Beckovskej brány a priľahlých území. *Práce Št. geol. Úst., Soš., 15, 5–32.*

Maglay, J. (ed.), Halouzka, R., Baňacký, V., Pristaš, J. & Janočko, J., 1999: Neotektonická mapa Slovenska. *Bratislava, MŽP SR, GS SR.*

Maglay, J., Pristaš, J., Kučera, M. & Ábelová, M., 2009: Geologická mapa kvartéru Slovenska. *Bratislava, Geol. Úst. D. Štúra.*

Maheľ, M., 1985: Geologická stavba Strážovských vrchov. *Bratislava, Geol. Úst. D. Štúra, 1–221.*

Maheľ, M. (ed.), Andrusov, D., Čechovič, V., Kamenický, L., Kuthan, M. & Matějka, A., 1964: Geologická mapa ČSSR 1 : 200 000, M-34-XXV Žilina. *Praha, Ústř. Úst. geol.*

Maheľ, M. (ed.), Kahan, Š., Gross, P., Vaškovský, I. & Salaj, J., 1982: Geologická mapa Strážovských vrchov 1 : 50 000. *Bratislava, Geol. Úst. D. Štúra.*

Marko, F., 2012: Kenozoické napäťové pole a zlomová aktivita severného okraja Dunajskej panvy (Západné Karpaty, Slovensko). *Miner. Slov., 44, 3, 213–230.*

Marko, F., Andriessen, P. A. M., Tomek, Č., Bezák, V., Fojtíková, L., Bošanský, M., Piovarči, M. & Reichwalder, P., 2017: Carpathian Shear Corridor – a strike-slip boundary of an extruded crustal segment. *Tectonophysics, 703–704, 119–134.*

Márton, E., Grabowski, J., Tokarski, A. K. & Túnyi, I., 2016: Palaeomagnetic results from the fold and thrust belt of the Western Carpathians: an overview. In: Pueyo, E. L., Cifelli, F., Sussman, A. J. & Oliva-Urcia, B. (eds.): Palaeomagnetism in Fold and Thrust Belts: New Perspectives. *London, Geol. Soc., Spec. Pub., 425, 7–36.*

Mazúr, E. & Kalaš, L., 1963a: Metódy kvartérnych výskumov na príklade stredného Považia. *Geol. Práce, Zoš., 64, 35–40.*

Mazúr, E. & Kalaš, L., 1963b: Vývoj doliny stredného Váhu v mladom pleistocéne. *Geogr. Čas., 2, 115–131.*

Mazúrová, V., 1972: Príspevok k poznaniu vývoja doliny stredného Váhu v kvartéri. *Geogr. Čas., 24, 1, 31–38.*

Mello, J., Potfaj, M., Teťák, F., Havrila, M., Rakús, M., Buček, S., Filo, I., Nagy, A., Salaj, J., Maglay, J., Pristaš, J. & Fordinál, K., 2005: Geologická mapa Stredného Považia 1 : 50 000. *Bratislava, Št. Geol. Úst. D. Štúra.*

Mello, J. (ed.), Boorová, D., Buček, S., Filo, I., Fordinál, K., Havrila, M., Iglárová, Ľ., Kubeš, P., Liščák, P., Maglay, J., Marcin, D., Nagy, A., Potfaj, M., Rakús, M., Rapant, S., Remšík, A., Salaj, J., Siráňová, Z., Teťák, F., Zuberec, J., Zlinská, A. & Žecová, K., 2011: Vysvetlivky ku geologickej mape Stredného Považia 1 : 50 000. *Bratislava, Št. Geol. Úst. D. Štúra,* 1–378.

Miall, A. D., 2000: Principles of sedimentary basin analysis. 3rd ed. *Berlin – Heidelberg, Springer, 616 p.*

Mišík, M., 1997a: Slovakia. In: Moores, E. M. & Fairbridge, R. W. (eds.): Encyclopedia of European and Asian Regional Geology. *Dodrecht, Springer, 656–664.*

Mišík, M., 1997b: The Slovak part of the Pieniny Klippen Belt after the pioneering works of D. Andrusov. *Geol. Carpath., 48, 4, 209–220.*

Mlynarčík, M., 1998: Kvartér Trenčianskej kotliny a priľahlé mezozoikum, Q-M 038. *Manuscript. Bratislava, archive SGIDŠ (arch. no. 83132), 171 p.*

Nagymarosy, A., 2013: Accretion of ALCAPA Mega-Unit. In: Haas, J. (ed.): Geology of Hungary, Regional Geology Reviews. *Heidelberg, Springer Verlag, 81–102.*

Nemcok, M., Hok, J., Kovac, P., Marko, F., Coward, M. P., Madaras, J., Houghton, J. J. & Bezak, V., 1998: Tertiary extension development and extension / compression interplay in the West Carpathian mountain belt. *Tectonophysics, 290, 137–167.*

Oszczypko-Clowes, M., Oszczypko, N., Piecuch, A., Sotak, J. & Boratyn, J., 2018: The Early Miocene residual flysch basin at the front of the Central Western Carpathians and its palaeogeographic implications (Magura Nappe, Poland). *Geol. Quart., 62, 3, 597–619.*

Pešková, I., Teťák, F., Pelech, O., Sentpetery, M., Olšavský, M., Kováčik, M. & Vlačiky, M., 2020: Geologická mapa regiónu Biele Karpaty – sever v mierke 1 : 50 000. *Manuscript. Bratislava, archive SGIDŠ.*

Picha, F. J., Stráník, Z. & Krejčí, O., 2006: Geology and hydrocarbon resources of the Outer Western Carpathians and their foreland, Czech Republic. In: Golonka, J. & Picha, F. J. (eds.): The Carpathians and their foreland: Geology and hydrocarbon resources. *Tulsa, Amer. Assoc. Petrol. Geol. Mem., 84, 49–175.*

Planderová, E., 1990: Miocene microflora of Slovak Central Paratethys and its biostratigraphical significance. *Bratislava, Geol. Úst. D. Štúra, 1–137.*

Plašienka, D., 2018a: Continuity and episodicity in the early Alpine tectonic evolution of the Western Carpathians: How large-scale processes are expressed by the orogenic architecture and rock record data. *Tectonics, 37, 7, 2029–2079.*

Plašienka, D., 2018b: The Carpathian Klippen Belt and types of its klippen – an attempt at a genetic classification. *Miner. Slov., 50, 1, 1–24.*

Plašienka, D. & Soták, J., 2015: Evolution of Late Cretaceous--Palaeogene synorogenic basins in the Pieniny Klippen Belt and adjacent zones (Western Carpathians, Slovakia): Tectonic controls over a growing orogenic wedge. *Ann. Soc. geol. Pol., 85, 43–76.*

Plašienka, D., Bučová, J. & Šimonová, V., 2020: Variable structural styles and tectonic evolution of an ancient backstop boundary: the Pieniny Klippen Belt of the Western Carpathians. *Int. J. Earth Sci. (Geol. Rdsch.), 109, 1355–1376.*

Poprawa, D. & Nemčok, J. (eds.), 1988: Geological atlas of the Western Carpathians and their foreland 1 : 500,000. *Warszawa, Panstw. Inst. Geol., 9 p.*

Pospíšil, Z., Chrobok, J., Loupanec, M., Mašek, F., Novák, P. & Plesník, K., 1971: Zpráva o výpočte zásob podzemných vôd kvartéru stredného toku Váhu. Manuscript. *Bratislava, archive SGIDŠ (arch. no. 25459),1–184.*

Potfaj, M., 2005: Textové vysvetlivky k účelovej geologickej mape. Súbor regionálnych máp geologických faktorov životného prostredia regiónu Myjavská pahorkatina a Biele Karpaty. *Manuscript. Bratislava, archive SGIDŠ (arch. no. 86620), 1–35.*

Potfaj, M., Teťák, F. (eds.), Havrila, M., Filo, I., Pešková, I., Olšavský, M. & Vlačiky, M., 2014: Geologická mapa Bielych Karpát (južná časť) a Myjavskej pahorkatiny v mierke 1 : 50 000. *Bratislava, Št. Geol. Úst. D. Štúra.*

Pristaš, J. (ed.), Elečko, M., Maglay, J., Fordinál, K., Šimon, L., Gross, P., Polák, M., Havrila, M., Ivanička, J., Határ, J., Vozár, J., Mello, J. & Nagy, A., 2000: Geologická mapa Podunajskej nížiny – Nitrianskej pahorkatiny 1 : 50 000. *Bratislava, Št. Geol. Úst. D. Štúra.*

Rakús, M., Mišík, M., Michalík, J., Mock, R., Ďurkovič, T., Koráb, T., Marschalko, R., Mello, J., Polák, M. & Jablonský, J., 1988: Paleogeographic Development of the West Carpathians: Anisian to Oligocene. In: Rakús, M., Dercourt, J. & Nairn, A. E. M. (eds.): Evolution of the Northern Margin of Tethys, Vol. III. *Mém. Soc. géol. France (Paris), Nouv. Ser., 154, 11, 39–62.*

Rybár, S., Halásová, E., Hudáčková, N., Kováč, M., Kováčová, M., Šarinová, K. & Šujan, M., 2015: Biostratigraphy, sedimentology and paleoenvironments of the northern Danube Basin: Ratkovce 1 well case study. *Geol. Carpath.,* 66, 51–67.

Salaj, J., 1988: Geologická štúdia širšieho okolia Považskej Bystrice. *Manuscript. Bratislava, archive SGIDŠ (arch. no. 66756), 1–51.*

Salaj, J., Began, A., Horniš, J., Nagy, A., Modlitba, I., Iglárová, Ľ., Remšík, A. & Vozárová, A., 1989: Vysvetlivky ku geologickej mape 24-441 (Považská Bystica). *Manuscript. Bratislava, archive SGIDŠ (arch. no. 70510), 1–112.*

Salaj, J. & Zlinská, A., 1991: Spodnomiocénne sedimenty slienitej fácie od Považskej Teplej. *Miner. Slov., 23, 2, 173–178.*

Salaj, J., 1995: Geológia Stredného Považia. Bradlové a pribradlové pásmo so súľovským paleogénom a mezozoikom severnej časti Strážovských vrchov – 2. časť. *Zem. Plyn Nafta, 39, 4, 297–395.*

Samuel, O. (ed.), Biely, A., Eliáš, M., Fusán, O., Jablonský, J., Ložek, V. & Michalík, J., 1988: Stratigrafických slovník Západných Karpát 3. *Bratislava, Geol. Úst. D. Štúra, 1–292.*

Schmid, S. M., Fügenschuh, B., Kounov, A., Matenco, L., Nievergelt, P., Oberhänsli R., Pleuger, J., Schefer, S., Schuster, R., Tomljenović, B., Ustaszewski, K. & van Hinsbergen, D. J. J., 2020: Tectonic units of the Alpine collision zone between Eastern Alps and western Turkey. *Gond. Res., 78, 308 – 374.*

Seneš, J., 1960: Burdigalská fauna v slienitých sedimentoch Považia. *Geol. Práce, Zpr., 17, 105–114.*

Soták, J., Pereszlenyi, M., Marschalko, R., Milička, J. & Starek, D., 2001: Sedimentology and hydrocarbon habitat of the submarine-fan deposits of the Central Carpathian Paleogene Basin (NE Slovakia). *Mar. Petrol. Geol., 18, 87–114.*

Steininger, F. F. & Seneš, J., 1971: M1 – Eggenburgien. Chronostratigraphie und Neostratotypen. *Bratislava, Veda, 827 p.*

Stráník, Z., Hrouda, F., Otava, J., Gilíková, H. & Švábenická, L., 2007: The Upper Oligocene – Lower Miocene Krosno lithofacies in the Carpathian Flysch Belt (Czech Republic): sedimentology, provenance and magnetic fabrics. *Geol. Carpath., 58, 4, 321–332.*

Šalagová, V., Tyleček, B. & Drahoš, M., 1990: Ilavská kotlina – kvartér a neogén. *Manuscript. Bratislava, archive SGIDŠ (arch. no. 87965), 1–118.*

Ślączka, A., Krugłov, S., Golonka, J., Oszczypko, N. & Popadyuk, I., 2006: Geology and hydrocarbon resources of the Outer Carpathians, Poland, Slovakia, and Ukraine: General geology. In: Golonka, J. & Picha, F. J. (eds.): The Carpathians and their foreland: Geology and hydrocarbon resources. *Tulsa, Amer. Assoc. Petrol. Geol. Mem., 84, 221–258.*

Šimonová, V. & Plašienka, D., 2011: Kinematická a paleonapäťová analýza zlomov v butkovskom lome (manínska jednotka, Západné Karpaty). *Acta Geol. Slov., 3, 1, 21–31.*

Teťák, F. & Potfaj (eds.), M., Havrila, M., Filo, I., Pešková, I., Boorová, D., Žecová, K., Laurinc, D., Olšavský, M., Siráňová, Z., Buček, S., Kucharič, Ľ., Gluch, A., Šoltés, S., Pažická, A., Iglárová, Ľ., Liščák, P., Malík, P., Fordinál, K., Vlačiky, M. & Köhler, E., 2015: Vysvetlivky ku geologickej mape Bielych Karpát (južná časť) a Myjavskej pahorkatiny v mierke 1 : 50 000. *Bratislava, Št. Geol. Úst. D. Štúra, 1–306.*

Teťák, F., 2017: Neogene sediments between Podbranč and Hradište pod Vrátnom, Vienna Basin. *Acta Geol. Slov., 9, 1, 1–14.*

Uhlig, V., 1903: Bau und Bild der Karpaten. In: Diener, K., Hoernes, R., Suess, F. E. & Uhlig, V. (eds.): Bau und Bild der Österreichs. *Wien – Leipzig, Verlag F. Tempsky, Verlag G. Greytag, 651–911.*

Vass, D., 2002: Litostratigrafia Západných Karpát: neogén a budínsky paleogén. *Bratislava, Št. Geol. Úst. D. Štúra, 1–202.*

Vass, D., Kováč, M., Konečný, V. & Lexa, J., 1988: Molasse basins and volcanic activity in West Carpathian Neogene: Its evolution and geodynamic character. *Geol. Zbor. Geol. carpath., 39, 5, 539–561.*

Vass, D., Elečko, M. & Fordinál, K., 2002: Závada – Bielice Rise – a buried elevation between Bánovce and Rišňovce Depressions in the Danube Basin. *Slovak Geol. Mag., 8, 1, 13–20.*

Vozár, J., Šantavý, J. (eds.), Potfaj, M., Szalaiová, V., Scholtz, P., Tomek, Č., Šefara, J., Machková, N., Gnojek, I., Šály, B., Pereszlényi, M., Hrušecký, I., Hlavatý, I., Jureňa, V., Rudinec, R., Magyar, J. & Slávik, M., 1999: Atlas hlbinných reflexných seizmických profilov Západných Karpát a ich interpretácia. *Bratislava, GS SR, 1–76.*

Vrana, K., Fendek, M., Panáček, A., Drexler, V., Szalaiová, V. & Reháková, D., 2009: Geotermálny vrt GZV-1 Nové Mesto nad Váhom – Zelená voda. Záverečná správa geologickej úlohy. *Manuscript. Bratislava, archive SGIDŠ (arch. no. 89661), 1–90.*

Zaťko, M., Mičian, Ľ., Škvarček, A., Zatkalík, F., Minár, J., Brnka, K., Machová, Z. & Krajčovičová, Ľ., 1988: Svahové deformácie a geomorfologické pomery v časti Bielych Karpát a Trenčianskej kotliny v oblasti Bošáca – Záblatie. *Manuscript. Bratislava, archive SGIDŠ (arch. no. 75451_19), 1–123.*

Zbořil, L., Halmešová, S., Nromec, J., Král, M., Kurkin, M., Puchnerová, M., Stránska, M. & Hladík, P., 1984: Trenčianska kotlina – Piešťanská priehlbeň. *Manuscript. Bratislava, archive SGIDŠ (arch. no. 59631), 1–54.*

**Tab. 2**
Nannoplankton alphabetical faunal list. For sample localization see Tab. 1.

| | Locality | | |
|---|---|---|---|
| **Species** | **1** | **2** | **3** |
| *Arkhangelskiella cymbiformis* Vekshina | x | | x |
| *Biscutum constans* (Górka) Black in Black & Barnes | | | x |
| *Broinsonia* sp. Bukry | | x | |
| *Calcidiscus leptoporus* (Murray & Blackman) Loeblich & Tappan | | | x |
| *Calcidiscus* sp. Kamptner | | | x |
| *Calculites obscurus* (Deflandre) Prins & Sissingh in Sissingh | | | x |
| *Clausicoccus fenestratus* (Deflandre & Fert) Prins | | | x |
| *Coccolithus formosus* (Kamptner) Wise | | x | x |
| *Coccolithus eopelagicus* (Bramlette & Riedel) Hay, Mohler & Wade | | x | |
| *Coccolithus pelagicus* (Wallich) Schiller | x | x | x |
| *Coronocyclus nitescens* (Kamptner) Bramlette & Wilcoxon | | | x |
| *Cribrosphaerella ehrenbergii* (Arkhangelsky) Deflandre in Piveteau | | x | x |
| *Cyclagelosphaera margereliii* Noël | | | x |
| *Cyclicargolithus abisectus* (Muller) Wise | | x | x |
| *Cyclicargolithus floridanus* (Roth & Hay, in Hay et al.) Bukry | x | x | x |
| *Discoaster* sp. Tan | x | | x |
| *Discoster deflandrei* Bramlette & Riedel | | x | |
| *Discoaster lodoensis* Bramlette & Riedel | | x | |
| *Discoaster multiradiatus* Bramlette & Riedel | | x | |
| *Discoaster nodifer* (Bramlette & Riedel) Bukry | | x | |
| *Eiffellithus eximius* (Stover) Perch-Nielsen | | | |
| *Eiffellithus turriseiffelii* (Deflandre in Deflandre & Fert) Reinhardt | | | x |
| *Ellipsolithus distichus* (Bramlette & Sullivan) Sullivan | | | x |
| *Ellipsolithus macellus* (Bramlette & Sullivan) Sullivan | | | x |
| *Fasciculithus* sp. Bramlette & Sullivan | | | x |
| *Fasciculithus tympaniformis* Hay & Mohler in Hay et al. | | x | |
| *Helicolithus trabeculatus* (Górka) Verbeek | | | x |
| *Helicosphaera* sp. Kamptner | x | | |
| *Helicosphaera ampliaperta* Bramlette & Wilcoxon | | x | x |
| *Helicosphaera* cf. *ampliaperta* Bramlette & Wilcoxon | x | | |
| *Helicosphaera bramlettei* (Müller) Jafar & Martini | | x | |
| *Helicosphaera carteri* (Wallich) Kamptner | x | | x |
| *Helicosphaera compacta* Bramlette & Wilcoxon | x | x | |
| *Helicosphaera recta* (Haq) Jafar & Martini | | x | |
| *Helicosphaera* cf. *scissura* Miller | x | | |
| *Helicosphaera scissura* Miller | | x | |
| *Helicosphaera seminulum* Bramlette & Sullivan | x | x | |
| *Holodiscolithus macroporus* (Deflandre, in Deflandre & Fert) Roth | | | x |
| *Chiasmolithus* sp. Hay et al. | | | x |
| *Lucianorhabdus maleformis* Reinhardt | x | | |
| *Lanternithus minutus* Stradner | | | x |
| *Manivitella pemmatoidea* (Deflandre in Manivit) Thierstein | | | x |
| *Markalius inversus* (Deflandre) Bramlette & Martini | x | x | |
| *Micrantholithus* sp. Deflandre in Deflandre & Fert | | | x |
| *Micula staurophora* (Gardet) Stradner | x | | x |
| *Neochiastozygus* sp. Perch-Nielsen | | | x |
| *Neococcolithes dubius* (Deflandre) Black | | x | |
| *Owenia hillii* Crux | | | x |
| *Pemma* sp. Klumpp | | | x |
| *Pontosphaera* sp. Lohmann | | | x |
| *Pontosphaera alta* Roth | | x | |
| *Pontosphaera duocava* (Bramlette & Sullivan) Romein | | x | x |
| *Pontosphaera enormis* (Locker) Perch-Nielsen | | | |
| *Pontosphaera latelliptica* (Báldi-Beke, in Báldi-Beke & Báldi) Perch-Nielsen | | | x |
| *Pontosphaera latoculata* (Bukry & Percival) Perch-Nielsen | x | x | |
| *Pontosphaera multipora* (Kamptner ex Deflandre in Deflandre & Fert) Roth | | x | x |
| *Pontosphaera pulcheroides* (Sullivan) Romein | | | x |
| *Pontosphaera pulchripora* (Reinhardt) Aubry | | | |
| *Pontosphaera punctosa* (Bramlette & Sullivan) Perch-Nielsen | x | | |

**Tab. 2** – continuation

| | Locality | | |
|---|---|---|---|
| **Species** | **1** | **2** | **3** |
| *Prediscosphaera cretacea* (Arkhangelsky) Gartner | | x | x |
| *Prinsius* sp. Hay & Mohler | x | | |
| *Retecapsa* sp. Black | x | | |
| *Retecapsa crenulata* (Bramlette & Martini) Grün in Grün & Allemann | | x | x |
| *Retecapsa ficula* (Stover) Burnet | | x | |
| *Reticulofenestra* sp. Hay, Mohler & Wade | x | | x |
| *Reticulofenestra bisecta* (Hay, Mohler & Wade) Roth | x | x | x |
| *Reticulofenestra daviesii* (Haq) Haq | x | x | |
| *Reticulofenestra dictyoda* (Deflandre) Stradner | x | x | |
| *Reticulofenestra excavata* Lehotayová | | | x |
| *Reticulofenestra haqii* Backman | | | x |
| *Reticulofenestra lockeri* Müller | x | x | x |
| *Reticulofenestra minuta* Roth | | | x |
| *Reticulofenestra ornata* Müller | x | x | x |
| *Reticulofenestra reticulata* (Gartner & Smith) Roth & Thierstein | | x | x |
| *Reticulofenestra stavensis* (Levin & Joerger) Varol | | x | x |
| *Reticulofenestra umbilicus* (Levin) Martini & Ritzkowski | x | x | x |
| *Reticulofenestra wadae* Bown | | x | |
| *Rhagodiscus* sp. Reinhardt | | | x |
| *Sphenolithus belemnos* Bramlette & Wilcoxon | | | x |
| *Sphenolithus moriformis* (Bronnimann & Stradner) Bramlette & Wilcoxon | | x | x |
| *Syracosphaera* sp. Lohmann | | | x |
| *Thoracosphaera* sp. Kamptner | | | x |
| *Toweius* sp. Hay & Mohler | | | x |
| *Toweius crassus* Bramlette & Sullivan | | x | |
| *Toweius gammation* (Bramlette & Sullivan) Romein | | | x |
| *Tranolithus minimus* (Bukry) Perch-Nielsen | | | x |
| *Tribrachiatus orthostylus* Shamrai | | x | x |
| *Triquetrorhabdulus carinatus* Martini | | | x |
| *Umbilicosphaera rotula* (Kamptner) Varol | | | x |
| *Watznaueria barnesiae* (Black in Black & Barnes) Perch-Nielsen | x | x | x |
| *Watznaueria britannica* (Stradner) Reinhardt | x | | |
| *Zeugrhabdotus* sp. Reinhardt | | x | x |
| *Zeugrhabdotus bicrescenticus* (Stover) Burnet | x | | |
| *Zeugrhabdotus embergeri* (Noël) Perch-Nielsen | x | | x |
| *Zygrhablithus bijugatus* (Deflandre in Deflandre & Fert) Deflandre | | x | x |

**Tab. 3**

Foraminifers alphabetical faunal list. For sample localization see Tab. 1. (*) marks thin section samples.

| | Locality | | | |
|---|---|---|---|---|
| **Species** | **1** | **3** | **4*** | **6*** |
| *Ammonia* cf. beccari (Linne) | | | x | |
| *Bolivina hebes* Macfad. | x | | | |
| *Bulimina schischkinskaye* (Samoilova) | | x | | |
| *Cibicidoides* sp. | | x | x | |
| *Cibicidoides ungerianus* (Orb.) | x | | | |
| *Globigerina* sp. | | x | | |
| *Globigerina ciperoensis* Bolli | x | x | | |
| *Globigerina ottnangiensis* Roegl | x | | | |
| *Globigerina praebulloides* Blow | x | | | |
| *Globigerinoides trilobus* (Rss.) | | x | | |
| *Globoturborotalita ouachitaensis* (Howe & Wallace) | | x | | |
| *Hanzawaia boueana* (Orb.) | x | | | |
| *Heterolepa dutemplei* (Orb.) | | x | | |
| *Lenticulina melvilli* (Cush. & Renz) | | x | | |
| *Melonis pompilioides* (Fichtel & Moll) | | x | | |
| *Pullenia bulloides* (Orb.) | x | x | | |
| *Quinqueloculina* sp. | | | x | |

**Tab. 3** – continuation

| | Locality | | | |
|---|---|---|---|---|
| **Species** | **1** | **3** | **4*** | **6*** |
| *Semivulvulina* sp. | | | | x |
| *Stilostomella* sp. | | x | | |
| *Tenuitellinata angustiumbilicata* (Bolli) | x | | | |
| *Textularia* sp. | | | | x |
| *Textularia gramen* Orb. | | x | | |
| *Turborotalita quinqueloba* (Natland) | | x | | |
| *Uvigerina* cf. *vicksburgensis* Cush. & Ellisor | | x | | |
| *Valvulineria complanata* (Orb.) | | x | | |
| * Thin-section samples | | | | |

# Trenčianska kotlina a Ilavská kotlina – zvyšky invertovanej nesenej spodnomiocénnej panvy

Trenčianska kotlina a Ilavská kotlina predstavujú erózne relikty spodnomiocénnej panvy nachádzajúcej sa na rozhraní Vonkajších Západných Karpát a Vnútorných Západaných Karpát (sensu Hók et al., 2019; obr. 1 a 2) a prekrývajú celky karpatského bradlového pásma a vnútrokarpatských mezozoických príkrovov (tatrikum, fatrikum a hronikum). Výskum sa opiera o výsledky geologického mapovania v severozápadnej časti Trenčianskej kotliny a najzápadnejšej časti Ilavskej kotliny a sumarizuje doterajšie (bio)stratigrafické, sedimentologické, geofyzikálne a vrtné údaje (vrty PB-1 a HVJ-25; obr. 4 a 10) zo širšieho regiónu. Sedimentárna výplň paniev pozostáva z egenburských klastík čausianskeho, karpatského a závodského súvrstvia a mladších pliocénnych a kvartérnych fluviálnych a eolických uložením (obr. 4). Sedimenty pelitickej litofácie čausianskeho súvrstvia vystupujú priamo pod kvartérnymi sedimentmi na viacerých miestach. Ide o šíromorské sedimenty, čo dokladá prítomnosť nanoplanktónu (obr. 8, tab. 2) a foraminifer (tab. 3; Salaj a Zlinská, 1991). Spodnomiocénne sedimenty transgresívne a diskordantne prekrývajú staršiu príkrovovú stavbu bradlového pásma. Prítomnosť sedimentov otnanského veku sa nepodarilo uspokojivo potvrdiť. Je pravdepodobné, že v panve pôvodne mohli byť prítomné, ale dnes sú odstránené eróziou (napr. Salaj a Zlinská, 1991). Celková hrúbka miocénnej výplne Trenčianskej kotliny dosahuje v jej centrálnej časti asi 1 000 m (obr. 3), v Ilavskej kotline sa pohybuje okolo 250 m (Kilény a Šefara, 1989). Presné poznatky o ich najhlbších častiach a predkenozoickom podloží nie sú známe pre chýbajúce vrty v ich centrálnych depresiách. Výsledky výskumu naznačujú, že Trenčianska kotlina a Ilavská kotlina pôvodne tvorili súčasť väčšieho spodnomiocénneho sedimentačného bazénu typu nadklinovej panvy, ktorá siahala zo severu Viedenskej panvy cez blatniansku priehlbinu do Bánovskej kotliny, Hornonitrianskej kotliny a Turčianskej kotliny. Pôvodná stavba bola dezintegrovaná inverziou, rotáciou blokov, spätným nasúvaním a výzdvihom okolitých pohorí (Kováč et al., 1994; Danišík et al., 2004; Marko et al., 2017), ktoré prebiehali v karpate až strednom miocéne. Inverzia v pliocéne až kvartéri mala za následok modelovanie kotlín do dnešnej podoby. Neexistujú žiadne presvedčivé argumenty na interpretáciu týchto kotlín ako paniev typu pull-apart, ako sa uvažovalo v minulosti, i keď šikmá (transtenzia) až horizontálna deformácia mohla v malej miere ich vývoj ovplyvniť.

Doručené / Received: 26. 3. 2020
Prijaté na publikovanie / Accepted: 11. 8. 2020

*Mineralia Slovaca, Web ISSN 1338-3523, ISSN 0369-2086*
*52, 1 (2020), 23 – 32,* 

# Main geological and mineralogical characteristics of the Cajálbana lateritic deposit, Pinar del Río, Cuba

JUAN RUIZ QUINTANA[1], GERARDO ANTONIO OROZCO MELGAR[2], ALAIN CARBALLO PEÑA[2] and KENYA ELVIRA NÚÑEZ CAMBRA[3]

[1]Ministerio de Energía y Minas, Salvador Allende No. 666, La Habana, Cuba, CP: 10300. jruiz@minem.gob.cu
[2]Universidad de Moa, Avenida Calixto García Iñiguez #15 entre Av. 7 de Diciembre y Calle Reynaldo Laffita Rueda, Reparto Caribe, Moa, Holguín, Cuba, CP: 83330; gorozco@ismm.edu.cu; acarballo@ismm.edu.cu
[3]Instituto de Geología y Paleontología, Calle Vía Blanca No. 1002. San Miguel del Padrón, La Habana, Cuba. CP 11000; kenya@igp.minem.cu

**Abstract:** This paper submits the main geological and mineralogical characteristics of the Cajálbana lateritic deposit located in Pinar del Río, Cuba, a perspective deposit for the Cuban nickel industry. Presented study took into account altogether 470 samples from 80 vertical boreholes. The contents of principal elements and compounds of Fe, Ni, Co, Mn, $SiO_2$, $Al_2O_3$, MgO and $Cr_2O_3$ were determined by the Inductively Coupled Plasma (ICP) method. The results of geological field research, combined with mineralogical and geophysical previous investigations, have revealed that the serpentinized pyroxene peridotites with increased iron, nickel and chrome contents represent the primary source of Ni and Fe mineralization in laterites of the Cajálbana deposit.

**Key words:** lateritic deposit, peridotite, serpentinite, Cajálbana

**Graphical abstract**

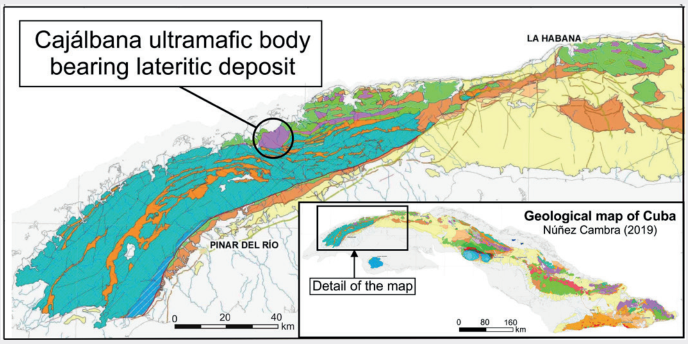


**Highlights**

- Paper informs about regional geology, ancient exploration and new research methodology applied in the Cajálbana lateritic deposit including processing and evaluation of mineralogical and geochemical data.
- Positive results obtained improve nickel reserves in Cuba and may contribute to beneficial mining in the Cajálbana locality.

## Introduction

Lateritic deposits worldwide are of importance, as they are the source of 59 % of primary nickel (Nickel Institute, 2017). In Cuba, lateritic deposits, associated with nickel and iron-bearing weathering crusts, occur in several regions. They have been studied for more than sixty years from geological and technological points of view due to their importance for the Cuban nickel industry, producing one of the main goods of the Cuban economy (Ruiz Quintana, 2016). Because the deposits currently exploited in the eastern part of the country will be gradually exhausted, it is essential to assure their replacement by new ones to sustain nickel production. This is the reason of increased research of the deposits in the western regions of Cuba such as the Cajálbana lateritic deposit in the Pinar del Río province.

## History of exploration in cajálbana area

First exploration for nickel in the Cajálbana serpentinite massif was committed by the American company *Cuban Iron* in 1939–1943. This exploration covered the western part of the area with lateritic weathering crust present *in situ*, as well as its redeposited occurrences, located north of the province of Pinar del Río (Commercial Caribbean Nickel, 2009) in the Sierra del Rosario of La Palma municipality (GeoCuba, 2002; Figs. 1–3).

The works of the Soviet geologist Ogarkov (e.g. Ogarkov, 1970) stand out by the *limonite* ore resources calculation in this Cuban mineral deposit, using earlier data of the *Cuban Iron* Company.

Other investigations in this area are related to exploration of ferruginous minerals for the use in metallurgical industry (Yujvit et al., 1966), or as an iron corrector at cement production (Gómez, 1988). Research was limited to study the upper part of the vertical lateritic profile with high iron content (zone of the unstructured ochre with pellets – iron concretions – OICP) and redeposited laterites to the area at the edges of the Cajálbana serpentine massif. This research did not contribute new knowledge of their ores.

Following geological research in the Cajálbana massif and its surroundings aimed to evaluate the nickel and iron potential (Carmona, 1995), as well as precious metals (Martín et al., 1998). This investigation improved existing geological data, by applying fieldwork and interpretation of geophysical and relief maps.

The *Geominera Oriente* Company developed the most recent works in the period 2008–2009 (Cardoso Velázquez et al., 2018), retrieved by *Commercial Caribbean Nickel* (project in 2009; see reference), constituting the basis of our investigation.

Other researchers have managed to generalize the geological information related to the formation of chromite deposits, associated with ophiolites, as well as their quantitative evaluation, modeling and estimation of possible new deposits (Díaz et al., 1987).

Concerning the volume of reserves, it is generally considered that the most important genetic type for Cuba is that having the lateritic-saprolitical vertical profile (Ariosa Iznaga et al., 2003). Cajálbana mineral deposit belongs into this group also.

For the studies of Cajálbana mineral deposit, the geophysical methods such as magnetic susceptibility have been also used for estimating the weathering crust mineral quality (Hernández Ramsay, 2018).

Therefore, the fundamental objective of this work is to present main geological and mineralogical characteristics of the Cajálbana lateritic mineral deposit for possible metallurgical use, taking advantage of the technologies recently used by the Cuban nickel industry (Ruiz Quintana, 2016; Figs.1–4).

The working hypothesis of this research states that, depending on the physical, chemical and mineralogical characteristics of the Cajálbana mineral deposit, the decision on its possible industrial use can be made.

## Geological setting of the Cajálbana deposit

The western part of Cuba is framed by the Guaniguanico Terrain with Cangre metamorphic belt, both representing the Mesozoic basement, as well as by the zone of **Mesozoic ophiolitic assemblage**, encompassing also the remnants of the **Cretaceous volcanic arc** (Fig. 2). Part of ophiolites is the **Cajálbana ultramafic body**, which perspective Ni/Fe mineralization was investigated and the results are presented in this study. Due to the Paleocene-Eocene convergence of oceanic crust on Mesozoic basement


**Fig. 1.** Exploration in the Cajálbana laterite deposit. 1 – Drilling facility UGB-50 with drilling capacity up to 100 m with spiral drilling and 65 mm of diameter, 2–3 – Cajálbana area is typical with red lateritic soil and contains traces after exploration works, 4 – complementary drilling for *limonitic* ore applying the Atlas Copco portable drill.

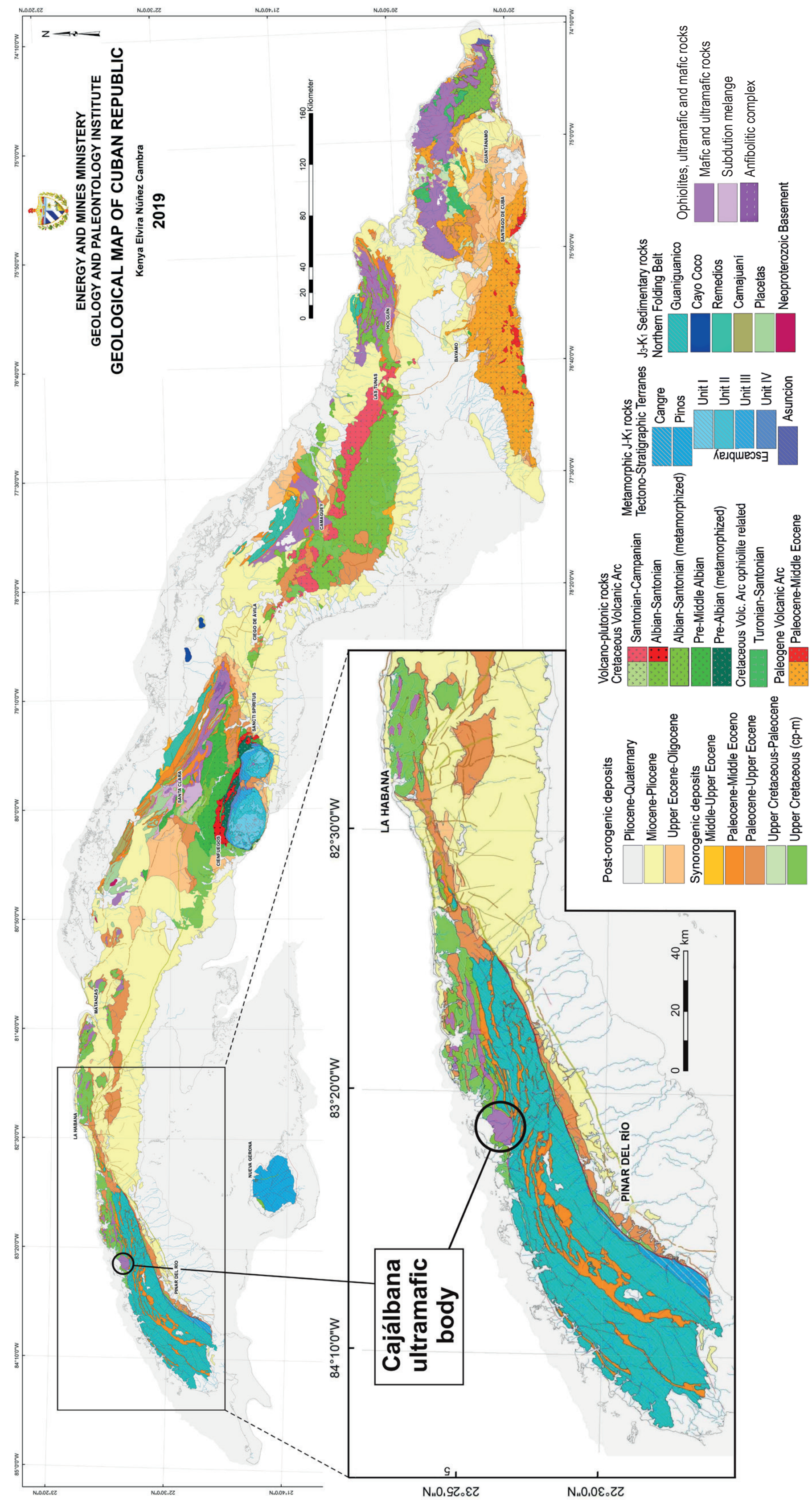


**Fig. 2.** Geological map of Cuba (taken after Núñez Cambra, 2019).

(Pardo, 2009; Núñez Cambra, 2019), the Paleogene sequences are folded and faulted and the post-obduction cover is represented by Late Eocene-Quaternary sediments. The ultramafic ophiolitic sequences after exhumation and obduction underwent lateritic weathering and became a source of economic Ni mineralization, contributing to Cuban raw material potential.

The **Cajálbana ophiolites** of the northern belt of Cuba crop out in a series of elongated bodies between localities of Baracoa to the east and Cajálbana to the west. The deformed tabular bodies of ophiolites, sometimes thick up to 6 km, were during their placement intermixed with tectonic slices of Cretaceous volcanic arc. Currently, the Cajálbana ophiolites lie in a tectonic position on sequences of the Sierra de Guaniguanico and are covered with tectonic slices of volcanites of the Bahía Honda Formation. This situation is best observable south of the Guaniguanico area in the Sierra del Rosario (Commercial Caribbean Nickel, 2009).

The Cajálbana deposit represents part of the ferro-nickeliferous crusts of the Cajálbana ultrabasic massif, which is located in the province of Pinar del Río, 13 and 38 km from the towns of La Palma to the West and Bahía Honda to the East respectively and 70 km from the city of Pinar del Río to the SW – the provincial capital (Oficina Nacional de Recursos Minerales, 2018).

### *Tectonites of peridotites*

In the Cajálbana massif, the peridotite complex has a depleted lherzolite character and distinct foliation produced by convergent processes. The lineation predominantly trends to the north and is well observable in the field. Under the microscope, a strong preferred orientation of the olivine was revealed, which indicates an intense high-temperature ductile deformation. The deformation inventory includes also pull-apart microstructures, undulose extinction in olivine, lamellae solution of clinopyroxenes in orthopyroxenes, kink band boundaries, etc. According to Fonseca (1989) the peridotites and their serpentinite equivalents exhibit a primitive and relatively uniform composition of their main metals.

In the Cajálbana area all contacts of peridotites with underlying and surrounding geological units are tectonic – the boundary is represented either by their thrust plane or vertical faults. The area is penetrated with two main fault systems trending generally NE-SW and NW-SE (Fig. 4). They influence the courses of some rivers, which is verified through geological criteria such as the alignment of the river beds and is visible also in the digital model of the relief. Subordinate to and associated with main faults, a system of lower-order faults was observed. The local cracks in the outcrop scale are filled with calcium and

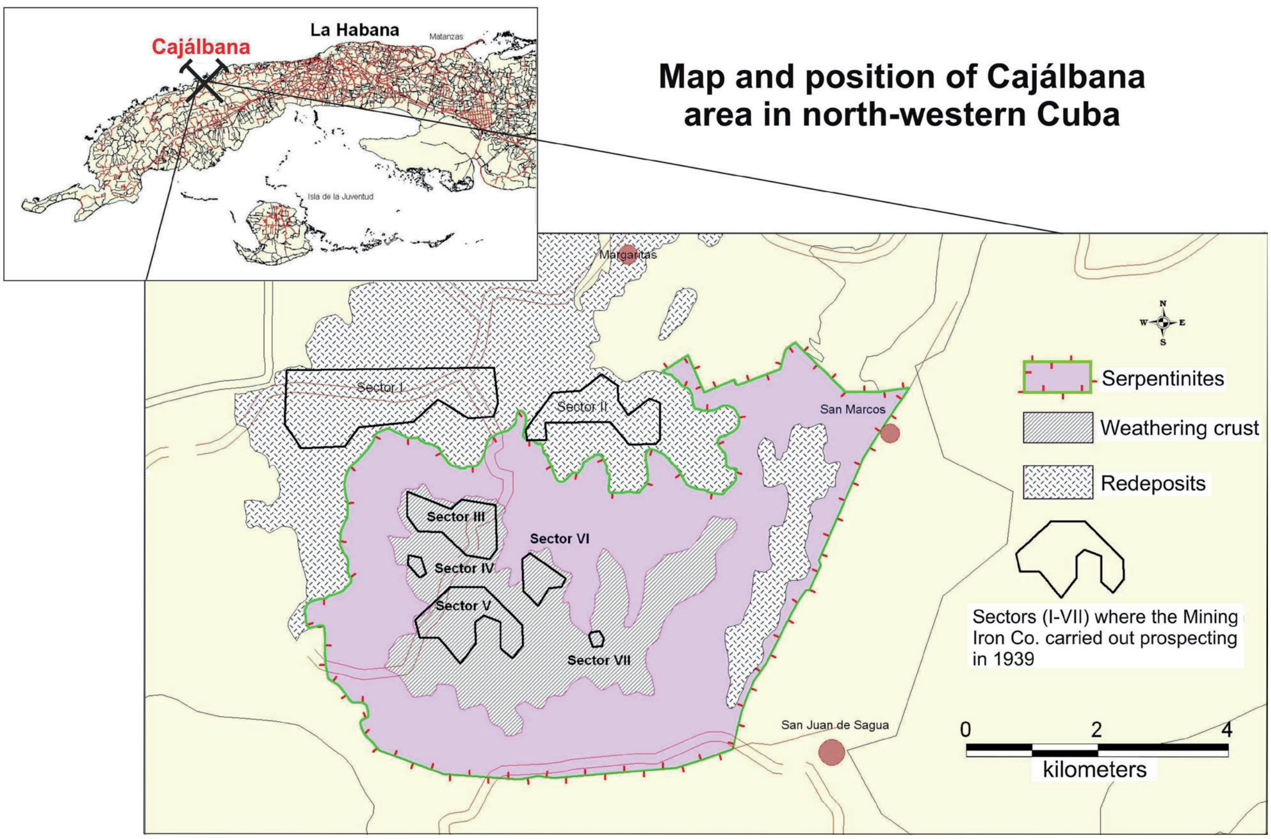


**Fig. 3.** Geographical location of Cajálbana (Oficina Nacional de Recursos Minerales, 2018).

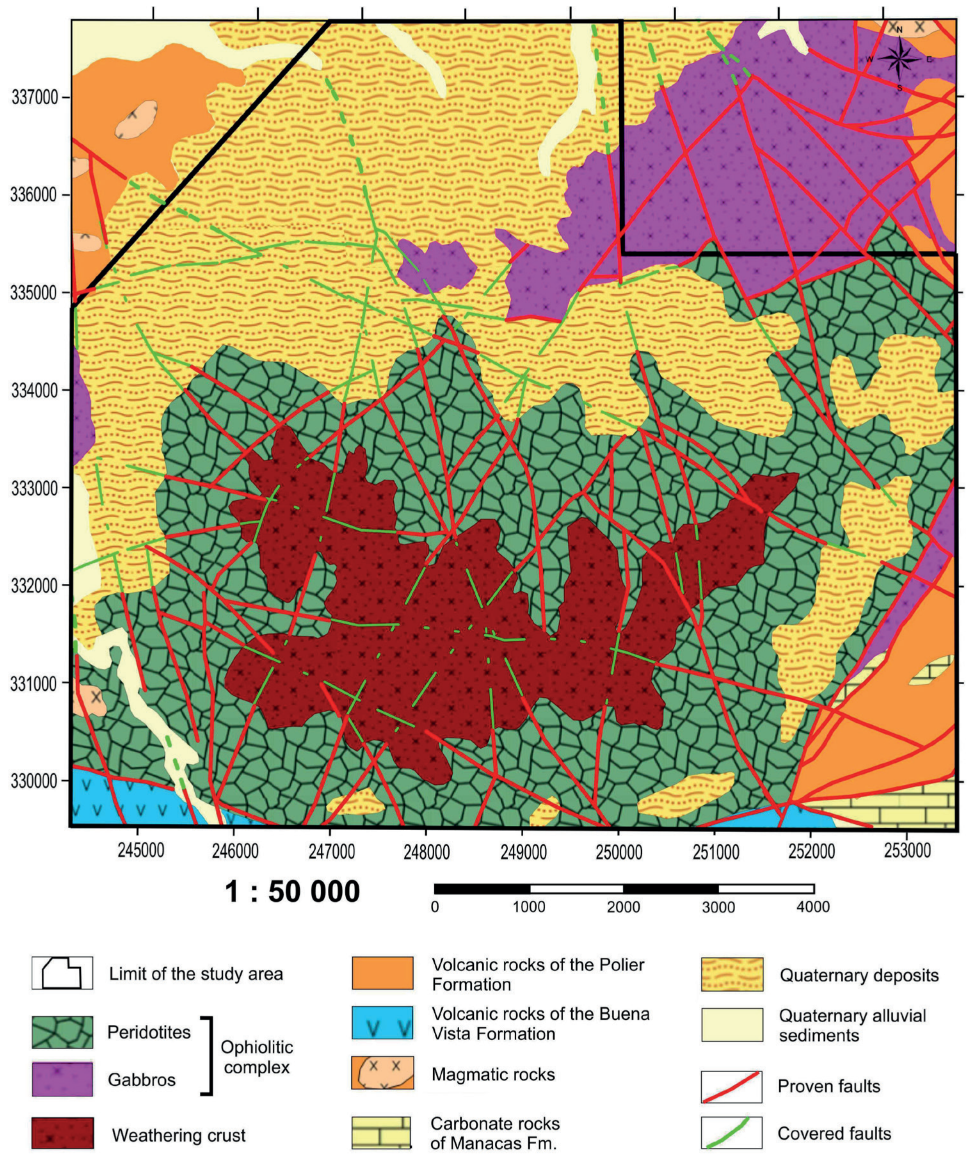


**Fig. 4.** Geological-tectonic map of the Cajálbana research area, prepared from the original map of Maximov et al. (1978). The Ophiolitic complex, Polier Fm., Buena Vista Fm., are from Cretaceous and Manacas Fm., from the lower Eocene (fore deep).

magnesium carbonate mineralization that we relate to the origin of the faults.

Tectonics represents one of the factors conditioning the formation of mineral deposits. Especially in the case of lateritic deposits the brittle faults play an important role, facilitating the circulation of surface water through the host rocks and enabling leaching and transport of soluble elements and by this way directly influencing also the geometry of the deposits and the distribution of ore types.

The recent version of the geological-tectonic map of the Cajálbana deposit research area (Fig. 4) was prepared from the geological map at a scale of 1 : 50 000 (Maximov et al., 1978), in which assumed faults were verified, digitized and reported. Likewise, Digital Relief Model (DEM) was constructed, as well as the different vector layers for faults, rivers and streams, have contributed in our research to decipher the brittle discontinuities – the pathways for the water penetration that facilitates the weathering.

## Materials and methods of mineralogical study

For achieving the research objectives the combination of methods of chemical, and mineralogical analyses was applied.

### *Sampling*

A sampling network was based on expert criteria for representative sampling in the studied Cajálbana lateritic mineral deposit, based on Geological Exploration Project (Commercial Caribbean Nickel, 2009). Technological and mineralogical samples were taken with the Hollow Auger

Integral drilling method applying 89 mm diameter spiral augers, providing granulometric fractions, which were selected for the study from individual lithological horizons (Fig. 5). The sampling within the same lithology was also done, as variations in the physical and mineralogical characteristics had been observed macroscopically during the field geological research (lithological profiles, accompanying mineralization and fundamental colour change).

### *Analytical techniques used*

Chemical analyses were performed using mainly the Inductively Coupled Plasma (ICP) method for determinations of the main element. The oxides were calculated using a stoichiometry conversion factor for $Al_2O_3$, $SiO_2$, MgO, $Cr_2O_3$, MnO, $Fe_2O_3$, NiO, CoO, FeO, FeO-Cr. The losses by ignition (LOI– Loss on ignition, in Spanish PPI) were determined by gravimetric method using a muffle furnace with the temperature range from 350 ºC to 850 ºC.

Mineralogical analyses were carried out by X-ray diffractometer – model Panalytical X'PERT3, under the following working conditions: Gonio-type scan in [° 2θ] angular register from 4.0042 to 79.9962 with step distance in ° 2θ of 0.0080 with Cu radiation and nickel filter. Difference of potential equal to 40 kV, current of 30 mA and calibration of the equipment with external silicon standard. Finally the mineralogical and chemical recalculations were performed per sample.

## Results and discussion

### *Lithological characteristics of the ore in the Cajálbana lateritic mineral deposit*

The presence of vertical lithological profiles of the lateritic-saprolitical type was verified. According to the terminology defined by Lavaut Copa (2003), there is a predominance of the Structurally Incomplete Saprolitical Laterite that from the surface of the cut to its base has chemical characteristics shown in Fig. 6.

**Tab. 1**

Average contents of the main chemical elements in lithology of the Cajálbana lateritic mineral deposit.

| Vertical lithological profiles | Chemical elements (%) | | | | | |
|---|---|---|---|---|---|---|
| | Ni | Fe | Co | Si | Mg | Al |
| OICP | 0.96 | 41.0 | 0.072 | 3.6 | 1.1 | 7.9 |
| OI | 1.14 | 43.1 | 0.057 | 2.9 | 1.0 | 6.5 |
| OEF | 1.07 | 36.2 | 0.136 | 7.2 | 2.6 | 5.8 |
| OEI | 1.26 | 20.7 | 0.041 | 16.1 | 9.0 | 3.4 |
| RML | 1.17 | 8.6 | 0.018 | 20.0 | 16.5 | 1.6 |

Note: For an explanation of abbreviations in the left column see Fig. 6.

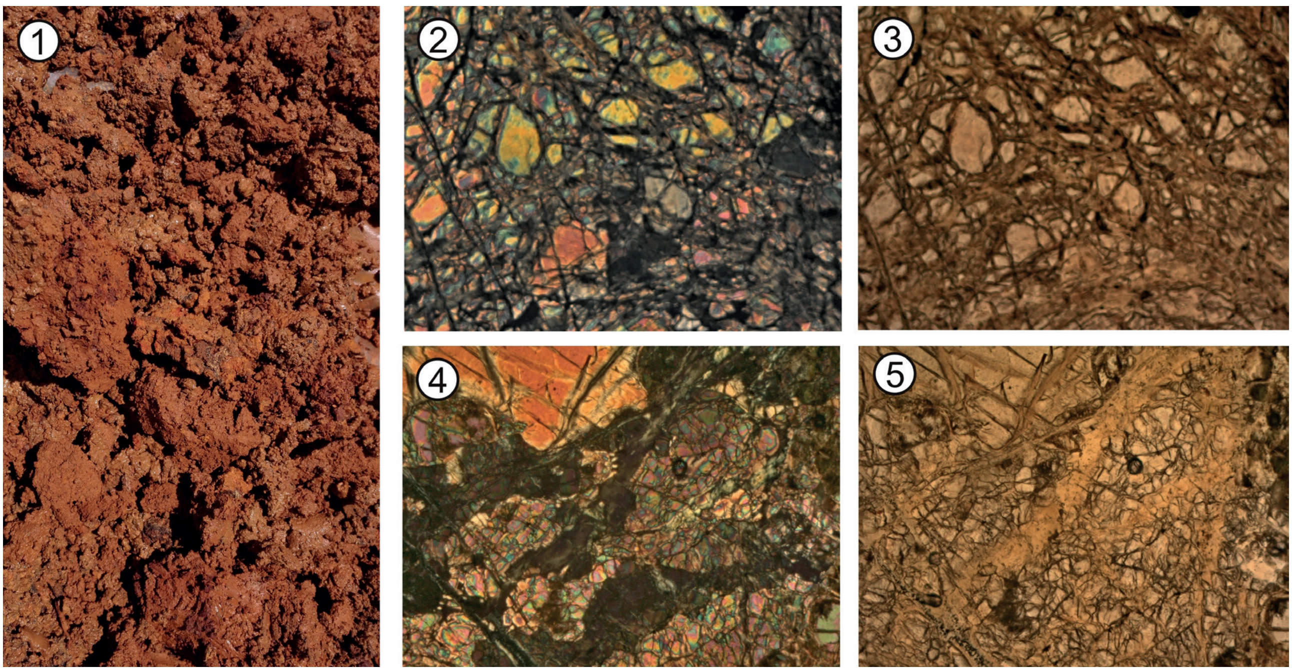


**Fig. 5**. Typical *limonite*-bearing weathering crust (1; width of view 20 cm) and photomicrograph of harzburgite from Cajálbana area (2–3; crossed and parallel nicols; x10) with dominating olivine (rounded) and clinopyroxene as well as small proportion of plagioclase. Serpentinized harzburgites (4–5; crossed and parallel nicols; x25) have newly formed chrysotile minerals. Photomicrographs 2–5 were done by the AXIO-LAB.A1 polarized light microscope with camera AXIOCAM ERs 5s.

The behaviour of the average contents of the main chemical elements in vertical lithological profiles shows a depthward increase in the content of nickel, silica and magnesium; while the trend of iron, cobalt and aluminum contents is generally the opposite. Table 1 presents a characteristic composition of elements in lateritic profile, the contents are considered to be perspective for the Cuban nickel industry.

It was corroborated that the study area is characterized by the dominating presence of ultramafic rocks (harzburgites and related serpentinites, lherzolites, websterites and more sparsely dunites). They are usually green, with shades ranging from light to dark, of massive structure, constituted by bastitized orthopyroxenes, olivine (relict or serpentinized) and minerals of the serpentine group, as shown in Fig. 7.

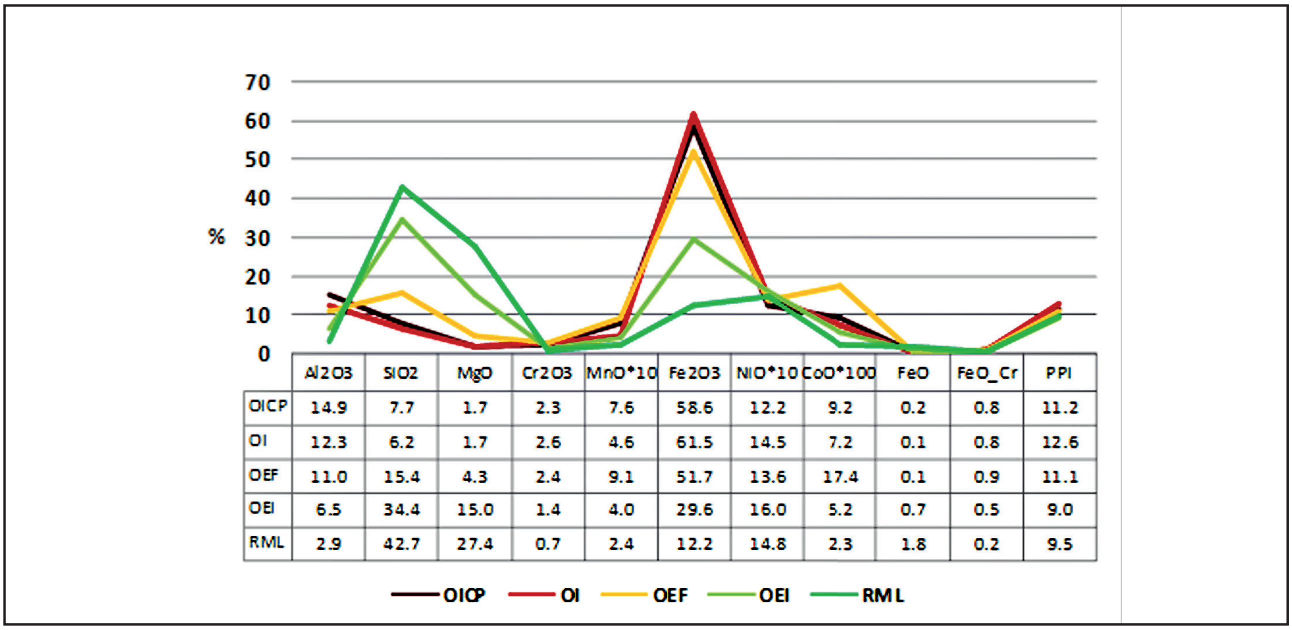


**Fig. 6.** Average content of oxides in lithological profiles in the Cajálbana lateritic mineral deposit. Used symbology: OICP – Unstructured ochre with iron concretions; OI – Unstructured ochre without iron concretions; OEF – Final structural ochre; OEI – Initial structural ochre; RML – Leaped and disintegrated serpentinites. Ordering OICP → OI → OEF → OEI → RML is from the top of lithological profile depthward.

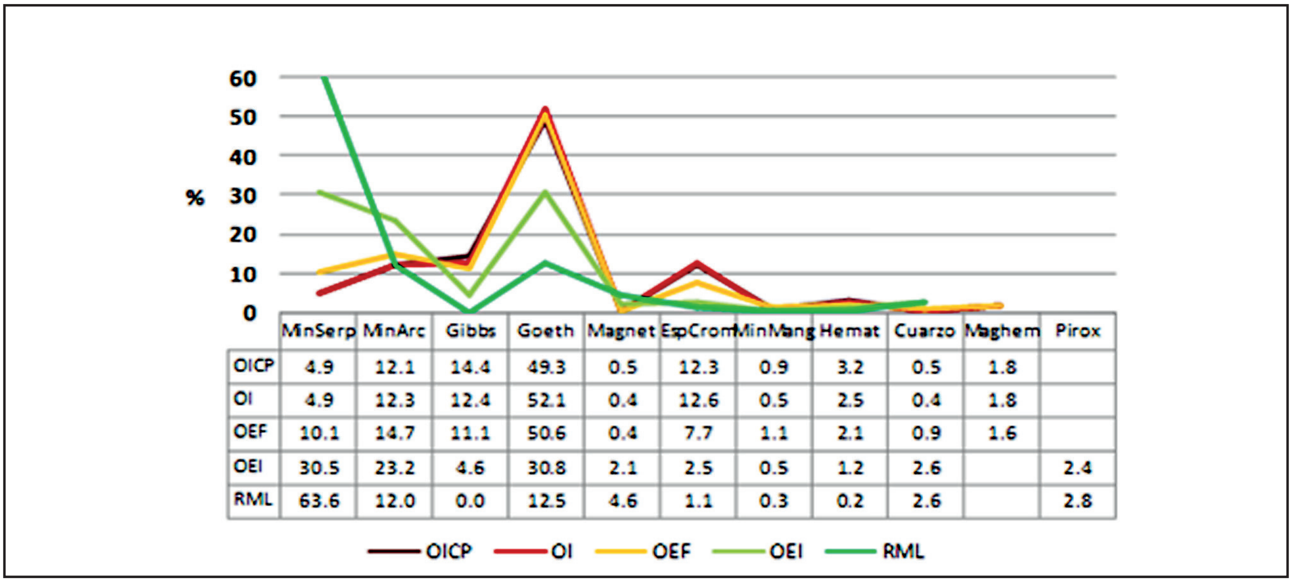


**Fig. 7.** Average mineralogical composition by lithological profiles in the Cajálbana lateritic mineral deposit. MinSerp – serpentine, MinArc – clay, Gibbs – gibbsite, Goeth – goethite, Magnet – magnetite, EspCrom – chromiferous spinel, MinMag – magnesite, Hemat – hematite, Cuarzo – quartz, Mghem – maghemites, Pirox – pyroxenes. For further symbology see Fig. 6.

### *Characteristics of ores*

The most abundant ore consists of *limonite* and in vertical lithological profiles it is mainly located from the OICP to the OEF, whose recalculation results are shown in Fig. 8.

Mineralogically, the ores of this deposit are characterized by the dominant presence of goethite, serpentine and clay minerals as shown in Fig. 9:

### *Main results of the Cajálbana deposit characterization*

The overall mineralization coefficient of the study area is 70.74 %, consisting mainly of structurally incomplete lateritic profiles developed in ultramafic protolith (peridotites) and very subordinate mafic rocks (ca. 11 %).

The mineralization present in the explored area is derived mainly from the pyroxenic peridotite rocks. Tectonically, the study area is dissected with the main fault systems trending NE-SW and NW-SE. They are interpreted as crucial for the surface water circulation.

A Database was created with the results of 470 samples analysed by ICP, taking into account the interpretation of the results of aero-geophysical flights from the 1980s (Díaz, Padilla & Corbea, 1987) in order to estimate the deposit thickness for modelling with the geological-mining software Micromine®, being the result the total tonnage of ore with the Ni cut off greater than or equal to 0.7 % determined is 51 million tons in the inferred category. The results by type of ore shown in Table 2.

As can be seen in Table 2, the ***limonite* ore (Lm)** has high mineralization values (48.99 %), with relatively high Fe, MgO, $Al_2O_3$ and $Cr_2O_3$ contents and an average value very similar to that of the Moa deposits in Cuba. Limonite prevailed in the Cajálbana area, representing 48.99 % of the total tonnage and this is very important for the Cuban nickel industry in the acid leaching processing plant as it is more suitable for this type of hydrometallurgical process.

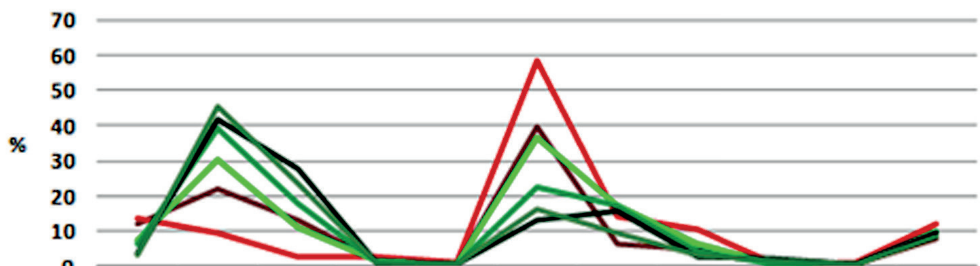


| | Al2O3 | SiO2 | MgO | Cr2O3 | MnO*10 | Fe2O3 | NiO*10 | CoO*100 | FeO | FeO_Cr | PPI |
|---|---|---|---|---|---|---|---|---|---|---|---|
| NM | 12.0 | 21.9 | 13.1 | 1.7 | 0.5 | 39.6 | 6.4 | 4.6 | 1.3 | 0.5 | 7.9 |
| Lm | 13.0 | 8.9 | 2.3 | 2.5 | 0.7 | 58.2 | 13.9 | 10.3 | 0.1 | 0.8 | 11.8 |
| Spb | 7.3 | 30.5 | 10.6 | 1.7 | 0.5 | 36.5 | 17.3 | 6.4 | 0.4 | 0.7 | 9.3 |
| Spd | 6.2 | 39.2 | 17.8 | 1.1 | 0.3 | 22.6 | 16.8 | 3.7 | 0.5 | 0.4 | 9.7 |
| SD | 3.2 | 41.7 | 27.6 | 0.7 | 0.2 | 12.8 | 15.4 | 2.5 | 1.7 | 0.2 | 9.3 |
| RE | 3.1 | 45.3 | 23.0 | 0.8 | 0.3 | 16.0 | 9.4 | 2.9 | 1.1 | 0.3 | 8.0 |

**Fig. 8.** Average content of oxides per ore in the Cajálbana lateritic mineral deposit. Used symbology: NM – ferricrete with nickel content below 0.7 %, Lm – *limonite*, Spb – soft saprolite, Spd – hard saprolite, SD – hard serpentine, RE – sterile rock.

**Tab. 2**
Average content of the main chemical elements by type of ore in the Cajálbana lateritic mineral deposit.

| Ore | Chemical contents (%) | | | | | | | | |
|---|---|---|---|---|---|---|---|---|---|
| | Fe | Ni | Co | MgO | $Al_2O_3$ | MnO | $Cr_2O_3$ | Pm.i (m) | Cm (%) |
| Lm | 41.41 | 1.03 | 0.081 | 2.59 | 12.84 | 0.60 | 2.57 | 2.73 | 48.99 |
| Spb | 27.41 | 1.11 | 0.058 | 10.65 | 9.16 | 0.54 | 1.79 | 2.58 | 7.80 |
| Spd | 16.62 | 1.07 | 0.033 | 21.10 | 4.57 | 0.34 | 1.03 | 5.76 | 10.32 |
| Sd | 10.07 | 1.24 | 0.021 | 27.94 | 2.52 | 0.21 | 0.65 | | 2.10 |
| Average contents in whole deposit | 40.10 | 1.05 | 0.060 | 17.70 | 8.90 | 0.50 | 1.85 | 5.26 | |

**Explanations:** Lm – *limonite*, Spb – soft saprolite, Spd – hard saprolite, Sd – hard serpentinite, Pm.i – Industrial average potential (thickness in meters), Cm – Coefficient of mineralization (%).

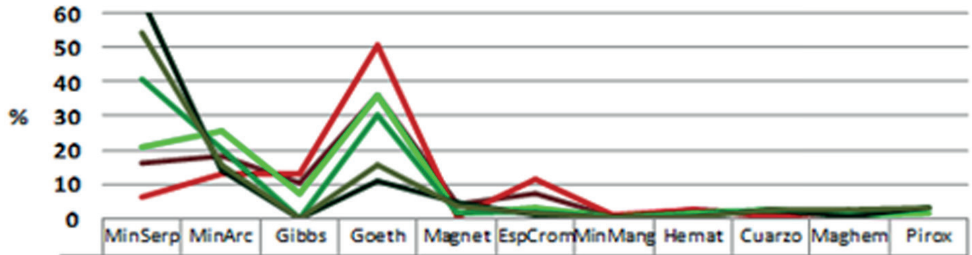


| | MinSerp | MinArc | Gibbs | Goeth | Magnet | EspCrom | MinMang | Hemat | Cuarzo | Maghem | Pirox |
|---|---|---|---|---|---|---|---|---|---|---|---|
| NM | 16.3 | 18.4 | 10.6 | 36.1 | 4.1 | 7.0 | 0.6 | 2.6 | 1.3 | 1.2 | |
| Lm | 6.0 | 12.9 | 13.0 | 50.5 | 0.4 | 11.5 | 0.8 | 2.6 | 0.5 | 1.7 | |
| Spb | 20.7 | 25.3 | 7.1 | 36.0 | 1.4 | 3.1 | 0.5 | 1.5 | 2.7 | 1.1 | 1.7 |
| Spd | 40.8 | 20.2 | 0.0 | 30.4 | 1.4 | 2.2 | 0.3 | 0.9 | 2.3 | 0.7 | 2.9 |
| SD | 64.3 | 13.8 | 0.0 | 11.1 | 4.7 | 1.1 | 0.3 | 0.3 | 2.5 | 0.4 | 2.8 |
| RE | 54.6 | 15.7 | 0.0 | 15.7 | 3.3 | 1.2 | 0.3 | 0.6 | 2.7 | 2.5 | 3.0 |

**Fig. 9.** Average mineralogical composition of ore in the Cajálbana lateritic mineral deposit: For symbology see Fig. 6 and 7.

On the other hand, **soft saprolite (Spb)** reaches an average mineralization coefficient of 7.80 %, with an extremely unstable character, which exhibits a very limited diffusion due to the existence of non-mineralized boreholes with average Fe, Ni and Co contents corresponding to the characteristics of the deposits of Punta Gorda, Moa, in the northeast part of the country.

**Hard saprolite (Spd)** has mineralization coefficient of 10.32 %, with extremely unstable character and limited diffusion, although somewhat higher than that of soft saprolite (Spb). The **hard serpentine (SD)** has a limited development, characterized by mineralization coefficient of 2.1 % and is extremely dispersed or unstable.

In general, it can be considered that the minerals from the Cajálbana lateritic mineral deposit in the municipality of La Palma, Pinar del Río province, have average contents of the main chemical elements that are currently being studied by the Cuban nickel industry, similar as those from lateritic nickel and iron deposits of the eastern region of Cuba, with an average ore potential of 5.26 m and mineralization of 17.3 %, which is proved by revealed main physical and chemical characteristics of this prospective deposit for the Cuban nickel industry.

From the mineralogical point of view, the Cajálbana deposit consists mainly of Fe and Ni bearing minerals, specifically the goethite, followed by serpentine and clay minerals and in smaller extent the chromiferous spinels and pyroxenes. In addition, the predominance of iron, nickel and chromium ores in these peridotites is typical.

## Conclusions

The ore from the Cajálbana lateritic mineral deposit in the municipality of La Palma, Pinar del Río province, is characterized by chemical elements and compounds with contents similar to those in the eastern region of Cuba where these minerals are processed by the Cuban nickel industry, having the average iron content of 40.10 %, nickel 1.05 % and cobalt 0.06 %, representing beneficial elements.

The lateritic mineral deposit is characterized mineralogically by the presence of Fe and Ni bearing minerals, mainly goethite and serpentine minerals, which resemble nickel and iron deposits in the eastern region of Cuba.

Recent knowledge of geological and mineralogical characteristics of the Cajálbana lateritic deposit confirms its similarity to the rest of the Cuban lateritic minerals deposits, with great potential for industrial processing, applying existing technologies.

## Acknowledgement.

Authors express their thanks to reviewers Prof. Allan Pierra Conde, Prof. Štefan Ferenc, one anonymous reviewer, as well as Zoltán Németh for improving quality of primary manuscript.

## References

Ariosa Iznaga, J., Lavaut Copa, W., Bergues, P. & Díaz, J., 2003: Modelo geológico descriptivo para los yacimientos lateríticos de Fe-Ni-Co en la faja ofiolítica Mayarí-Baracoa de Cuba. *Miner. Geol.*, 33–44.

Cardoso Velázquez, L., Barrientos, K., Cadete, M., Lorente, M., Acosta, J. & Recouso Sanchez, P., 2009: Reconiocimiento geológico Cajálbana. *Santiago de Cuba, Geominera Oriente.*

Cardoso Velázquez, L., Ruiz Quintana, J., Hernadez Ramsay, A., Barrientos, K., Cadete, M., Lorente, M., Acosta J. & Recouso Sanchéz, P., 2018: Revisión de correcciones a informes de cálculo de recursos y reservas del deposito mineralmineral Cajálbana. *La Habana, Ofic. Nacion. Recur. Miner.*

Carmona, A., 1995: Recálculo de los recursos y reconocimiento de lateritas niquelíferas del macizo de Cajálbana. *Pinar del Río, Empresa Geominera Pinar del Río.*

Commercial Caribbean Nickel, 2009: Reconocimiento geológico Cajálbana. *Geominera Oriente, La Habana, Commercial Caribbean Nickel.*

Díaz, L., Padilla, I. & Corbea, L., 1987: Informe Sobre los Resultados del Levantamiento Aerogeofísico Complejo en el Territorio de las Provincias de la Habana (sector Habana), en la República de Cuba. *La Habana, Instituto Geol. Paleont.*

Fonseca, E., 1989: Geoquímica de la Asociación Ofiolítica de la provincia de Pinar del Río. *Rev. tecnol., 3–16.*

GeoCuba, 2002: Planchetas topográficas San Cristóbal y La Palma, escala 1:100 000. *La Habana, GeoCuba.*

Gómez, O., 1988: Informe sobre los trabajos de búsqueda orientativa y detallada a escala 1:10 000 para corrector de Fe para la producción de cemento “La Mulata”. *La Habana, Ofic. Nacion. Recur. Miner. Cuba.*

Hernández Ramsay, A., 2018: Contribución de métodos geofísicos para caracterizar, evaluar la calidad y seleccionar minerales lateríticos y saprolíticos del norte de Cuba oriental. *La Habana, Univer. Tecnol. Habana.*

Lavaut Copa, W., 2003: La Meteorización de la Ofiolita de Cuba Oriental. Modelos Geológicos y Terminología Cubana. *La Habana, Mem. GEOMIN.*

Martín, R., Barrios, E., Fernández de Lara, R. & Barbón, R., 1998: Reconocimiento geológico de metales preciosos (Au y Ag) en el macizo de Cajálbana y sus alrededores sectores Agustina, Burén y Yagruma. *La Habana, Ofic. Nacion. Recur. Miner.*

Maximov, A., Mediakov, S., Riabenko, B., Krasnov, A., Kateav, L., Hevia, V., Bello, R., Gomez, G., Park, I., Maximov, A., Mediakov, S., Riabenko, B., Krasnov, B., Kateav, A., Hevia, L., Bello, V., Gomez, R., & Park, G., 1978: Informe sobre los resultados de los trabajos complejos geólogos geofísicos a escala 1:50 000 en la zona Bahía Honda. ONRM. *La Habana, Inst. Geol. Paleont.*

Nickel Institute, 2017: Nickel – essential resources for future sustainable developmen. *Ganzhou, China International Nickel & Cobalt Industry Forum 2017.*

Núñez Cambra, K. E., 2019: Geological map of Cuban Republic. *La Habana, Inst. Geol. Paleont.*

Oficina Nacional de Recursos Minerales, 2018: Ficha resumida de los trabajos realizados en el depósito Cajálbana. *La Habana, Ofic. Nacion. Recur.*

Ogarkov, V., 1970: Conclusiones sobre las menas de níquel de la corteza laterítica de intemperismo de la Plataforma Cajálbana (yacimiento la Mulata). *La Habana, Ofic. Nacion. Recur. Miner.*

Pardo, G., 2009: The geology of Cuba. *Amer. Assoc. Petrol. Geol. Stud, Geol. Ser., 58, 1–361.*

Ruiz Quintana, J., 2016: La Minería en Cuba, una aproximación. *La Habana, Nuevo Milenio C y T.*

Yujvit, V., Fesenco, G. & Guzmán, L., 1966: Informe final sobre los trabajos de exploración geológica sobre los minerales ferruginosos, efectuados en la provincia de Pinar del Río 1964-1965. ONRM. *La Habana, Inst. Geol. Paleont.*

## Hlavné geologické a mineralogické charakteristiky lateritického ložiska Cajálbana v provincii Pinar del Río, Kuba

Príspevok charakterizuje geologickú stavbu zóny mezozoickej obdukovanej ofiolitovej sekvencie vystupujúcej paralelne s osou Kuby v jej severnej zóne (obr. 2) s dôrazom na nové perspektívne Fe-Ni ložisko Cajálbana pri obci La Palma v provincii Pinar del Río v západnej časti Kuby (obr. 1, 3 a 4). Toto ložisko vzniklo intenzívnym lateritickým zvetrávaním povrchovej časti obdukovaných serpentinizovaných peridotitov (obr. 1, 4 a 5), ktoré spolu s výskytmi hornín kriedového vulkanického oblúka sa v súčasnosti nachádzajú na mezozoickom fundamente Guaniguanico. Ložisko je prestúpené početnými zlomami smeru SV – JZ a SZ – JV, ktoré sú dôležité pri cirkulácii povrchovej vody a prispeli k intenzívnemu lateritickému zvetrávaniu.

Chemická analýza reprezentatívnych vzoriek z jednotlivých horizontov kôry zvetrávania (tab. 1) a tiež rudy z ložiska Cajálbana (obr. 6 a 8) pri celkovom počte 470 vzoriek z 80 vertikálnych vrtov preukázali porovnateľný obsah prvkov a zlúčením, ako sa už skôr zistil na ložiskách vo východnej časti Kuby, ktoré sa ťažia v súčasnosti – priemerný obsah Fe dosahuje 40,10 %, Ni 1,05 % a Co 0,06 % (tab. 2). Podobne aj mineralogický výskum doložil prítomnosť Fe a Ni minerálov, predovšetkým goethitu a serpentínových minerálov (obr. 7 a 9), korešpondujúcich s minerálmi na Ni a Fe ložiskách ťažených v súčasnosti.

Terénnym geologickým prieskumom opierajúcim sa o mineralogický a skorší geofyzikálny výskum sa potvrdilo, že primárnym zdrojom zvýšeného obsahu Fe, Ni a Co na ložisku Cajálbana sú serpentinizované peridotity a budúca ťažba ich lateriticky zvetraných častí bude ekonomickým prínosom pre krajinu.

Doručené / Received: 26. 3. 2020
Prijaté na publikovanie / Accepted: 11. 8. 2020

*Mineralia Slovaca, Web ISSN 1338-3523, ISSN 0369-2086*
*52, 1 (2020), 33 – 44,* 

# Differential stresses estimated from calcite veins in HP-LT Triassic Hallstatt Limestones (Northern Calcareous Alps, Austria)

BARBORA ŠČERBÁKOVÁ[1], HANS-JÜRGEN GAWLICK[2] and ZOLTÁN NÉMETH[3]

[1]Technical University Košice, Faculty of Mining, Ecology, Process Control and Geotechnology, Letná 9, SK-042 00 Košice, Slovakia; barbora.zakrsmidova@gmail.com
[2]Montanuniversität Leoben, Department of Applied Geosciences and Geophysics, Petroleum Geology, Peter Tunner Str. 5, A-8700 Leoben, Austria; gawlick@unileoben.ac.at
[3]State Geological Institute of Dionýz Štúr, Mlynská dolina 1, SK-817 04 Bratislava, Slovakia; zoltan.nemeth@geology.sk

**Abstract:** Using paleopiezometry we calculated differential stresses ($\sigma_D = \sigma_1 - \sigma_3$), recorded by calcite veins during final stages of deformation of exhumed HP-LT Triassic Hallstatt Limestone blocks in the Pailwand Mt. (central Northern Calcareous Alps). Extreme recrystallization of the micrite of Hallstatt Limestone, which had taken place earlier than the studied calcite veins originated, has not allowed us to use calcite paleopiezometry on host rock. Studied calcite veins were strained during the last deformation phase which the Hallstatt Limestone has underwent. High number of deformation twins per 1 mm in calcite grains (Twin Density; D = 21–47) with grain-size from 323 to 571 μm demonstrates the deformation at differential stresses from 184 to 234 MPa.

This paper supports earlier interpretation that the Hallstatt Limestone in the Northern Calcareous Alps represents a lateral equivalent of a part of the Bôrka nappe of Meliata unit in the Western Carpathians and both segments underwent Middle Jurassic subduction, followed by rapid Late Jurassic-Early Cretaceous exhumation and thrusting.

**Key words:** paleopiezometry, differential stress, calcite, Hallstatt Mélange, Eastern Alps, Meliata Unit, Western Carpathians

**Graphical abstract**

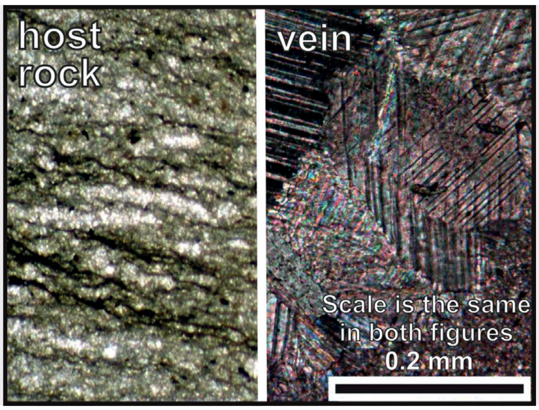


**Highlights**

- Research results contribute to further testing and upgrading of the methodology of calcite paleo-piezometry, as well as reconstruction of Cenozoic tectono-metamorphic events in E. Alps and W. Carpathians
- New paleopiezometric results (184–233 MPa) from the calcite veins in the Hallstatt Limestone Succession, as a lateral analogue of the Bôrka nappe rock succession of Meliatic unit (W. Carpathians), have completed the earlier paleopiezometric data – differential stresses acting during subduction (348–430 MPa) and exhumation (188–278 MPa) in the Bôrka nappe.

## Introduction

Southern zones of the Northern Calcareous Alps and the Western Carpathians represented in Triassic to Middle Jurassic time the northwestern shelf of the Neotethys (in this paper named as Meliata-Hallstatt) Ocean, striking from the Western Carpathians at least to the Hellenides (Fig. 1). According to one-ocean paleogeographic and geodynamic reconstructions (e.g. Krystyn & Lein in Haas et al., 1995; Gawlick et al., 1999, 2008; Schmid et al., 2008; Missoni & Gawlick, 2011a, b), the formation of Jurassic mélanges and an accretionary wedge is a result of a northwestward propagating thin-skinned orogen with the Middle to early Late Jurassic ophiolite obduction (i.e. Frisch & Gawlick, 2003; Plašienka, 2018, with references therein). Parts of the former outer shelf (Fig. 1: Meliata, Hallstatt and Zlambach facies zones) became imbricated, subducted and underwent a high-pressure–low-temperature metamorphism (Faryad, 1999; Faryad & Henjes-Kunst, 1997; Gawlick & Höpfer, 1999; Mock et al., 1998; Németh et al., 2012). From the Tithonian onwards, these metamorphosed slices were being exhumed.

Studied metamorphosed Triassic Hallstatt Limestones of the Pailwand Mt. (Figs. 2 and 3) are located roughly 50 km SE of Salzburg on the NE edge of the Tennengebirge Mts. They rest on the uppermost part of the Hallstatt

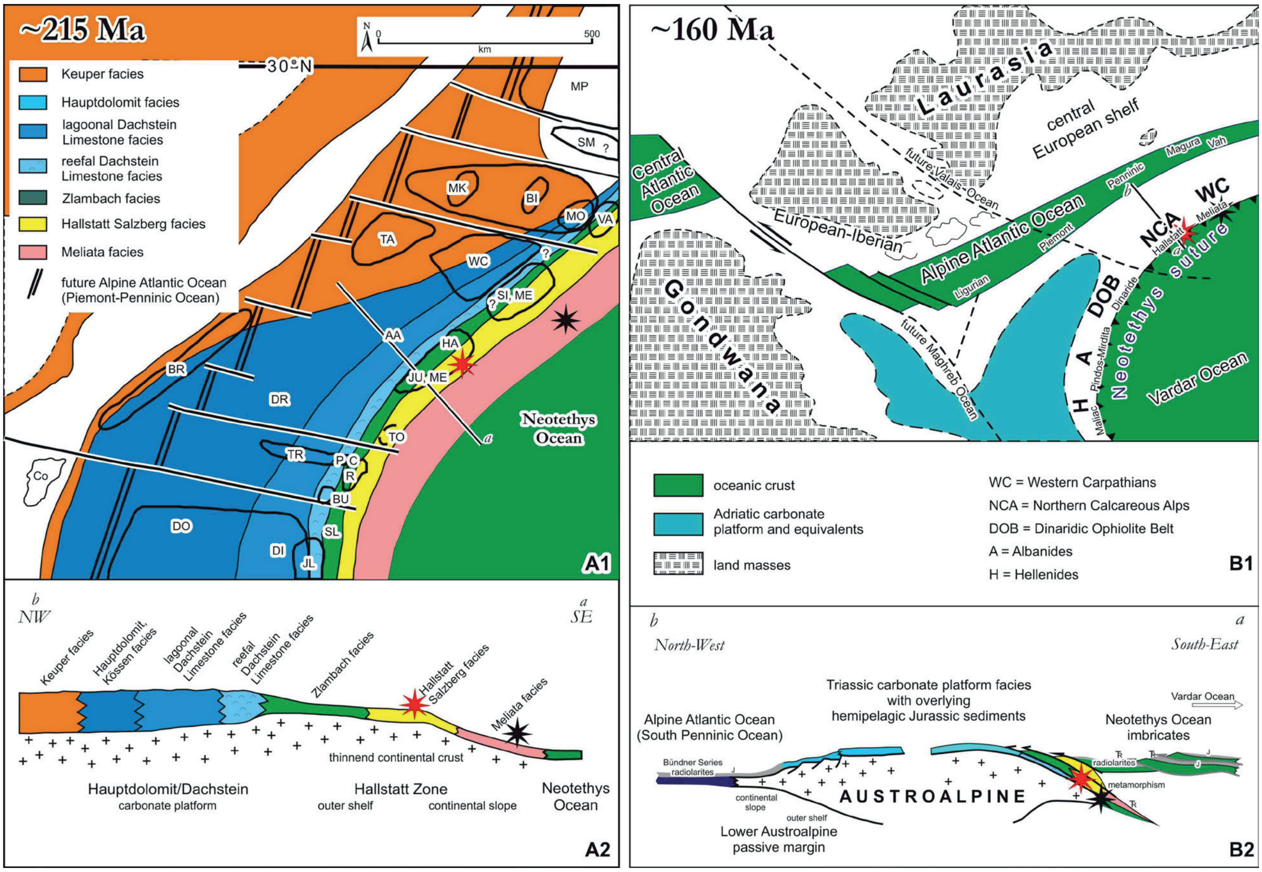


**Fig. 1.** ***A1*** – Paleogeographic reconstruction and facies distribution of the northwestern Neotethys realm in the Late Triassic time (paleogeographic position of the Austroalpine realm modified after Krystyn & Lein in Haas et al., 1995). *AA* Austroalpine; *BI* Biharia; *BR* Briançonnais; *BU* Bükk; *C* Csovar; *Co* Corsica; *DI* Dinarides; *DO* Dolomites; *DR* Drau Range; *HA* Hallstatt; *JU* Juvavicum; *JL* Julian Alps; *ME* Meliaticum; *MK* Mecsek; *MO* Moma Unit; *MP* Moesian platform; *P* Pilis-Buda; *R* Rudabanyaicum; *SI* Silicicum; *SL* Slovenian trough; *SM* Serbo-Macedonian Unit; *TA* Tatricum; *TO* Tornaicum; *TR* Transdanubian Range; *VA* Vascau Unit; *WC* - more internal zones of Western Carpathians located closer to Neotethys basin. ***A2*** – Schematic cross section through the Neotethys passive continental margin of the Austroalpine realm in the Late Triassic showing a typical passive continental margin facies distribution. ***B1*** **–** Paleogeographic position of the Northern Calcareous Alps as a part of the Austroalpine domain around the Middle/Late Jurassic boundary (after FRISCH, 1979). In this reconstruction, the Northern Calcareous Alps represent part of the Jurassic Neotethyan Belt (orogen) striking from the Carpathians to the Hellenides (Missoni & Gawlick, 2011a). The Neotethys suture is an equivalent to the West-Vardar ophiolite obduction (e.g., Dinaridic Ophiolite Belt) in the sense of Schmid et al. (2008) = far-travelled ophiolite nappes of the western Neotethys Ocean in the sense of Gawlick et al. (2008). The eastern part of the Neotethys Ocean remained open = Vardar Ocean (compare Missoni & Gawlick, 2011a). Toarcian to Early Cretaceous Adria-Apulia carbonate platform and equivalents are visualized according to Golonka (2002), Vlahovič et al. (2005) and Bernoulli & Jenkyns (2009). ***B2*** – Schematic cross section of the Austroalpine realm along the Alpine Atlantic margin towards the Neotethys realm around the Middle/Late Jurassic boundary showing the formation of the Neotethyan Belt (Missoni & Gawlick, 2011a). Red stars = study area, Pailwand. Black stars = comparison with the Bôrka nappe of the Meliatic Unit.

Mélange of the Lammer Basin, striking from the Saalach Unit in the west to the Gosaukamm Mt. in the east (e.g. Missoni & Gawlick, 2011a). Metamorphosed Hallstatt Limestone tectonic blocks occur on the top of the Middle to early Late Jurassic basin fill due to their northwest trending displacement. The Pailwand Mt. consists of amalgamated tectonic blocks of differing paleogeographic provenance and different diagenetic overprint ((see details in Gawlick & Königshof, 1993, and Gawlick & Höpfer, 1999).

The Hallstatt Limestone Succession metamorphic overprint in the Pailwand area, revealed by the Conodont Colour Alteration Index (CAI), calcite-dolomite solvus thermometry and the chlorite composition (clinochlore or pycnochlorite) with $Al^{IV}$ = 1.10–1.20 pfu (Gawlick & Königshof, 1993; Kralik et al., 1987; Gawlick & Höpfer, 1999; Frank & Schlager, 2006) took place at peak temperature 360–480 °C for the host rock recrystallization (CAI > 5.5 and CAI 6.0), The minimum pressures of 6–8 kb at 360 °C or 10 kb at 400 °C were deduced by microprobe analyses of the texturally different white micas with high celadonite content of 3.35–3.45 Si pfu. The metamorphic overprint of 155–152 Ma (Kimmeridgian) was determined by K-Ar and Rb-Sr on mica from fault

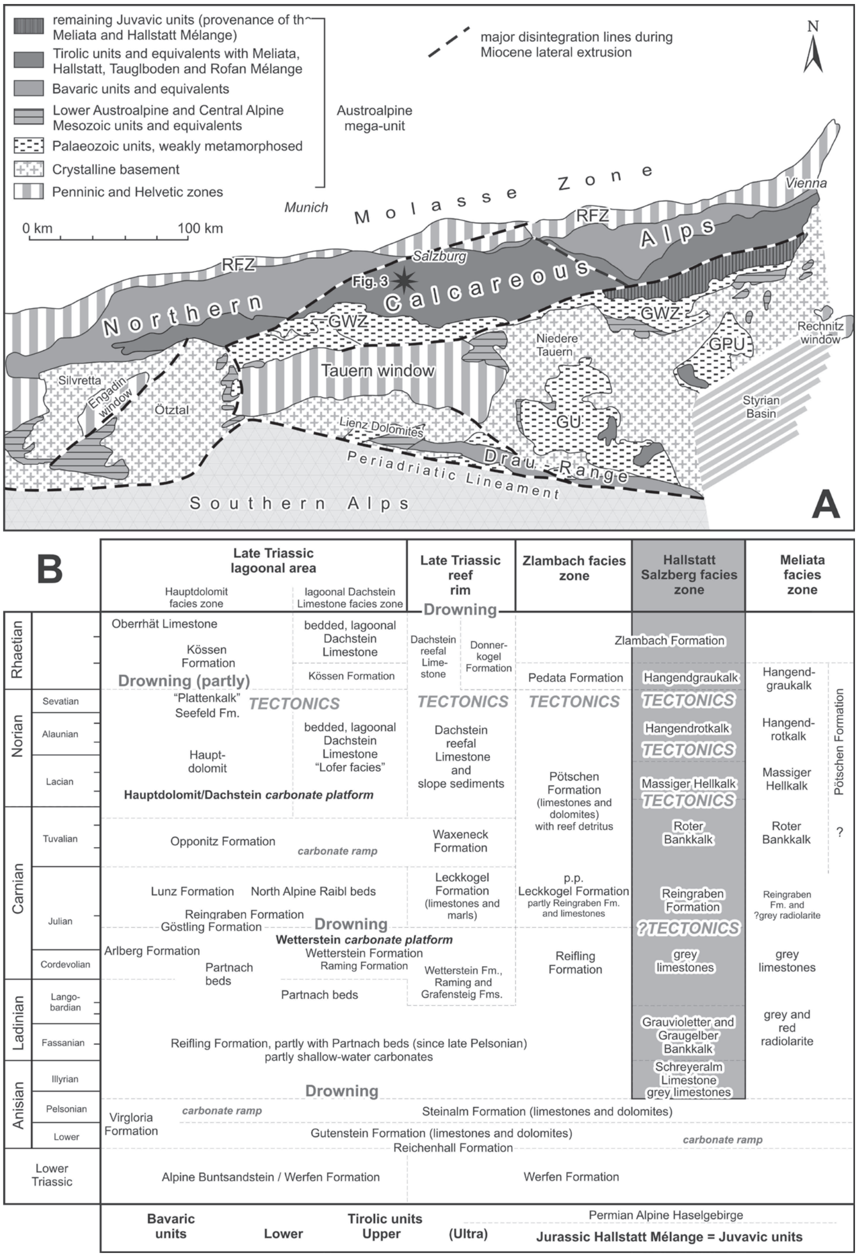


**Fig. 2.** ***A*** – Tectonic sketch map of the Eastern Alps with the Northern Calcareous Alps in their northern part showing the location of the study area (after Tollmann, 1977, and Frisch & Gawlick, 2003). *GPU* – Graz Paleozoic Unit. *GU* – Gurktal Unit. *GWZ* – Greywacke Zone. *RFZ* – Rhenodanubian Flysch Zone. Star indicates location of Fig. 3. ***B* –** Stratigraphic table of the Triassic formations and tectonic events in the Northern Calcareous Alps and equivalents (modified after Missoni & Gawlick, 2011a, b); compare Tollmann (1976). The Hallstatt Limestone Succession of the Pailwand is marked in grey.

gouges in the Hallstatt Limestones (Kralik et al., 1987), or a wide spectrum of Ar-Ar dating on mica (Frank & Schlager, 2006), providing the age clusters between 163–152 Ma and 141–132 Ma, as well as younger ages.

Recent research was motivated by previous studies in the HP-LT sequences of the Bôrka nappe in the Western Carpathians (Németh, 1996, 2005; Németh et al., 2007, 2012), aiming to obtain paleopiezometric data also from HP-LT Hallstatt Limestones of the Eastern Alps as a part of the Neotethyan Belt, too. This paper presents differential stress values ($\sigma_D = \sigma_1 - \sigma_3$) from calcite veins as products of the last stages of deformation of HP-LT Triassic Hallstatt Limestones of Pailwand Mt., because the very fine-grained (mylonitized) calcite grains (< 10 μm) in sheared layers in open-marine fine-grained Hallstatt Limestones of Pailwand (Fig. 4) did not allow application of paleopiezometry. Therefore, our research was focused on the youngest generation of calcite veins, penetrating the limestones, as well as penetrating older calcite veins, formed during an earlier stage of the diagenetic history of the Hallstatt Limestone Succession prior to their burial (Gawlick & Höpfer, 1999). The relative age of calcite veins was distinguished by overprinting relations.

## Methodology of paleopiezometry

The method of paleopiezometry, applied on deformed calcite grains – either in the calcitic marbles or calcite veins, allows to estimate paleo-stress, being expressed by the differential stress ($\sigma_D = \sigma_1 - \sigma_3$; *MPa*). The method is best calibrated for mono-mineral calcite marbles with a pervasive ductile deformation (Rowe & Rutter, 1990) and is useful for establishing the deformation gradient e.g. in a profile across a shear zone, or a normal or reverse fault plane with ductile deformation, The paleopiezometric measurements are based on the approaches by Jamison & Spang (1976), Lacombe (2007) and Laurent et al. (2000), who assume that the critical resolved shear stress (CRSS; $\tau_c$) is constant – about 10 MPa. According to Burkhard (1993), the deformation twins are developed at very low shear stress varying in between $\tau_c = 2–12$ MPa, what is depending on temperature, as well as the pressure conditions. The stress required to activate twinning is likely varying with the shear modulus and decreases with temperature (Rowe & Rutter, 1990). In general, the twinning represents one of

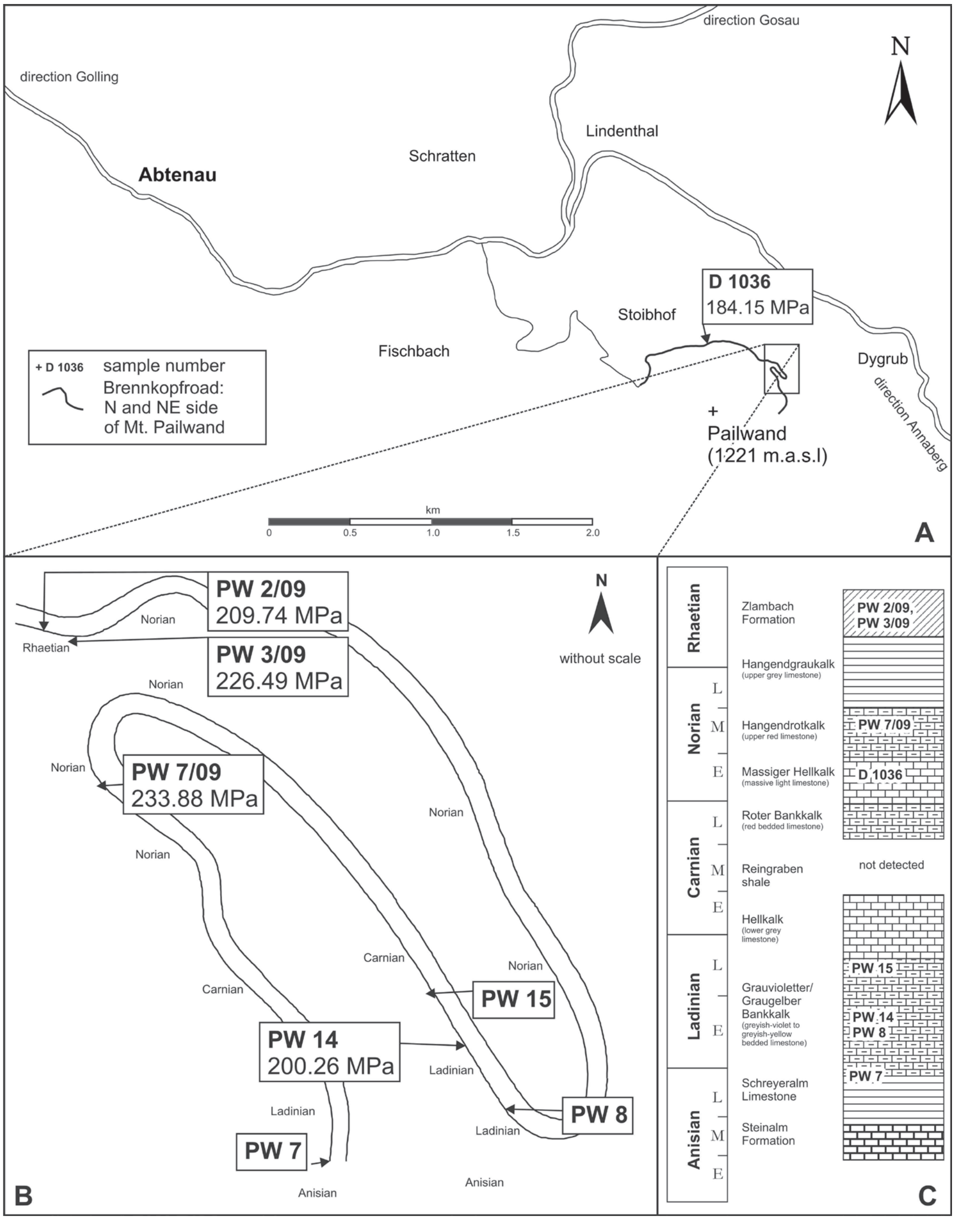


**Fig. 3.** ***A*** – Location of the study area in the southwestern central Northern Calcareous Alps east of Abtenau and the sample localities. ***B*** – Hallstatt Limestone Succession along the forest road at the northeastern side of Mt. Pailwand. Studied samples have added the values of differential stresses revealed in this study. ***C*** – Anisian to Rhaetian Hallstatt Limestone Succession of the Pailwand block and stratigraphic position of the studied samples.

important deformation mechanisms at LT-HP conditions (Groshong, 1972, 1988; Christian & Mahajan, 1995; Burckhard, 1993; Ferrill et al., 2004; Turner, 1964). The start of twinning is connected with the stress concentration on calcite crystals surfaces, grain boundaries, or various defects. Growth of twins is parallel to the twin boundary (Burkhard, 1993; Christian & Mahajan, 1995; Nicolas & Poirier, 1976).

*Calcite paleopiezometry* takes into account the size of recrystallized grains and the number and type of deformation twins. According to Rowe & Rutter (1990), there are two main independent ways for determining the differential stresses in calcitic rocks – the methods of *twinning incidence* ($I_t$ *= twinned grains / No. of grains total)* and *twin density (D = No. of twins / diameter of grains)*, both in *MPa*. (l.c.).

*Twinning incidence,* $I_t$, is defined as a percentage of grains having microscopically visible twins. Differential stress $\sigma_D$ ($\sigma_1 - \sigma_3$; MPa) can be estimated by the equation below, where d represents the size of grains in µm. The standard error in this technique, determined by Rowe & Rutter (1990), is up to 31 MPa.

$$\sigma_D = 523 + 2.13\ I_t - 204 \log d\ [\text{MPa}]$$

*Twin density, D*, is defined as the number of twins regarding the grain diameter, measured perpendicularly to the twins. As demonstrated by Friedman & Heard (1974), as well as Rybacki et al. (2013), twin density measurements using a flat stage match those measured with the U-stage to within 10 %. The standard error of this method is 43 MPa (Rowe & Rutter, 1990). The relation of the differential stress on twin density D is as follows:

$$\sigma_D = -52.0 + 171.1 \log D \text{ [MPa]}$$

To guarantee maximum representativeness of data, measurements were done systematically on profiles through thin sections, taking into account each neighbouring grain. Extreme dimensions (extremely small or large grains) were excluded from following calculations, using the variation coefficient 0.25 (Ranalli, 1984). Numerical processing used a procedure consisting of several steps (cf. Németh, 2005):

1. Separation and batching of obtained data according to the grain size.
2. Counting the number of grains in individual size categories, the grains without twins, as well as with twins. Values are used for calculation of twinning incidence $I_t$.
3. Counting of the number of twins in individual size categories and sums of all perpendicular diameters of grains related to twins. Values are used for calculation of twin density D.

For the maximum correctness, the calculation has been realized by six ways. Four calculations applied the variation coefficient below 0.25 (± 25 %; Ranalli, 1984), avoiding inaccuracy of results by calculations with extremely small and large grains.

Multiple determination of the differential stress by the method of Twinning Incidence:

1. Differential stresses have been calculated separately for each grain size class. The total differential stress has been calculated as their weighted mean. The variation coefficient was not implemented into calculations in this particular case.
2. Calculation with the total twinning incidence (without selective calculation for each grain size). Calculation with the coefficient of variation.
3. Determination of differential stress by the arithmetic mean from the partial results for individual categories. Calculation with the coefficient of variation.
4. Determination of differential stress by the weighted mean from the partial results for individual categories. Calculation with the coefficient of variation.

Multiple determination of the differential stress using method of Twin Density:

5. Calculation with application of mathematically determined twins number with respect to grain sizes perpendicular to twins without separation of calculation for individual size classes. The coefficient of variation was not implemented into calculation in this particular case.
6. The same way of calculation with implemented coefficient of variation.

In most of samples, results of both methods (Twinning Incidence and Twin Density), were comparable. Because a greater number of measured parameters, the Twin Density Method we consider as more precise and obtained results (with implementation of the coefficient of variation by Ranalli, 1984) seems to be well applicable for tectonic considerations.

## Results

The open-marine fine-grained metamorphosed Hallstatt Limestones have preserved a strong tectono-metamorphic and ductile deformation overprint, represented in some layers by very fine-grained (mylonitized) calcite crystals with grain-size of < 10 μm (Fig. 4). Such mylonites were not appropriate for paleopiezometric research. Therefore our attention was focused on younger calcite veins, bearing deformation twins (Fig. 5), which originated and were deformed later than the ductile deformation of the host rock occurred.

Generally 1–5 mm thick calcite veins (PW-2/09, PW-3/09, PW-7/09, PW-14 and D-1036; Figs. 3 and 5) were hosted by Hallstatt Limestone samples, which have an exact age control (Fig. 3C), and were used by one of authors (HJG) in his previous research.

Our systematic counting of the grain-size (d) and a number of deformation twins in 240 calcite grains along lines perpendicular to studied veins in thin sections has provided following results: the representative grain-sizes of calcite grains in veins are 323–571 μm, the twinning incidents determined by variation coefficient are 29–100, the numbers of twins per 1 mm of perpendicular diameter are 21–47 and calculated differential stresses are 184 to 234 MPa (Tab. 1).

Because twinning can accommodate only a limited amount of strain and always operates in specific crystallographic directions, if occurs the larger strain it can be accommodated by additional pressure solution dislocation creep or recrystallization (cf. Passchier & Trouw, 1996). In studied thin sections we have found also manifestations of three dislocation creep regimes of dynamic recrystallization (Fig. 5; cf. e.g. Dunlap et al. (1997), Stöckhert et al. (1999) and Zulauf (2001)) – the grain boundary area migration (GBAR), bulging (BLG) and sub-grain rotation (SGR), so the total differential stress can be even higher than that revealed by paleopiezometry.

Sample D-1036 with the mean grain-size diameter 515 μm, providing the lowest value of the differential stress ($\sigma_D$ = 184 MPa), contains also polygonal grains. They characterize the process of recovery with static recrystallization induced by temperature increase. The

**Tab. 1**
The results of Twinning Incidence (It) and Twin Density (D) paleopiezometric methods.

| | | TWINNIG INCIDENCE (It) | | | | | TWIN DENSITY (D) | | |
|---|---|---|---|---|---|---|---|---|---|
| | Representative grain-size | Calcul. without variation coeffic. | It for interval determined by variation coefficient | Calculation with variation coefficient | | | D – no. of twins per 1 mm of perpend. diameter | Calcul. without variation coeffic. | Calculat. with variation coeffic. |
| | | Calculat. with weight. mean | | Calculat. with the whole It | Arith. mean of σ for size classes | weight. mean of σ for size classes | | | |
| | µm | $\sigma_D$ (MPa) | | $\sigma_D$ (MPa) | $\sigma_D$ (MPa) | $\sigma_D$ (MPa) | | $\sigma_D$ (MPa) | $\sigma_D$ (MPa) |
| **PW-2/09** | 465.87 | 195.72 | 100 | 191.67 | 194.37 | 195.72 | 34 | 218.57 | **209.74** |
| **PW-3/09** | 365.26 | 360.24 | 20.68 | 44.29 | 38.49 | 38.49 | 21 | 215.31 | **226.49** |
| **PW-7/09** | 323.38 | 119.76 | 29.41 | 73.67 | 92.99 | 92.99 | 47 | 222.95 | **233.88** |
| **PW-14** | 571.25 | 200.26 | 76.92 | 124.45 | 121.97 | 124.81 | 30 | 189.51 | **200.26** |
| **D 1036** | 515.38 | 144.38 | 78 | 135.87 | 151.82 | 150.39 | 24 | 191.25 | **184.15** |

**Note:** Table presents the results of several ways of calculation of differential stresses ($\sigma_D$) in the studied samples from Pailwand (explained in the text). The results of Twin Density method, processed with the variation coefficient (the last right column), we suppose the most objective and applicable for further considerations.

→

**Fig. 4.** Deformation characteristics and microfacies of the Hallstatt Limestones of the Pailwand.

a – Early Ladinian Hallstatt Limestone. Sample **PW 8**. Sheared and recrystallized originally micritic limestone with filaments and radiolarians (see **b**). In the central part the original microfacies occur. In zones with the ductile deformation the limestone is totally recrystallized (see **c**). Scale bar = 500 µm.

b – Enlargement of **a** showing the well preserved microfacies characteristics of the filament-radiolarian wackestone. The preservation of the filaments and radiolarians is strongly affected by recrystallization. Scale bar = 150 µm.

c – Enlargement of **a** – sheared and totally recrystallized limestone. The extremely fine grain-size of this ultramylonitic limestone with signs of pressure solution and the absence of deformation twins do not allow to apply paleopiezometry. Scale bar = 75 µm.

d – Late Anisian Hallstatt Limestone. Sample **PW 7**. Shear zone in the original nodular limestone with ductile shearing and ultra-stylolitization. Whereas in the light grey parts the microfacies is well preserved, the calcite grains in the shear zone are completely mylonitized (see **e**). Scale bar = 500 µm.

e – Enlargement of **d** showing the completely recrystallized and mylonitized calcite crystals. Scale bar = 150 µm.

f – Late Anisian Hallstatt Limestone. Sample **PW 7**. Contact of a ductile deformed and recrystallized shear zone with a surrounding limestone matrix. In the lower part of the picture the limestone is practically not affected by shearing, having quite well preserved original microfacies. The rim of the shear zone is characterized by strong recrystallization and ultra-stylolitization. The central part of presented thin section represents the core of the shear zone with completely ductile recrystallized calcite grains. The asymmetric structures and porphyroclasts rotation are visible. Scale bar = 150 µm.

g – Sample **PW 7**. Completely recrystallized calcite grain in the shear zone showing newly formed phengites (greenish) at the rim of numerous sub-grains. In some cases (right and bottom parts of the calcite grain) the phengite forms larger accumulations. Scale bar = 150 µm.

h – Late Ladinian Hallstatt Limestone. Sample **PW 15**. Ductile deformed filament limestone showing complete recrystallization in the deformed parts. In the larger clasts the radiolarian and filaments ghosts are visible. Frequent porphyroclasts of sigma- and delta-type. Scale bar = 150 µm.

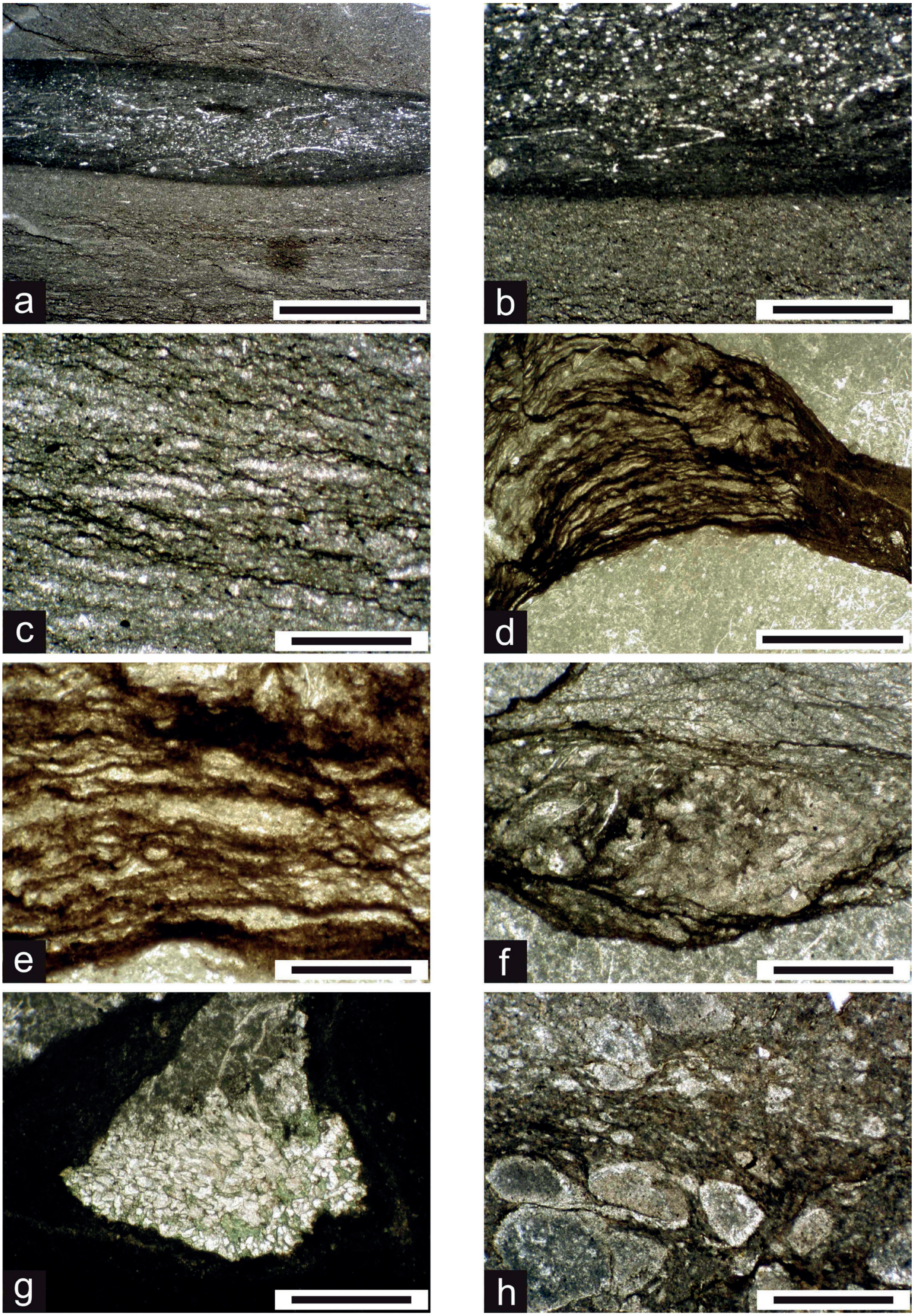
a
b
c
d
e
f
g
h

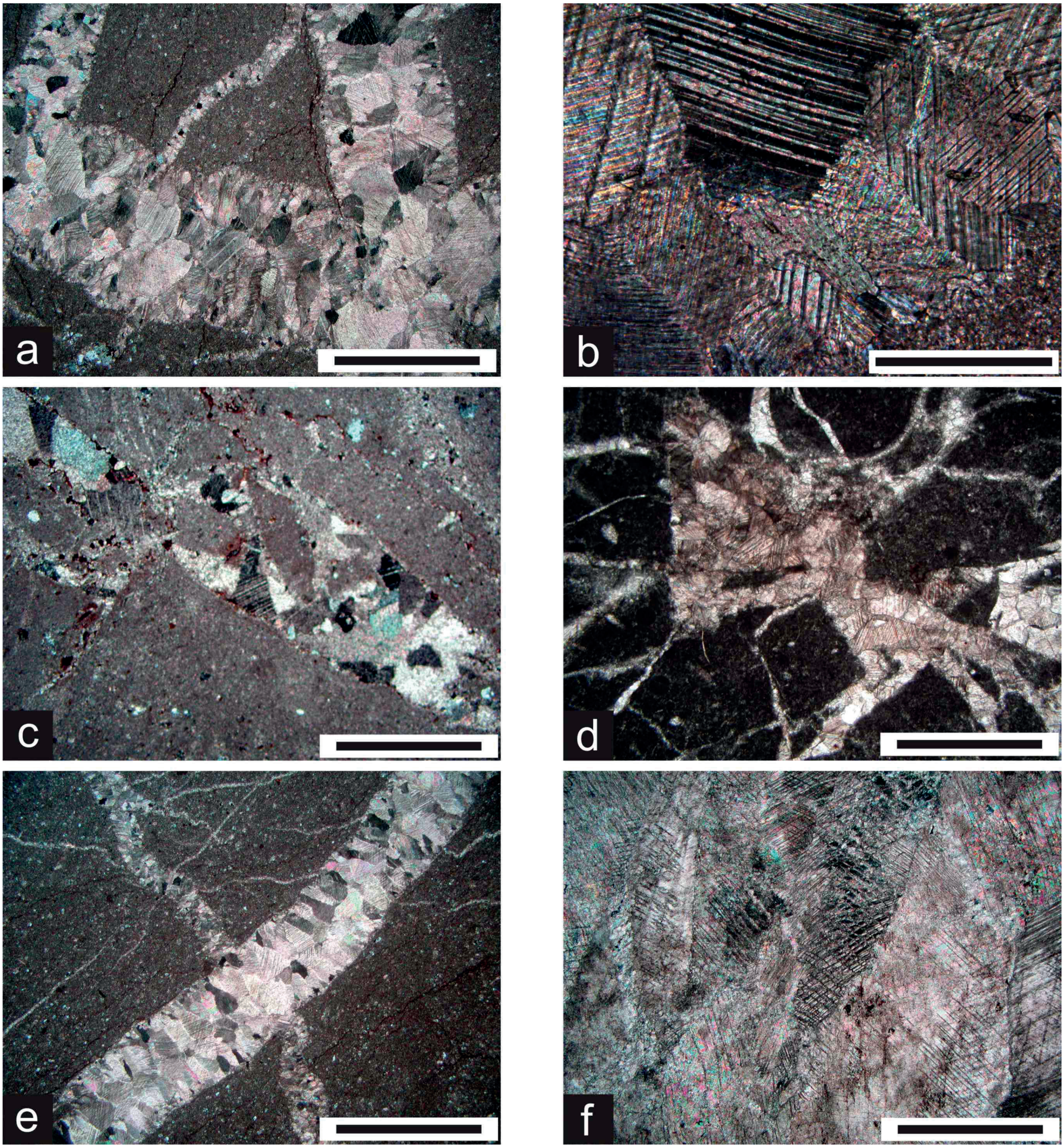


**Fig. 5.** Microphotographs of studied calcite veins. Description bellow relates the following parameters: d – average grain-size, It – Twinning incidence – the percentage of grains with deformation twins; D – Twin density – the average number of twins per 1 mm perpendicular to twin lamellae; $\sigma_D$ – differential stress (MPa). Compare Tab. 1.

a, b – Sample **PW 2/09**: d = 466 μm; It = 100 %; D = 219 MPa; $\sigma_D$ = 210 MPa. Scale bars = 2 mm (in a) and 200 μm (in detail b).

c – Sample **PW 3/09**: d = 365 μm; It = 21 %; D = 215 MPa; $\sigma_D$ = 227 MPa. Scale bar = 2 mm.

d – Sample **PW 7/09**: d = 323 μm; It = 29 %; D = 232 MPa ; $\sigma_D$ = 234 MPa. Scale bar = 2 mm.

e – Sample **PW 14**: d = 571 μm; It = 77 %; D = 190 MPa; $\sigma_D$ = 200 MPa. Scale bar = 2 mm.

f – Sample **D 1036**: d = 515 μm; It = 78 %; D = 191 MPa; $\sigma_D$ = 184 MPa. Scale bar = 200 μm.

increasing grain-size diameter (d) causes the decrease of differential stresses ($\sigma_D$), what is depicted in Tab. 1.

## Discussion

The Hallstatt Mélange in the southern zone of Northern Calcareous Alps (Frisch & Gawlick, 2003), as well as the Meliata Mélange, incl. the Bôrka nappe, resting on Gemeric Unit in the Western Carpathians (cf. Mello et al., 1998), represent two lateral parts of the Neotethyan orogenic belt (Missoni & Gawlick, 2011a).

For the metamorphosed rocks of the Meliata unit, included into the Bôrka nappe, numerous thermobarometric and geochronological data are available (Faryad, 1995; Faryad & Henjes-Kunst, 1997; Faryad & Hoinkes, 1999; Aubrecht et al., 2010; Ivan, 2002; Ivan et al., 2009; Ivan & Méres, 2009; Dallmeyer et al., 1993, 1996, 2005, 2008; Maluski et al., 1993; Putiš et al., 2011, 2012, 2014, 2019; Plašienka et al., 2019), depicting a Jurassic higher pressure overprint in the subduction process (170–150 Ma). In contrast, in the Northern Calcareous Alps the thermobarometric and geochronological data are scarce due to the fact, that carbonates represent practically the only preserved metamorphosed rocks, and more variegated rock suite and mineral asseblages for thermobarometry are absent (Gawlick & Frisch, 2003, with references therein).

Earlier paleopiezometric research of recrystallized limestones from the Bôrka nappe in the Western Carpathians (cf. Németh, 2005; Németh et al., 2012), has provided the peak differential stresses (348–430 MPa; l.c.), related to ductile deformation in the subduction slab. As interpreted by l.c., the recrystallization state of the rock, manifesting high differential stresses, was "frozen" by fast exhumation and they are recently positioned in the frontal part of the Bôrka nappe. The stresses in the subduction slab during later stages of exhumation were lowered probably due to the convection mantle heat input (cf. Németh et al., 2016; Zákršmidová et al., 2016), so ongoing static recrystallization lowered the differential stress (188–278 MPa; Németh, 2005).

Evolution in Pailwand we expect similar like in the Bôrka nappe, so it motivated us to document it by paleopiezometric data from both segments, resp. combine data if some are missing in one of these two segments.

We assume that in the case of studied Hallstatt Limestones, the differential stresses 184–234 MPa (Tab. 1) of deformed grains in penetrative calcite veins document the last stage of exhumation, similarly like it was found in the Bôrka nappe of Meliatic unit, whereas the earlier higher pressure metamorphism of continual subduction-exhumation process in the Hallstatt Limestones is manifested by their mylonitization / ultramylonitization (cf. Fig. 4; extreme grain-size reduction, origin of asymmetric shape of porphyroclasts, etc., origin of micro-shear zones). The grains (porphyroclasts), which originated in this higher pressure process, are so small which hinder to application of paleopiezometric measurements according to method by Rowe & Rutter (1990). It was the reason of focussing our paleopiezometric research on calcite grains in penetrative thin veins (thickness of 1–5 mm), which origin can be tied with the final stage of subduction-exhumation process when the dynamic recrystallization of calcite in veins was followed with the beginning of static recrystallization. This process was dated to (1) 146–135 Ma or (2) ~119–113 Ma (cf. Frank & Schlager, 2006). The first age group indicates an exhumation of the Neotethyan Belt (Missoni & Gawlick, 2011a) and the second group is related to the so-called Eo-Alpine evolution (cf. Frank & Schlager, 2006).

## Conclusions

The paleopiezometric investigation on deformed calcite veins within a metamorphosed Hallstatt Limestone Succession in the central Northern Calcareous Alps has

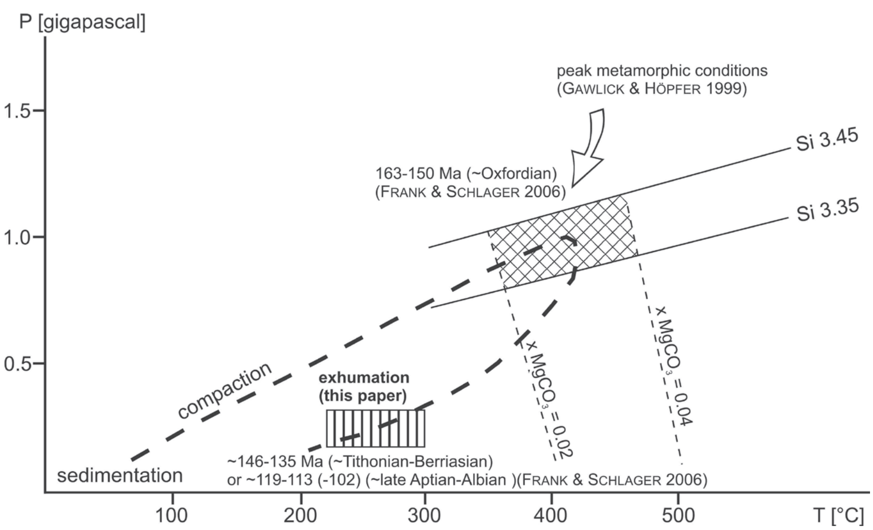


**Fig. 6.** Pressure-temperature path of subduction and exhumation of the Hallstatt Limestone Succession in the Pailwand area. Data from: Gawlick & Höpfer (1999), Frank & Schlager (2006) and this study

provided numeric data about the differential stresses ($\sigma_D = \sigma_1 - \sigma_3$) from the final stages of ductile deformation of the calcite veins, close to the onset of their static recrystallization. The number of deformation twins per 1 mm of perpendicular diameter of the grain (Twin Density, D = 21–47) at the grain-size (323–571 µm) has been produced by the deformation at differential stresses σ = 184–234 MPa. Recent paleopiezometric results from the calcite veins in the Hallstatt Limestone Succession, being interpreted as a lateral analogue of the corresponding rock succession in the Bôrka nappe of Meliatic unit in the Western Carpathians, have completed earlier paleopiezometric data – differential stresses acting during subduction process (348–430 MPa) and exhumation (188–278 MPa), revealed by previous research (Németh, 2005; Németh et al., 2012).

## Acknowledgements

Grants in the frame of the CEEPUS CIII-RO-0038 network for Barbora Zákršmidová (Ščerbáková) are gratefully acknowledged.

## References

Aubrecht, R., Gawlick, H. J., Missoni, S., Suzuki, H., Plašienka, D., Kronome, K. & Kronome, B., 2010: Middle Jurassic matrix radiolarians from the Meliata ophiolite mélange at the type Meliatic sites Meliata and Jaklovce (Western Carpathians): Paleogeographic evidence. *Geol. Balcanica, 39, 33–34.*

Bernoulli, D. & Jenkyns, H., 2009: Ancient oceans and continental margins of the Alpine-Mediterranean Tethys: Deciphering clues from Mesozoic pelagic sediments and ophiolites. *Sedimentology, 56, 149–190.*

Burkhard, M., 1993: Calcite twins, their geometry, appearance and significance as stress-strain markers and indicators of tectonic regime: a review. *J. struct. Geol., 15, 351–368.*

Christian, J. V. & Mahajan, S., 1995: Deformation twinning. *Progress Mater. Sci., 39, 1–157.*

Dallmeyer, R. D., Neubauer, F. & Pitiš, M., 1993: $^{40}Ar/^{39}Ar$ mineral age controls for the pre-Alpine and Alpine tectonic evolution of nappe complexes in the Western Carpathians. In: Pitoňak, P. & Spišiak, J. (eds.): Pre-Alpine Events in the Western Carpathians' Realm. *Stará Lesná, Confer. Excursions Guide, 11–20.*

Dallmayer, R. D., Neubauer, F., Handler, R., Fritz, H., Muller, W., Pana, D. & Putiš, M., 1996): Tectonothermal evolution of the internal Alps and Carpathians: Evidence from $^{40}Ar/^{39}Ar$ mineral and whole-rock data. *Eclogae geol. Helv., 89, 203–227.*

Dallmeyer, R. D., Németh, Z. & Putiš, M., 2005: Regional tectonometamorphic events in Gemericum and adjacent units (Western Carpathians, Slovakia): Contribution by the $^{40}Ar/^{39}Ar$ dating. *Slovak Geol. Mag., 11, 2–3, 155–163.*

Dallmeyer, R. D., Neubauer, F. & Fritz, H., 2008: The Meliata suture in the Carpathians: Regional significance and implications for the evolution of high-pressure wedges within collisional orogens. *J. Geol. Soc., London, 298, 101–115.*

Dunlao, W. J., Hirth, G. & Teyssier, C., 1997: Thermodynamical evolution of a ductile complex. *Tectonics, 16, 983–1000.*

Faryad, S. W., 1995: Phase petrology and P-T conditions of mafic blueshists from the Meliata Unit, West Carpathians, Slovakia. *J. Metamorph. Geol., 13, 701–714.*

Faryad, S. W., 1999: Exhumation of the Meliata high-pressure rocks (Western Carpathians): Petrological and structural records in blueshists. *Acta Montan. Slovaca, 2, 137–144.*

Faryad, S. W. & Henjes-Kunst, F., 1997: Petrological and K-Ar and Ar-40-Ar-39 age constraints for the tectonothermal evolution of the high-pressure Meliata unit, Western Carpathians (Slovakia). *Tectonophysics, 280, 141–156.*

Faryad, S. W. & Hoinkes, G., 1999: Two contrasting mineral assemblages in the Meliata blueshists, Western Carpathians. *Min. Mag., 63, 489–501.*

Ferrill, D. A., Morris, A. P., Evans, M. A., Burkhard, M., Groshong, R. H. J. & Onasch, C. A., 2004: Calcite twin morphology: A low-temperature deformation geothermometer. *J. struct. Geol., 26, 8, 1521–1529.*

Frank, W. & Schlager, W., 2006: Jurassic strike slip versus subduction in the Eastern Alps. *Int. J. Earth. Sci., 95, 431–450.*

Friedman, M. & Heard, H. C., 1974: Principal stress ratios in Cretaceous limestones from Texas Gulf Coast. *Bull. Amer. Assoc. Petrol. Geol., 58, 71–78.*

Frisch, W., 1979: Tectonic progradation and plate tectonic evolution of the Alps. *Tectonophysics, 60, 121–139.*

Frisch, W. & Gavlick, H. J., 2003: The nappe structure of the central Northern Calcareous Alps and its disintegration during Miocene tectonic extrusion: A contribution to understanding the orogenic evolution of the Eastern Alps. *Int. J. Earth. Sci., 92, 712–727.*

Gawlick, H. J. & Frisch, W., 2003: The Middle to Late Jurassic carbonate clastic radiolaritic flysch sediments in the Northern Calcareous Alps: Sedimenology, basin evolution, and tectonics – an overview. *Neu. Jb. Geol. Paläont., Abh., 230, 2/3, 163–213.*

Gawlick, H. J. & Königshof, P., 1993: Diagenese, niedrig- und mittelgradige Metamorphose in den südlichen Salzburger Kalkalpen – Paläotemperaturabschätzung auf der Grundlage von Conodont Color-Alteration-Index- (CAI-) Daten. *Jb. Geol. Bundesanst., 136, 39–48.*

Gawlick, H. J. & Höpfer, N., 1999: Stratigraphie, Fazies und Hochdruck-Mitteltemperatur-Metamorphose der Hallstätter Kalke der Pailwand (Nordliche Kalkalpen, Österreich). *Z. Dtsch. geol. Gesell., 150, 4, 641–667.*

Gawlick, H. J., Frisch, W., Vecsei, A., Steiger, T. & Böhm, F., 1999: The change from rifting to thrusting in the Northern Calcareous Alps as recorded in Jurassic sediments. *Geol. Rdsch., 87, 644–657.*

Gawlick, H. J., Frisch, S., Hoxha, L., Dumitrica, P., Krystyn, L., Lein, R., Missoni, S. & Schlagintweit, F., 2008: Mirdita Zone ophiolites and associated sediments in Albania reveal Neotethys Ocean origin. *Int. J. Earth. Sci., 97, 865–881.*

Golonka, J., 2002: Plate-tectonic maps of the Phanerozoic. *Spec. Publ. (Soc. econ. Paleontologists Mineralogists Tulsa), 72, 21–75.*

Groshong, R. H., Jr., 1972: Strain calculated from twinning in calcite. *Geol. Soc. Amer. Bull., 82, 2025–2038.*

Groshong, R. H., Jr., 1988: Low-temperature deformation mechanisms and their interpretation. *Geol. Soc. Amer. Bull., 100, 1329–1360.*

Haas, J., Kovács, S., Krystyn, L. & Lein, R., 1995: Significance of Late Permian-Triassic facies zones in terrane reconstructions in the Alpine-North Pannonian domain. *Tectonophysics, 242, 19–40.*

Ivan, P., 2002: Relics of the Meliata Ocean crust: Geodynamic implications of mineralogical, petrological and geochemical proxies. *Geol. Carpath., 53, 245–256.*

Ivan, P. & Méres, Š., 2009: Blueschist enclave in the Dobšiná quarry: The evidence of the relation of the ultrabasic body to the Hačava Fm. of the Bôrka nappe (Meliatic Unit, Slovakia). *Miner. Slov., 41, 4, 407–418.*

Ivan, P., Méres, Š. & Sýkora, M., 2009: Magnesioriebeckite in red cherts and basalts (Jaklovce Fm. of the Meliatic Unit, Western Carpathians): An indicator of initial stage of the high-pressure subduction metamorphism. *Miner. Slov., 41, 4, 419–432.*

Jamison, W. R. & Spang, J. H., 1976: Use of calcite twin lamellae to infer differential stress. *Geol. Soc. Amer. Bull., 87, 6, 868–872.*

Kralik, M., Klima, K. & Riedmüller, G., 1987: Dating fault gouges. *Nature, 327, 6126, 315–317.*

Kozur, H., 1991: The evolution of the Meliata Ocean and its significance for the early evolution of the Eastern Alps and Western Carpathians. *Palaeogeogr. Palaeoclimatol. Palaeoecol., 87, 109–135.*

Lacombe, O., 2007: Comparison of paleostress magnitudes from calcite twins with contemporary stress magnitudes and frictional sliding criteria in the continental crust: mechanical implications. *J. struct. Geol., 29, 86–99.*

Laurent, P., Kern, H. & Lacombe, O., 2000: Determination of deviatoric stress tensors based on inversion of calcite twin data from experimentally deformed monophase samples. Part II. Axial and triaxial stress experiments. *Tectonophysics, 327, 131–148.*

Maluski, H., Rajlich, P. & Matte, P., 1993: $^{40}Ar–^{39}Ar$ dating of the Inner Carpathians Variscan basement and Alpine mylonitic overprinting. *Tectonophysics, 223, 313–337.*

Mello, J., Reichwalder, P. & Vozárová, A., 1998: Bôrka nappe: High-pressure relic from the subduction-accretion prism of the Meliata Ocean (Inner Western Carpathians, Slovakia). *Slovak Geol. Mag., 4, 261–273.*

Missoni, S. & Gawlick, H. J., 2011a: Evidence for Jurassic subduction from the Northern Calcareous Alps (Berchtesgaden; Austroalpine, Germany). *Int. J. Earth. Sci., 100, 1605–1631.*

Missoni, S. & Gawlick, H. J., 2011b: Jurassic mountain building and Mesozoic-Cenozoic geodynamic evolution of the Northern Calcareous Alps as proven in the Berchtesgaden Alps (Germany). *Facies, 57, 137–186.*

Mock, R., Sýkora, M., Aubrecht, R., Ožvoldová, L., Kronome, B., Reichwalder, P. & Jablonský, J., 1998: Petrology and petrography of the Meliaticum near the Meliata and Jaklovce villages, Slovakia. *Slovak Geol. Mag., 4, 223–260.*

Németh, Z., 1996: First discovery of the Bôrka nappe in the eastern part of the Spiš-Gemer Ore Mts., Western Carpathians. *Miner. Slov., 28, 3, 175–184.*

Németh, Z., 2005: Paleopiezometry: Tool for determination of differential stresses for principal ductile shear zones of Gemericum, Western Carpathians. *Slovak Geol. Mag., 11, 2–3, 185–193.*

Németh, Z., Gazdačko, Ľ., Návesňák, D. & Kobulský, J., 2007: Polyphase tectonic evolution of Gemericum (the Inner Western Carpathians) outlined by review of structural and deformational data. In: Grecula, P., Hovorka, D. & Putiš, M. (eds.): Geological evolution of Western Carpathians. Monogr. *Miner. Slov., 215–224.*

Németh, Z., Radvanec, M., Kobulský, J., Gazdačko, Ľ., Putiš, M. & Zákršmidová, B., 2012: Allochthonous position of the Meliaticum in the North-Gemeric zone (Inner Western Carpathians) as demonstrated by paleopiezometric data. *Miner. Slov., 44, 1, 57–64.*

Németh, Z., Putiš, M. & Hraško, Ľ., 2016: The relation of metallogeny to geodynamic processes – the natural prerequisite for the origin of mineral deposits of public importance (MDoPI): The case study in the Western Carpathians, Slovakia. *Miner. Slov., 48, 119–134.*

Nicolas, J. & Poirier, J. P., 1976: Crystalline plasticity and solid state flow in metamorphic rocks. *London, Wiley.*

Passchier, C. W. & Trouw, R. A. J., 1996: Microtectonics. *Springer, 1–289.*

Plašienka, D., 2018: Continuity and episodicity in the Early Alpine tectonic evolution of the Western Carpathians: How large-scale processes are expressed by the orogenic architecture and rock record data. *Tectonics, 37.*

Plašienka, D., Méres, S., Ivan, P., Sýkora, M., Soták, J., Lačný, A., Aubrecht, R., Bellova, A. & Potočný, T., 2019: Meliatic blueschists and their detritus in Cretaceous sediments: New data constraining tectonic evolution of the West Carpathians. *Swiss J. Geosci., 112, 55–82.*

Putiš, M., Radvanec, M., Sergeev, S., Koller, F., Michálek, M., Snárska, B., Koppa, M., Šarinová, K. & Németh, Z., 2011: Metamorphosed succession of cherty shales with basalt and diastrophic breccia in olistolith of the Meliatic Jurassic accretion wedge near Jaklovce (Slovakia), dated on zircon (U-Pb SIMS SHRIMP). *Miner. Slov., 43, 1–18.*

Putiš, M., Koppa, M., Snárska, B., Koller, F. & Uher, P., 2012: The blueschist-associated perovskite-andradite--bearing serpentinized harzburgite from Dobšiná (the Meliata Unit), Slovakia. *J. Geosci., 57, 221–240.*

Putiš, M., Danišík, M., Ružička, P. & Schmiedt, I., 2014: Constraining exhumation pathway in an accretionary wedge by (U-Th)/He thermochronology – Case study on Meliatic nappes in the Western Carpathians. *J. Geodyn., 81, 80–90.*

Putiš, M., Soták, J., Li, Q.-L., Ondrejka, M., Li, X.-H., Hu, Z., Ling, X., Nemec, O., Németh, Z. & Ružička, P., 2019: Origin and age determination of the Neotethys Meliata Basin ophiolite fragments in the Late Jurassic-Early Cretaceous accretionary wedge mélange (Inner Western Carpathians, Slovakia). *Minerals, 9, 652, 1–38.*

Rannalli, G., 1984: Grain size distribution and flow stress in tectonics. *J. struct. Geol., 6, 443–447.*

Rowe, K. J. & Rutter, E. H., 1990: Paleostress estimation using calcite twinning: Experimental calibration and application to nature. *J. struct. Geol., 6, 443–447.*

Rybacki, E., Evans, B., Janssen, C., Wirth, R. & Dresen, G., 2013: Influence of stress, temperature, and strain on calcite twins constrained by deformation experiments. *Tectonophysics, 601, 20–36.*

Schmid, S. M., Bernoulli, D., Fügenschuh, B., Matenco, L., Schefer, S., Schuster, R., Tischler, M. & Ustaszewski, K., 2008: The Alpine-Carpathian-Dinaridic orogenic system: correlation and evolution of tectonic units. *J. Geosci., 101, 139–183.*

Stöckhert, B., Brix, M. R, Leinschrodt, R., Hurford, A. & Wirth, R., 1999: Thermochronometry and microstructures of quartz – a comparison with experimental flow laws and predictions on the temperature of the brittle-plastic transition. *J. struct. Geol., 21, 3, 351–369.*

Tollmann, A., 1976: Analyse des klassischen nordalpinen Mesozoikums. *Wien, Deuticke, 1–580.*

Tollmann, A., 1977: Geologie von Österreich. Band 1. *Wien, Deuticke, 1–766.*

Turner, F. J., 1964: Metamorphic Petrology: Mineralogy, field and tectonic aspects. *New York, McGraw Hill Book, 339–401.*

Vlahovič, I., Tišljar, J., Velič, I. & Matičec, D., 2005: Evolution of the Adriatic carbonate platform: Paleogeography, main events and depositional dynamics. *Palaeogeogr. Palaeoclimatol. Palaeoecol., 220, 333–360.*

Zulauf, G., 2001: Structural style, deformation mechanisms and paleodifferential stress along an exposed crustal section; constraints on the rheology of quartzfeldspatic rocks at supra- and infrastructural levels (Bohemian massif). *Tectonophysics, 332, 211–237.*

Zákršmidová, B., Jacko, S. & Németh, Z., 2016: Paleopiezometry – the new investigation method applied on the Penninic oceanic suture zone in comparison to the Meliata-Hallsttat suture zone. *Acta Montan. Slov., 21, 43–52.*

# Diferenciálne napätia z deformovaných kalcitových žíl vo vysokotlakovo-nízkoteplotne deformovaných triasových hallstattských vápencoch (Severné Vápencové Alpy, Rakúsko)

Aplikovaním metodiky paleopiezometrie sme vypočítali diferenciálne napätia ($\sigma_D = \sigma_1 - \sigma_3$), ktoré zaznamenali zrná v penetratívnych kalcitových žilách prestupujúcich hostiteľskou horninou – vysokotlakovo-nízkoteplotne metamorfovaným hallstattským vápencom (obr. 1 – 3) na lokalite Pailwand v centrálnej časti Severných Vápencových Álp (Rakúsko).

Hallstattský vápenec je interpretovaný ako laterálny ekvivalent karbonatickej sekvencie príkrovu Bôrky meliatika Západných Karpát a bol deformovaný aj počas jursko-spodnokriedového subdukčno-exhumačného procesu. Náš výskum mal za cieľ rozšíriť poznatky o charaktere a parametroch jeho duktilnej deformácie, podobne, ako sme to skôr zistili v príkrove Bôrky. Paleopiezometrické údaje z kalcitických mramorov príkrovu Bôrky zdokumentovali pôsobiace diferenciálne napätia, a to v prípade skôr exhumovaných frontálnych častí príkrovu Bôrky (348 až 430 MPa), rovnako ako z jeho neskôr exhumovaných tylových častí (188 až 278 MPa), ktoré už zaznamenali aj začiatok statickej rekryštalizácie (cf. Németh, 2005; Németh et al., 2012).

V prípade hallstattských vápencov sme zistili, že ich skoršia extrémna duktilná deformácia (obr. 4) spájaná so subdukčným procesom spôsobujúca vznik mylonitových až ultramylonitových deformačných pásov s extrémnou redukciou veľkosti kalcitových porfyroklastov (rozmery max. niekoľko desiatok µm) tvoriacich asymetrické štruktúry, rovnako ako absencia deformačných lamiel v kalcitových zrnách, neumožňuje zrealizovať paleopiezometrické merania a vyčísliť deformačný gradient ich deformácie pri subdukčnom procese.

Dôležité bolo ale zistenie, že hallstattské vápence s už dotvorenou duktilnou stavbou sú prestúpené mladšími kalcitovými žilami, na ktoré po ich vzniku tiež pôsobilo napäťové pole a zaznamenali sukcesívne mladšiu duktilnú deformáciu s diferenciálnymi napätiami 184 až 234 MPa (tab. 1). Túto mladšiu deformačnú epizódu je možné interpretovať ako dôsledok exhumačného procesu, prípadne príkrovového presunu alebo ponásunového odstrešovania. Deformácia kalcitových zŕn v týchto žilách (obr. 5) sa vyznačuje tvorbou vysokého počtu deformačných lamiel v zrnách (21 – 47 lamiel na 1 mm kolmej vzdialenosti oproti lamelám) pri zistenej veľkosti zŕn 323 – 571 µm. Niektoré časti žíl už indikovali aj začiatok statickej rekryštalizácie (polygonizáciu zŕn)

Zrealizovaný výskum a nové paleopiezometrické výsledky z lokality Pailwand diferenciálnymi napätiami zdokumentovali len najmladšiu duktilnodeformačnú udalosť, ale mikroštruktúrne bol zaznamenaný aj mylonitizačný proces hlavnej subdukčnej duktilnej deformácie. Napriek tomu prinášajú ďalší dôkaz o vhodnosti paralelizácie hallstattských vápencov s karbonatickou sukcesiou príkrovu Bôrky a indikujú podobnosť priebehu subdukčno-exhumačného procesu v tejto časti neotetýdnej zóny (obr. 6).

Doručené / Received: 28. 10. 2019
Prijaté na publikovanie / Accepted: 11. 8. 2020

*Mineralia Slovaca, Web ISSN 1338-3523, ISSN 0369-2086*
*52, 1 (2020), 45 – 56,* 

# Hydrogeological parameters trend analysis in the Slanec village landslide area (Slovakia), crossed by transit gas pipeline of European imporance

MARIÁN STERCZ, DANIEL GREGA, KATARÍNA PAČAJOVÁ and ĽUBOMÍR PETRO

State Geological Institute of Dionýz Štúr, Mlynská dolina 1, SK-817 04 Bratislava, Slovakia

**Abstract:** Time change of hydrological parametres was analysed in the landslide area near the Slanec village in the time span of 2003–2019. Five branches of international gas pipeline of European importance are crossing this landslide area, as well as two branches of international Družba pipeline, optical telecomunication lines and high-voltage power-lines.

Regime observations included measuring the groundwater levels in 11 observation boreholes and outflow in 20 drainage boreholes, concentrated in 5 outposts. The data file was supplemented by monthly precipitations from the nearby meteorological station.

Conducted trend analysis, using Mann-Kendall (MK) test, did not proved the existence of statistically important trend in the data file of monthly and yearly precipitations, even after calculations for each month – no statistical change in average amount of precipitations was revealed. Concerning drainage boreholes, MK test proved statistically importand declining trend of outflow for the whole measured period and for each of 5 outposts. This result can indicate e.g. clogging of drainage boreholes. The groundwater levels values demonstrated an average lowering by one meter during examined period. This result indicates lowering of the groudwater amount in the landslide and long time improvement of geotechnical parametres of the landslide slope.

**Key words:** trend analysis, monitoring, regime observation, remedial measures, landslide, Slanec, Mann-Kendall test, Sen's slope

**Graphical abstract**

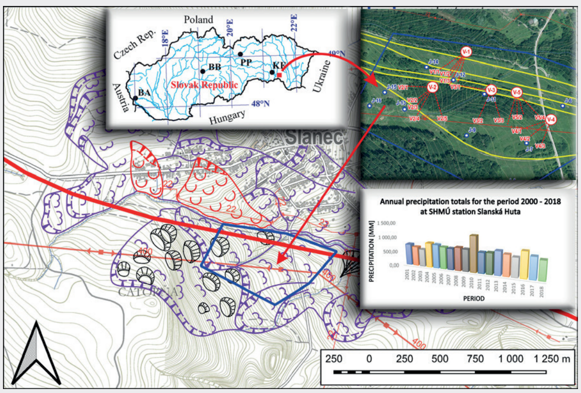


**Highlights**

- The Mann-Kendall test did not confirm any statistically important evolution trend of rain precipitations on the landslide area.
- Despite lowering of outflow in drainage subhorizontal boreholes, the lowering trend of groundwaters was revealed in almost all vertical boreholes.
- The results of trend analysis show that at standard climate conditions, the drainage measures have sufficient effect.

## Introduction

This contribution deals with time changes of hydrogeological situation parameters in the landslide area near the Slanec village. They were gathered as a part of regime observations between years 2003 and 2019. Results of those evaluations can help with overall reassessment of the situation and functionality of remediation measures and also the actual situation of monitored landslide area.

The Slanec village is located on the southern and southeastern slopes of Milič stratovolcano, developed on the southern side of the Slanské vrchy hills. Geomorphologically accurate location is – part of Slanské Hills, subassembly Milič, Východoslovenská pahorkatina unit and Podslanská pahorkatina subassembly (Mazúr & Lukniš, 1986). Whole village and surrounding area are situated in large landslide area. Large amount of residential or farm buildings are affected by landslide, similarly as the 2nd class state road. Five branches of transit gas pipeline, two branches of international pipeline Družba, telecommunication and optical lines and also high-voltage powerlines are crossing the landslide, too. Route of underground lines is crossing the valley of the Bradlo creek between villages Slanec and Nový Salaš, and the Slanské vrchy hills through the pass near Rákoš village (Fig. 1). Morphological and geological conditions

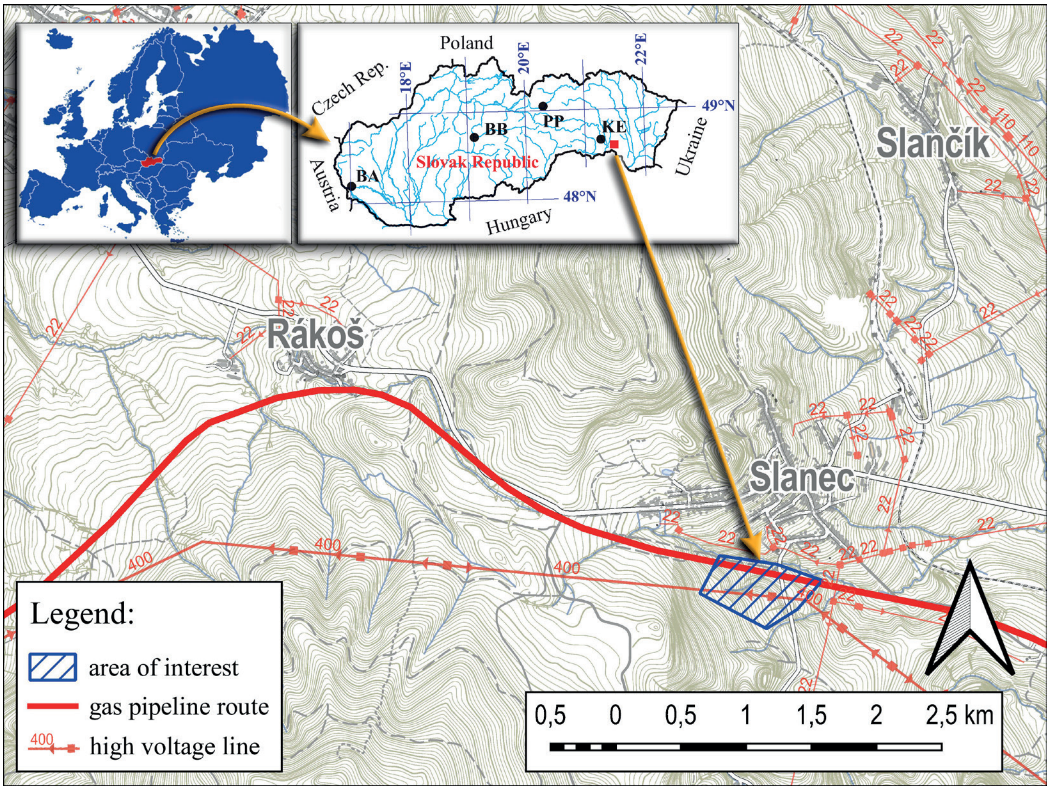


**Fig. 1.** Position of interest area in Slovakia with the gas pipeline route (thick red line).

of surrounding area of the current route – continuous mountain range of the Slanské vrchy hills, ranging from the north to south – made it impossible to apply different route for engineering networks.

Investigated landslide area is located south of the Slanec village. Because of numerous networks are traversing here, the location of Slanec was in 2003 included into set of regular measurements within a project of "Partial Monitoring System – Geological Factors" (PMS GF), where the State Geological Institute of Dionýz Štúr became the main research organization. The PMS GF forms an integral part of national environmental monitoring network. It is focused mainly on so-called geologic hazards, representing harmful natural or anthropogenic geological processes, which threat natural environment and ultimately also humans (www.geology.sk).

From a geological point of view, examined area is formed of Neogene sediments of Stretava Formation, in particular of clays and claystones, tuffitic clays, sands and volcanic rocks. Quaternary sedimetns are presented by colluvial sediments, less by fluvial deposits. In the overlay of grey Neogene clays with general dip 5–10° in the direction of the slope, which were verified by drilling works throughout the measured territory, the geodynamic processes are active until today (Fig. 2). Ongoing movements can be classified as very slow, with significant influence of the groundwater (Míka & Boľha, 2000).

Considering the extreme overload of geological environment by anthropogene interventions and high sensitivity of underground networks to potential slope instabilities, engineering geological survey was performed in 2000, and extensive remediation measures were designed (Míka & Boľha, 2000). Recently, performed monitoring is mainly focused on changes of the groundwater levels and outflow from drainage boreholes after realized remediation, which proved its functionality (Ondrejka et al., 2017).

## Monitoring

The regime observations at Slanec area consist of monitored level changes in 11 vertical observation boreholes and outflow from 20 subhorizontal drainage boreholes. The drainage boreholes are gathered into 5 outposts (Fig. 2). The surface drainage measures are not monitored.

Measurements, performed from 2003, are done applying a tape with Rang´s well whistle or electric water level meter without automatic recording at regular intervals, but with a minimum frequency of 10 measurements a year. Data file is supplemented by monthly rain precipitations from rain gauge station situated in Slanská Huta with indicative number 51160, operated by Slovak Hydrometeorological Institute (SHMI). Names of

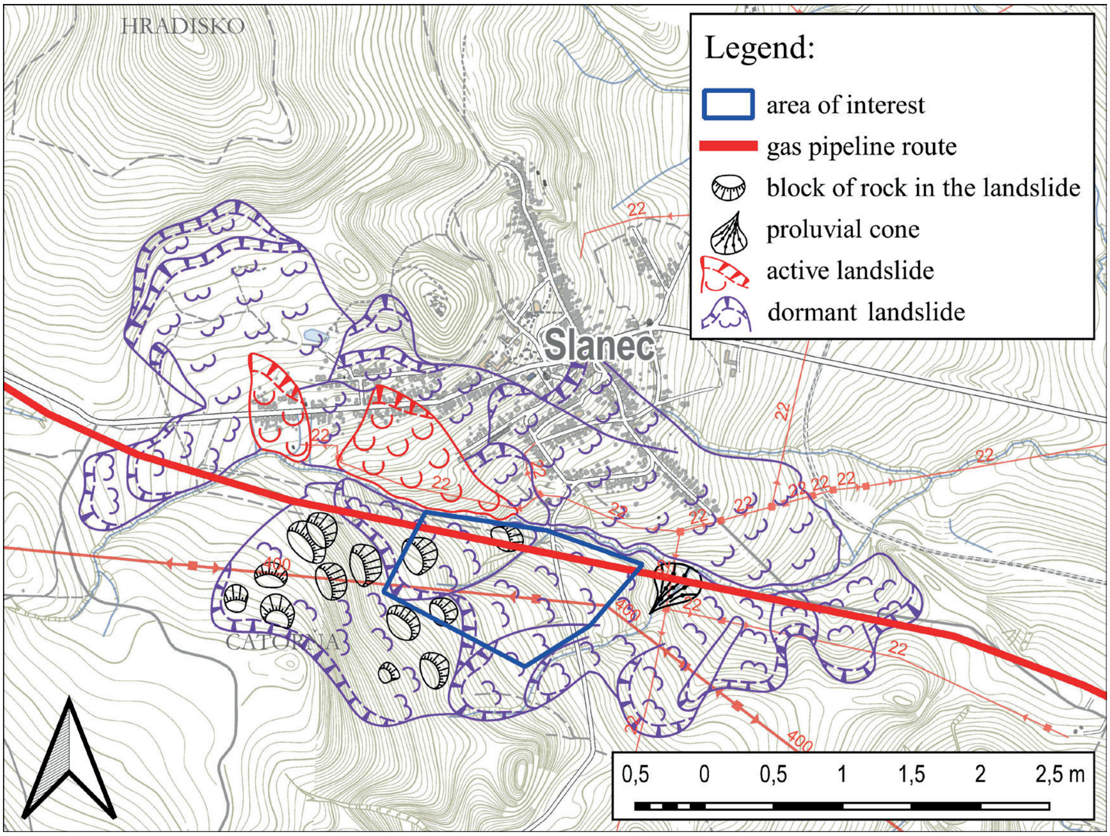


**Fig. 2.** Slope deformations in Slanec village and its vicinty, position of study area (polygon bordered by blue line).

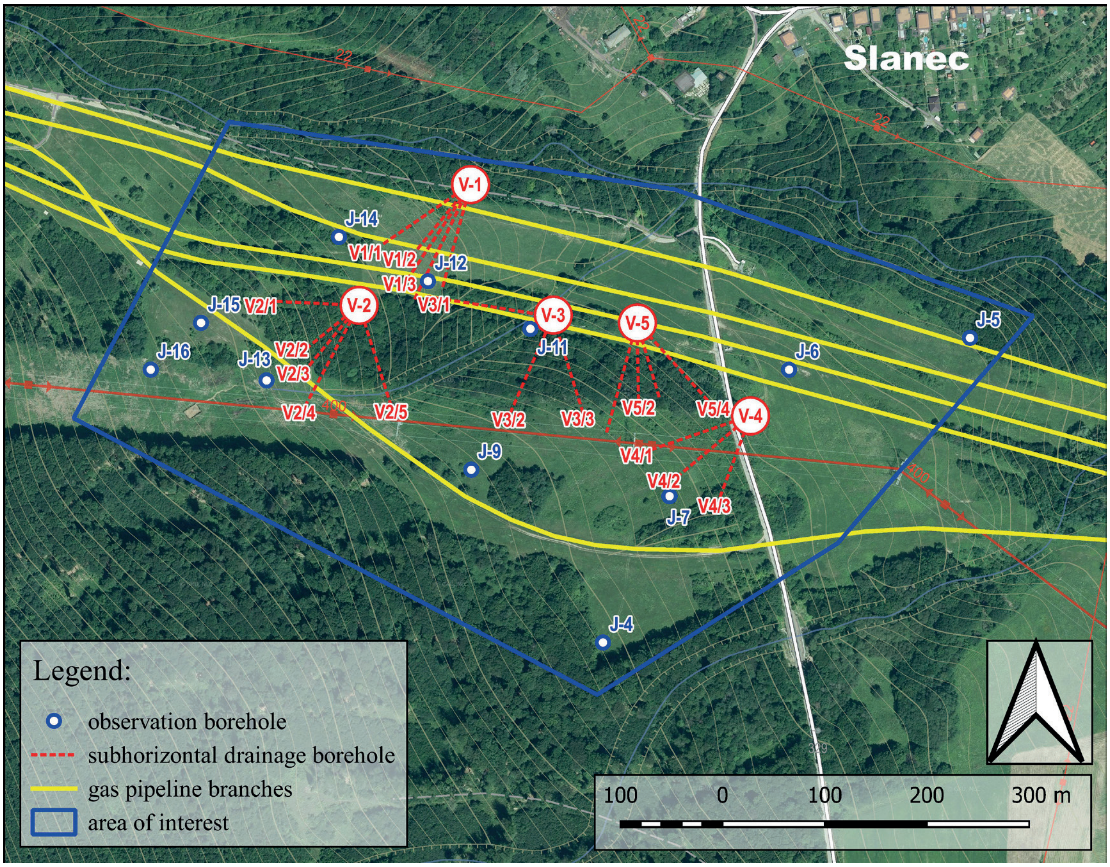


**Fig. 3.** Situation of remediation technical measures and monitoring – observation boreholes.

the boreholes, included in regime measurements, are listed with their basic characteristic in following table (Tab. 1).

### Trend analysis – methodics

One of goals of the evaluation of regime mea-surements is represented by investigation and demonstration of the presence of statistically significant trends in timed values of individual measured datasets.

From various statistical procedures used for analysis of time series, suitable for processing of environmental data (Gibbons et al., 1955), unparametrical Mann-Kendall trend test (MK-test) is most common. As an unparametrical test, MK-test does not create any premise for division of probability of random variable. Using of unparametrical technique offers better way to deal with data that differ from normality, while being tested. It is known, that unparametrical techniques are less suggestible with values more distant from the average (so-called remote) values (Zeleňáková et al., 2016).

Original author of the test – H. B. Mann – published it in 1945. In 1975 it was improved by M. G. Kendall – the founder of respective statistics. This type of test was widely applied for trend analysis in environmental sciences and its results showed up as very consistent (Önöz & Bayazit, 2003). It is more suitable for a larger statistical files. The MK-tests assess in time series without specification, if those are linear or non-linear trends.

Mann-Kendall test is based on value S (Önöz & Bayazit, 2003), which is defined as:

$$S = \sum_{i=1}^{n-1} \sum_{j=i+1}^{n} sgn(x_j - x_i)$$

wher **n** – total number of processed values
$x_i$ a $x_j$ – individual values in time i and j

For value $sgn(x_j - x_i)$ the following relationship applies:

$$sgn(x_j - x_i) = \begin{cases} 1 \;\; if \; (x_j - x_i) > 0 \\ 0 \;\; if \; (x_j - x_i) = 0 \\ -1 \;\; if \; (x_j - x_i) < 0 \end{cases}$$

**Tab. 1**
List of technical objects for regime observations.

| **Observation boreholes** (11 boreholes) | | | | | | | |
|---|---|---|---|---|---|---|---|
| borehole | coordinate X (S-JTSK) | coordinate Y (S-JTSK) | depth (m) | borehole | coordinate X (S-JTSK) | coordinate Y (S-JTSK) | depth (m) |
| J-4 | -247 227.32 | -1 250 757.36 | 14 | J-12 | -247 398.66 | -1 250 403.68 | 9 |
| J-5 | -246 868.07 | -1 250 459.24 | 20.2 | J-13 | -247 556.59 | -1 250 500.82 | 10.8 |
| J-6 | -247 045.14 | -1 250 490.30 | 17 | J-14 | -247 485.78 | -1 250 360.44 | 10 |
| J-7 | -247 162.18 | -1 250 614.13 | 16 | J-15 | -247 620.76 | -1 250 444.48 | 14 |
| J-9 | -247 356.20 | -1 250 588.26 | 23 | J-16 | -247 669.95 | -1 250 490.26 | 14 |
| J-11 | -247 298.35 | -1 250 450.36 | 8.8 | | | | |
| **Subhorizontal drainage boreholes** (20 boreholes in 5 groups) | | | | | | | |
| borehole | coordinate X (S-JTSK) | coordinate Y (S-JTSK) | length (m) | borehole | coordinate X (S-JTSK) | coordinate Y (S-JTSK) | length (m) |
| V1/1 | -247 356.91 | -1 250 309.19 | 110 | V3/1 | -247 275.95 | -1 250 436.89 | 120 |
| V1/2 | -247 356.91 | -1 250 309.19 | 90 | V3/2 | -247 275.95 | -1 250 436.89 | 100 |
| V1/3 | -247 356.91 | -1 250 309.19 | 110 | V3/3 | -247 275.95 | -1 250 436.89 | 100 |
| V1/4 | -247 356.91 | -1 250 309.19 | 120 | V4/1 | -247 082.87 | -1 250 535.53 | 100 |
| V1/5 | -247 356.91 | -1 250 309.19 | 100 | V4/2 | -247 082.87 | -1 250 535.53 | 100 |
| V2/1 | -247 466.02 | -1 250 427.33 | 90 | V4/3 | -247 082.87 | -1 250 535.53 | 90 |
| V2/2 | -247 466.02 | -1 250 427.33 | 80 | V5/1 | -247 193.60 | -1 250 444.57 | 110 |
| V2/3 | -247 466.02 | -1 250 427.33 | 90 | V5/2 | -247 193.60 | -1 250 444.57 | 80 |
| V2/4 | -247 466.02 | -1 250 427.33 | 110 | V5/3 | -247 193.60 | -1 250 444.57 | 80 |
| V2/5 | -247 466.02 | -1 250 427.33 | 100 | V5/4 | -247 193.60 | -1 250 444.57 | 110 |

Value S in MK-test presents sum of all considered values sgn ($x_j - x_i$). If S > 0, examined values, placed in time series later tend to be larger than values that are recorded in time series earlier. The opposite is true in case, if S < 0. Value S indicates the direction of the investigated trend (if it exists) – in case of positive value it will have increasing tendency, in the case of negative value the trend will be decreasing.

Assessment of the statistical significance of the trend is done by testing of hypothesis. In trend MK-test is tested null hypothesis ($H_0$), which assumes, that there is trend and the data are random and independent. Alternative hypothesis ($H_1$) is, that in tested file the trend exists. If the total number of values is n > 10, the statistics of the test can be aproximate by normal distribution and then normalized statistics $Z_S$ can be calculated. (Helsel & Hirsch, 1992):

$$Z_S = \begin{cases} \dfrac{S-1}{\sigma_S} & if\ S > 0 \\ 0 & if\ S = 0 \\ \dfrac{S+1}{\sigma_S} & if\ S < 0 \end{cases}$$

where $\boldsymbol{\sigma}_s$ is standard deviation: $\sigma_S = \sqrt{Var(S)}$

Var(S) is variation:

$$Var(S) = \frac{1}{18}[n(n-1)(2n+5) - \sum_{i=1}^{m} t_i(t_i - 1)(2t_i + 5)]$$

n – total number of data
m – number of linked groups (zero values between the compared groups)
$t_i$ – number of data in i-ish bounded group

The p-value can be used to decide the validity or invalidity of the null hypothesis:

$$p = 2(1 - P(Z \le Z_S))$$

where ($Z \le Z_S$) – the value of the distribution function of the standardized normal distribution in point $Z_S$.

The P-value expresses probability, by using of under the validity of the hypothesiss $H_0$ we get the same or less probable value of tested statistics. In comparison with determined level of significance α (generally α = 5 %) is hypothesis $H_0$ rejected in case, if p-value is lower than value α. In this case it means, that hypothesis $H_1$ is confirmed, so in file under consideration the existence of statistically important trend is confirmed in confidence interval 95 %.

Determining the size of the proven statistically significant trend can be done using of Sen´s slope. The Sen's slope method expects a linear trend in time series and is widely used for the determination of the size of trends e.g. in hydro-climatic time series (Zeleňáková et al., 2016). In this method the regression line directive is calculated as follow:

$$\beta = median\left(\frac{x_j - x_k}{j - k}\right)$$

where $x_j$, $x_k$ are data in time j and k (j > k)

Positive value of the directive β indicates growing trend and negative value indicates decreasing trend in time series. Median is the number in the middle of variation series.

For confidence interval 1-α for Sen's slope, upper and lower limit can be calculated:

lower limit: $lower = \beta_{(N-k)/2}$
upper limit: $upper = \beta_{(N+k)/2+1}$

where N is number of pairs in time series $N = C(n, 2)$

k is inverse distribution function of the standardized normal distribution for the selected level of significance α

$$k = \sigma_S . Z_\alpha$$

## Results of statistical analysis

*Set of precipitation totals*

Near the site (ca 3.5 km) the hydrometeorological station of SHMI Slanská Huta is located. The trend analysis of regime observations in the frame of PMS GF encompasses monthly total precipitations, provided by SHMI, which are measured on this station (Fig. 4).

Monthly data since 2001 are avilable for monitoring purposes. Because the direct precipitations represent primary and probably the most important phenomenon, which influences the hydrogeological situation of the area, it was appropriate to analyse also this data file.

The file in question included 216 elements. Within the Mann-Kendall test, hypothesis $H_0$ was tested, on the basis of the test results we could confirm or deny the existence of statistically important trend within the confidence interval of 95 % (for α = 0.05). Results are shown in table (Tab. 2).

In order to exclude the effects of cyclically recurring effects with a one-year period (e.g. the intensity of evapotranspiration), trends for individual months (Tab. 3), as well as annual precipitation totals (Tab. 4) for the entire measured period were tested using the same methodology.

Based on calculations in tested file of monthly and annual total precipitations from rain gauge station of SHMI Slanská Huta, no statistically important trend of the significance level α = 0.05 was demonstrated. So the presented data have character of independend and random data.

**Tab. 2**
Results of MK-test for file of monthly total rain precipitations.

| Mann-Kendall test for monthly precipitation totals in the period 2001 - 2019 | | | | | | | |
|---|---|---|---|---|---|---|---|
| n | α | S | Var(S) | $\sigma_S$ | Zs | p | trend |
| 216 | 0.05 | 308 | 94864 | 1061.814 | 0.289 | 0.772 | NO |

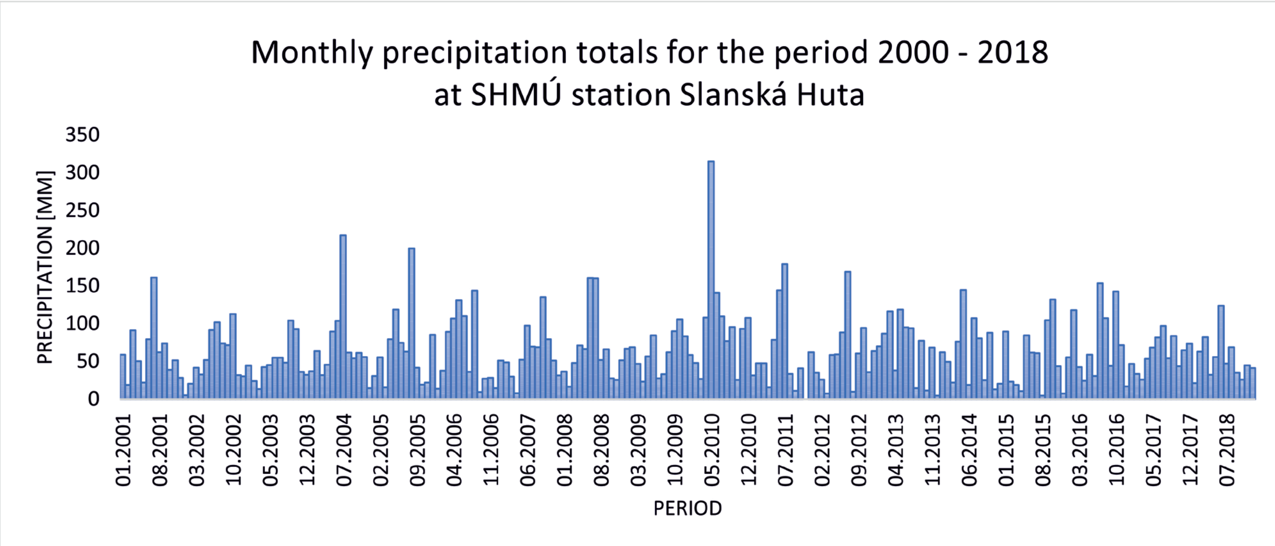


**Fig. 4.** Graphic representation of monthly total precipitations.

*Set of groundwater level measurements*

Statistical evaluation of hydrogeological data results from measurements, collected since 2003. These are periodical monthly measurements in 11 observation boreholes which represents set of data, sufficient for long term trend evaluation.

In terms of annual cycle, lowest average groundwater levels were measured in August – November, and highest average levels were measured in spring months March and May, while in this period, also largest variance of levels were recorded (Figs. 5, 6 and 7).

Trend analysis was conducted separately for each borehole. Range of tested files, corresponding to number of measurements was 162. In the case of boreholes J-6, J-7, J-9 and J-16, for technical reason not all measurements were made, so the range of files was lower (Tab. 5).

As is evident from Tab. 6, trend on statistically important level was confirmed in 10 of 11 cases. For this

**Tab. 3**
Results of the MK-test for monthly precipitation totals for individual months.

| MK-test for monthly precipitation totals for individual months in the period 2001 - 2019 | | | | | | | | |
|---|---|---|---|---|---|---|---|---|
| mounth | n | α | S | Var(S) | $\sigma_S$ | Zs | p | trend |
| JAN | 18 | 0.05 | 27 | 697 | 26.40 | 0.98 | 0.32 | NO |
| FEB | 18 | 0.05 | 39 | 697 | 26.40 | 1.44 | 0.15 | NO |
| MAR | 18 | 0.05 | -7 | 697 | 26.40 | -0.23 | 0.82 | NO |
| APR | 18 | 0.05 | -15 | 697 | 26.40 | -0.53 | 0.60 | NO |
| MAY | 18 | 0.05 | 31 | 697 | 26.40 | 1.14 | 0.26 | NO |
| JUN | 18 | 0.05 | -5 | 697 | 26.40 | -0.15 | 0.88 | NO |
| JUL | 18 | 0.05 | -13 | 697 | 26.40 | -0.45 | 0.65 | NO |
| AUG | 18 | 0.05 | -24 | 696 | 26.38 | -0.87 | 0.38 | NO |
| SEP | 18 | 0.05 | -15 | 697 | 26.40 | -0.53 | 0.60 | NO |
| OKT | 18 | 0.05 | 7 | 697 | 26.40 | 0.23 | 0.82 | NO |
| NOV | 18 | 0.05 | 15 | 697 | 26.40 | 0.53 | 0.60 | NO |
| DEC | 18 | 0.05 | 7 | 697 | 26.40 | 0.23 | 0.82 | NO |

**Tab. 4**
Results of the MK-test for annual precipitation totals.

| Mann-Kendall test for annual precipitation totals in the period 2001 - 2019 | | | | | | | |
|---|---|---|---|---|---|---|---|
| n | α | S | Var(S) | $\sigma_S$ | Zs | p | trend |
| 18 | 0.05 | -11 | 697 | 26.401 | -0.379 | 0.705 | **NO** |

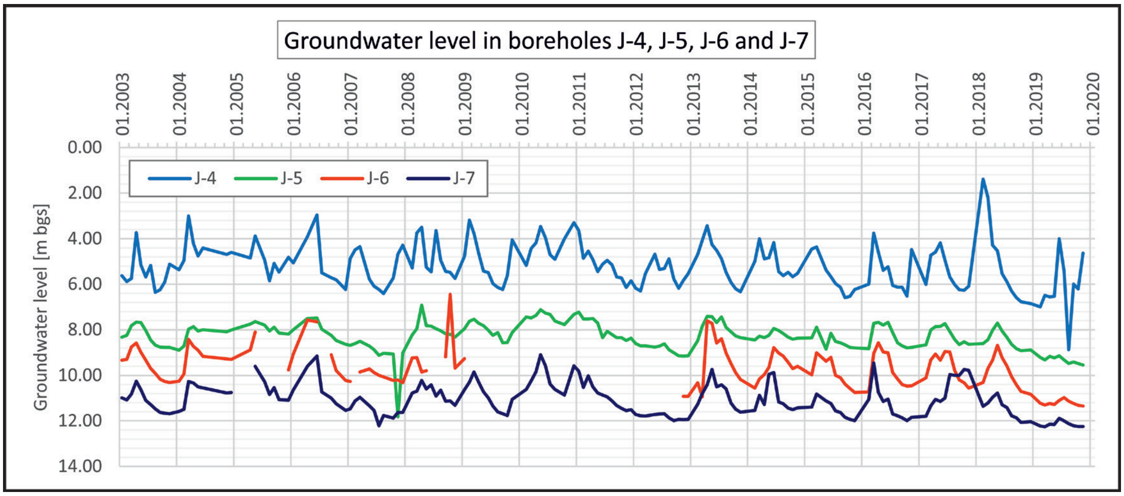


**Fig. 5.** Graphs of groundwater levels in boreholes J-4, J-5, J-6 and J-7.

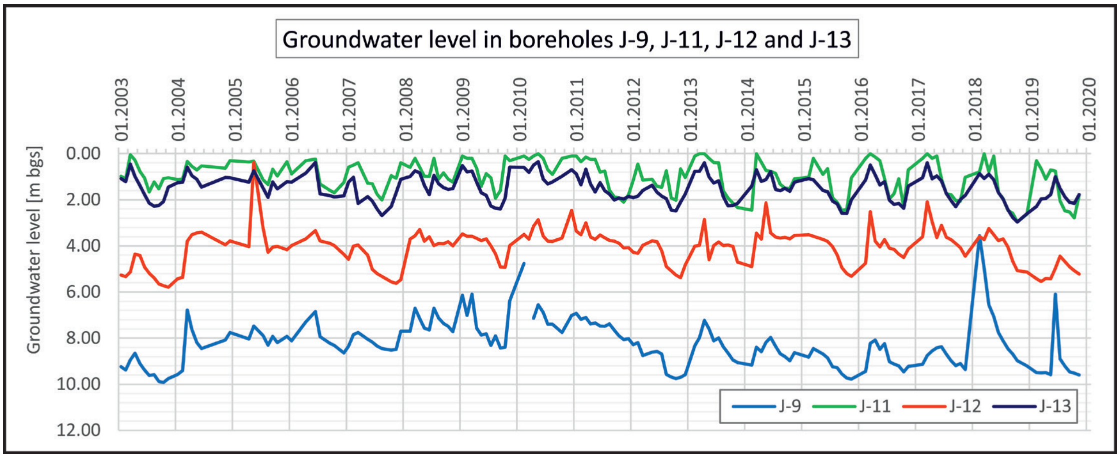


**Fig. 6.** Graphs of groundwater levels in boreholes J-9, J-11, J-12 and J-13.

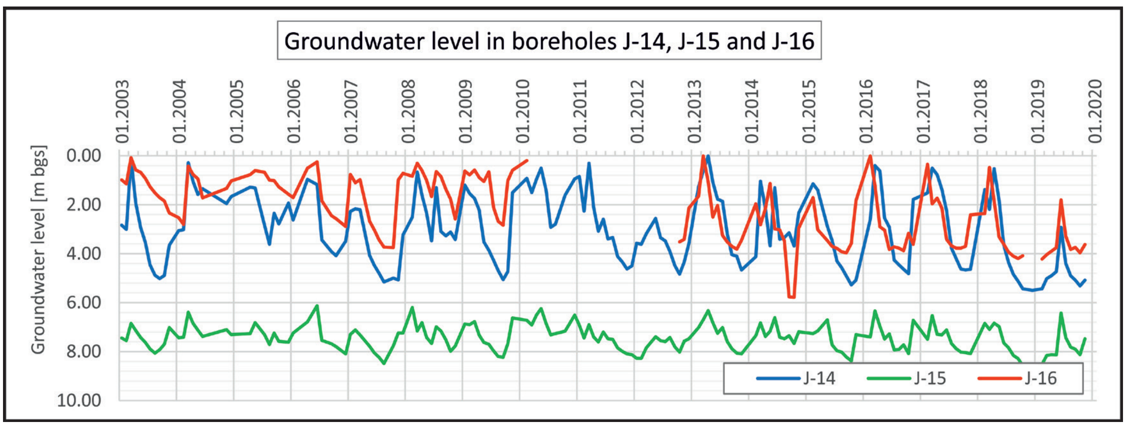


**Fig. 7.** Graphs of groundwater levels in boreholes J-14, J-15 and J-16.

**Tab. 5**
Results of MK-test for set of measurements of groundwater levels.

| Mann-Kendall test | Monitored boreholes | | | | | | | | | | |
|---|---|---|---|---|---|---|---|---|---|---|---|
| | J-4 | J-5 | J-6 | J-7 | J-9 | J-11 | J-12 | J-13 | J-14 | J-15 | J-16 |
| n | 162 | 162 | 124 | 161 | 161 | 162 | 162 | 162 | 162 | 162 | 136 |
| α | 0.05 | 0.05 | 0.05 | 0.05 | 0.05 | 0.05 | 0.05 | 0.05 | 0.05 | 0.05 | 0.05 |
| S | 2185 | 2560 | 1833 | 2928 | 2391 | 1727 | -396 | 1781 | 2236 | 1719 | 3969 |
| Var(S) | 476671 | 476648 | 214190 | 467908 | 467931 | 476356 | 476647 | 476656 | 476695 | 476632 | 282511 |
| $\sigma_S$ | 690.414 | 690.397 | 462.807 | 684.038 | 684.055 | 690.185 | 690.397 | 690.403 | 690.431 | 690.386 | 531.518 |
| Zs | 3.163 | 3.707 | 3.958 | 4.279 | 3.494 | 2.501 | -0.572 | 2.578 | 3.237 | 2.488 | 7.465 |
| p | 0.00156 | 0.00021 | 0.00008 | 0.00002 | 0.00048 | 0.01239 | 0.56723 | 0.00993 | 0.00121 | 0.01283 | 8.3E-14 |
| trend | YES | YES | YES | YES | YES | YES | NO | YES | YES | YES | YES |

**Tab. 6**
Calculation results of Sen's slope for set of groundwater level measurements.

| Sen's slope | Monitored boreholes | | | | | | | | | | |
|---|---|---|---|---|---|---|---|---|---|---|---|
| | J-4 | J-5 | J-6 | J-7 | J-9 | J-11 | J-12 | J-13 | J-14 | J-15 | J-16 |
| trend (MK) | YES | YES | YES | YES | YES | YES | NO | YES | YES | YES | YES |
| α | 0.05 | 0.05 | 0.05 | 0.05 | 0.05 | 0.05 | | 0.05 | 0.05 | 0.05 | 0.05 |
| N | 13041 | 13041 | 7626 | 12879 | 12880 | 13041 | | 13041 | 13041 | 13041 | 9180 |
| $\sigma_S$ (MK) | 690.414 | 690.397 | 462.807 | 684.038 | 684.055 | 690.185 | | 690.403 | 690.431 | 690.386 | 531.518 |
| Zα(MK) | 1.960 | 1.960 | 1.960 | 1.942 | 1.960 | 1.960 | | 1.960 | 1.960 | 1.960 | 1.960 |
| k | 1353.19 | 1353.15 | 907.09 | 1328.35 | 1340.72 | 1352.74 | | 1353.16 | 1353.22 | 1353.13 | 1041.76 |
| β | 0.0053 | 0.0038 | 0.0090 | 0.0050 | 0.0063 | 0.0035 | | 0.0027 | 0.0088 | 0.0023 | 0.0206 |
| β-lower | 0.0021 | 0.0019 | 0.0044 | 0.0029 | 0.0028 | 0.0005 | | 0.0007 | 0.0033 | 0.0005 | 0.0154 |
| β-upper | 0.0083 | 0.0056 | 0.0128 | 0.0071 | 0.0095 | 0.0063 | | 0.0048 | 0.0136 | 0.0042 | 0.0252 |
| Δh[m] | 0.9 | 0.6 | 1.1 | 0.8 | 1.0 | 0.6 | | 0.4 | 1.4 | 0.4 | 2.8 |
| Δh-lower | 0.3 | 0.3 | 0.5 | 0.5 | 0.5 | 0.1 | | 0.1 | 0.5 | 0.1 | 2.1 |
| Δh-upper | 1.3 | 0.9 | 1.6 | 1.1 | 1.5 | 1.0 | | 0.8 | 2.2 | 0.7 | 3.4 |

data files, the slope of trend β was then calculated by using Sen's slope method – it is regression line slope.

*Set of drainage boreholes measurements*

Statistical file of data from boreholes for underground drainage of area covers period from the end of 2001 until the start of 2019. For simplification, data are covered for 5 outposts, where the water is collected, drained from the area by subhorizontal drainage boreholes in count of 3–5 boreholes for outpost. Summary figure for outpost is formed as a sum of outflows from each borehole. Set of measurements for examined period is plotted in following graph (Fig. 8):

Trend analysis was realized similar to groundwater levels by MK-test. When testing, the hypothesis $H_0$ was in each of 5 cases denied and statistically important trend on the significance level α = 0,05 was confirmed (Tab. 7). By using of Sen's method, for each outpost, trend regression line direction was calculated. Results are listed in tables 5 and 6.

## Discussion

According to SHMI study (Zeleňáková et al., 2016), time series of rain precipitations in Slovak rain gauge stations have mostly growing trend, mainly in July. Analysis of annual trend of time series of rain gauges by means of MK-test has identified statistically important trend in 452 from 487 evaluated rain gauge stations of SHMI, which is 93 % of evaluated stations. Important negative trends were indentified in northern part of Slovakia, near Orava water reservoir, important positive trends were indentified all across Slovakia.

Based on our processed statistical file of monthly precipitations from Slanská Huta station, the growing trend was not confirmed, in the 95 % interval of reliability, the data appear as random and independent. This reality

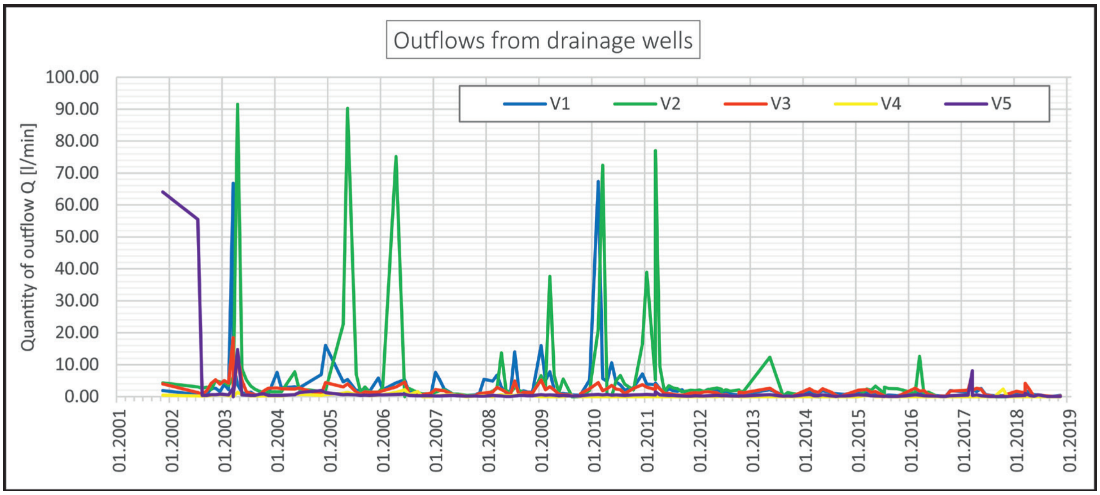


**Fig. 8.** Graphs display of outpot outflows – each outpot V1–V5 consists of 2–5 subhorizontal drainage boreholes (their location is visualized in Fig. 3).

**Tab. 7**
Results of MK-test for set of measurements of drainage wells outflows.

| Mann-Kendall test | Names of drainage boreholes groups | | | | |
|---|---|---|---|---|---|
| | V1 | V2 | V3 | V4 | V5 |
| n | 151 | 150 | 150 | 150 | 150 |
| α | 0.05 | 0.05 | 0.05 | 0.05 | 0.05 |
| S | -3485 | -4187 | -2951 | -4894 | -4057 |
| Var(S) | 386285 | 371863 | 378669 | 309256 | 378511 |
| $\sigma_S$ | 621.518 | 609.806 | 615.361 | 556.108 | 615.232 |
| Zs | -5.606 | -6.864 | -4.794 | -8.799 | -6.593 |
| p | 2.07E-08 | 6.67E-12 | 1.64E-06 | 1.38E-18 | 4.32E-11 |
| trend | YES | YES | YES | YES | YES |

**Tab. 8**
Results of Sen's slope for measurements set of drainage boreholes outflows.

| Sen's slope | Names of drainage boreholes groups | | | | |
|---|---|---|---|---|---|
| | V1 | V2 | V3 | V4 | V5 |
| trend (MK) | YES | YES | YES | YES | YES |
| α | 0.05 | 0.05 | 0.05 | 0.05 | 0.05 |
| N | 11325 | 11175 | 11175 | 11175 | 11175 |
| $\sigma_S$ (MK) | 621.518 | 609.806 | 615.361 | 556.108 | 615.232 |
| Zα(MK) | 1.960 | 1.960 | 1.960 | 1.960 | 1.960 |
| k | 1218.15 | 1195.20 | 1206.08 | 1089.95 | 1205.83 |
| β | -0.0128 | -0.0190 | -0.0102 | -0.0017 | -0.0027 |
| β-lower | -0.0183 | -0.0265 | -0.0150 | -0.0026 | -0.0035 |
| β-upper | -0.0078 | -0.0132 | -0.0057 | -0.0006 | -0.0020 |
| ØQ [l/min] | 3.15 | 5.51 | 1.80 | 0.20 | 1.33 |
| ΔQ [l/m] | -1.9 | -2.8 | -1.5 | -0.3 | -0.4 |
| ΔQ-lower | -2.8 | -4.0 | -2.3 | -0.4 | -0.5 |
| ΔQ-upper | -1.2 | -2.0 | -0.9 | -0.1 | -0.3 |

had to be taken into account while evaluation other parts of regime measurements.

Generally assumed, these measured values of regime measuremens are dependent on amount of rain precipitations. However, in this case no correlation analysis was performed, because for its correct realization, data with comparable method of collection were required, which is not the case. When comparing timelapse data, such as monthly rain precipitations with point data, like groundwater measurements in monthly intervals, inaccuracies can appear, which can discard the analysis. But results of unparametrical trend analysis can be compared regardless of input data character.

Despite the fact that we assume dependence of groundwater levels on amount of precipitations and data file shows no trend, in a set of groundwater level measurements the increasing trend was confirmed in the vast majority of evaluated boreholes. Because those data present depth of groundwater levels – that means distance of level from the surface, the increasing trend means that groundwater levels are decreasing in time. After recalculation of Sen´s slope β (trend line guideline), it is possible to quantify this trend and calculate statistical decrease of groundwater level in each borehole during the measured period. This value is in the range between 0.4 m in the borehole J-13 up to 2.8 m in the borehole J-16T (credibility of value in J-16 is debatable, because borehole had collapsed during measurements and on its place a new borehole was drilled to restore functionality of remediation messures). Average statistical decrease of the groundwater level for the whole measured period is 1.0 m, while within the interval of reliability 95 % it can reach value from 0.5 to 1.5 m. Despite the results are relatively favourable, they are quite unexpected, because in general, remediation issues lose their effectiveness after some time and there is rather an repeated increase in the groundwater level.

Decreasing amount of the water, drained by remediation issues from the measured area is observable from the trend analysis of outflow from drainage boreholes. It should be noted, that in original data file of each borehole a large variance of values is evident, because some boreholes, strongly responsive to precipitations, can in short amount of time drain water from rock enviromnent with outflow 100-times bigger, than is its average outflow. These are mainly boreholes V2 and V4, where the outpost was often flooded over the outlet because of high outflow, so the immediate outflow was only estimated. This is why high values (over 100 l/min) were omitted from tested file. Considering, that high values were omitted throughout the period of data collection and considering the unparametrical character of the test, we do not expect important affect of its results.

The MK-test demonstrated in all groups of drainage boreholes statistically important decreasing trend – the groundwater levels in rock environment were decreasing in time. Applying the Sen´s slope calculation we tried to quantify this proces. After recalculation on the whole period of data collection, 37 % statistical decrease of outflow has occured, representing a decrease of outflow by 5.3 l/min at average outflow by 14.3 l/min. By using calculations of Sen´s slope for 95 % confidence interval, it can be stated, that statistical decrease of the outflow in drainage boreholes can reach values in interval from 2.4 to 8.5 l/min, which corresponds to 20–60 % decrease. It can be assumed, that decreasing outflow of drainage boreholes relates with their clogging (colmatation), or there is a relation with total statistical decrease of the groundwater volume in rock environment of the landslide area?

## Conclusion

Trend analysis proved decreased outflow of drainage boreholes during the measurement period by 37 % in average. It also confirmed decrease in the groundwater levels in almost all measured boreholes by 1 m during whole measured period in average. As the decreasing trend of rain precipitations was not confirmed, there must be another explanation of this phenomenon:

It is possible, that groundwater in the measured area had the character of static volumes (Mika & Boľha, 2000) and remediaton measures caused their gradual drainage.

The groundwater levels had lowered under level, which can be reached by drainage boreholes.

Because under the regime observations, effectiveness of surface measurements was not evaluated – surface drain and drainage ribs, proposed together with deep drainage of the groundwater (Mika & Boľha, 2000). It is possible, that they result into important decrease in transporting of the rainwater into the rock.

Based on meteorological observations, there is some change in climate (Zeleňáková et al., 2016) – and even if there was not confirmed decreasing trend of amount of rain precipitations, their character can change – the torrential rains are becoming more frequent, where the rainwater drains more frequently on the surface (with a significant contribution of the surface remediation measures) and less intensive subsidizes the rock environment.

Despite the fact that long-term trends indicate positive state in the development of hydrogeological situation of the landslide area, emergency situations arise during extreme weather fluctuations. It is necessary to keep, or even increase the capacity of drainage units, so they can sustain the extreme situations and drain even the extreme amount of the rain precipitations away from the landslide area.

**Acknowledgement.**

Authors express their thanks to reviewers M. Bednarik and M. Briestenský for high-quality remarks and suggestions to primary manuscript which increased its quality.

## References

Gibbons, R. D., Bhaumik, D. K. & Aryal, S., 1955: Statistical methods for groundwater monitoring. *New York, Wiley, 366 p.*

Helsel, D. R. & Hirsch, R. M., 1992: Statistical methods in water resources. Part 12: Trend analysis. *Stud. Environ. Sci., 49, 323–355.*

Mazúr, E. & Lukniš, M., 1986: Geomorfologické členenie SSR a ČSSR. Časť Slovensko. In: Atlas Slovenskej socialistickej republiky. *Bratislava, Slovenská kartografia* (in Slovak and English).

Mika, R. & Boľha, Ľ., 2000: Záverečná správa z podrobného inžinierskogeologického prieskumu „Slanec". *Manuscript. Bratislava, archive SPP* (in Slovak).

Ondrejka, P., Petro, Ľ., Iglárová, Ľ., Liščák, P., Dananaj, I., Mašlár, E., Mašlárová, I., Ondrášiková, B., Magalová, D., Ondrus, P. & Wagner, P., 2017: Čiastkový monitorovací systém – Geologické faktory, Podsystém 01 Zosuvy a iné svahové deformácie, Správa za rok 2017. *Manuscript. Bratislava, archive St. Geol. Inst. D. Štúr* (in Slovak).

Önöz, B. & Bayazit, M., 2003: The power of statistical tests for trend detection. *Turkish J. Eng. Envi. Sci., 27, 247–251.*

Zeleňáková, M., Purczb, P., Poórovác, Z., Alkhalafd, I., Hlavatá, H. & Portelaf, M. M., 2016: Monthly trends of precipitation in gauging stations in Slovakia. *Proc. Engineer., 162, 106–11.*

# Trendová analýza hydrogeologických parametrov zosuvného územia v trase tranzitného plynovodu európskeho významu pri obci Slanec

Príspevok sa zaoberá hodnotením časových zmien parametrov charakterizujúcich hydrogeologickú situáciu v zosuvnom území v blízkosti obce Slanec. Údaje boli namerané v rámci režimových pozorovaní v rokoch 2003 – 2019. Závery z týchto hodnotení môžu prispieť k celkovému posúdeniu stavu a funkčnosti realizovaných sanačných opatrení, ako aj aktuálnej situácie monitorovaného zosuvného územia.

Obec Slanec leží na južnej strane Slanských vrchov na svahoch stratovulkánu Milič v rozsiahlom zosuvnom území (obr. 2), ktorým prechádza trasa dôležitých podzemných a nadzemných vedení. V tejto súvislosti bola lokalita Slanec v roku 2003 zaradená do súboru monitorovaných lokalít v rámci projektu *Čiastkový monitorovací systém – Geologické faktory* (ČMS GF). ČMS GF tvorí neodmysliteľnú súčasť národnej environmentálnej monitorovacej siete so zameraním na tzv. geologické hazardy – škodlivé prírodné alebo antropogénne geologické procesy ohrozujúce prírodné prostredie a človeka.

Geodynamické procesy prebiehajúce na tomto území je možné klasifikovať ako veľmi pomalé svahové pohyby, podstatne ovplyvnené podzemnou vodou (Míka a Boľha, 2000). Monitorovacie práce vykonávané v súčasnosti sa preto sústreďujú na hydrogeologické parametre územia – merania zmien výšky hladiny podzemnej vody vo vrtoch a výdatnosti odvodňovacích zariadení, realizovaných v rámci sanácie geologického prostredia, čím sa overuje ich funkčnosť (Ondrejka et al., 2017).

V rámci režimových pozorovaní sa na lokalite Slanec monitoruje hladina podzemnej vody v 11 pozorovacích vrtoch a meria sa výdatnosť 20 odvodňovacích zariadení (subhorizontálnych odvodňovacích vrtov) sústredených do 5 stanovíšť (obr. 3). Súbor údajov je doplnený o mesačné zrážkové úhrny z blízkej meteorologickej stanice Slanská Huta, poskytované Slovenským hydrometeorologickým ústavom (SHMÚ).

Jedným z cieľov vyhodnotenia režimových meraní je preukázanie prítomnosti štatisticky významných trendov v časových radoch monitorovaných údajov.

Z rôznych štatistických postupov používaných na analýzu časových radov vhodných na spracovanie environmentálnych údajov (Gibbons et al., 1955) je najbežnejší neparametrický Mannov-Kendallov trendový test (MK-test). Tento typ testu bol široko aplikovaný na analýzy trendov v environmentálnych vedách a jeho výsledky sa ukázali veľmi konzistentné (Önöz a Bayazit, 2003).

Posúdenie štatistickej významnosti trendu sa robí testovaním hypotéz. V trendovom MK-teste sa testuje nulová hypotéza ($H_0$), ktorá predpokladá, že v testovanom súbore neexistuje trend a že údaje sú náhodné a nezávislé. Alternatívnou hypotézou ($H_1$) je, že v testovanom súbore trend existuje. Stanovenie veľkosti preukázaného štatisticky významného trendu je možné realizovať výpočtom Sen-koeficientu. Senova metóda predpokladá lineárny trend v časových radoch a široko sa využíva na určenie veľkosti trendov napr. v hydroklimatických časových radoch (Zeleňáková et al., 2016).

### Výsledky štatistickej analýzy

Súčasťou trendovej analýzy režimových pozorovaní v rámci ČMS GF sú mesačné úhrny zrážok zo zrážkomernej stanice Slanská Huta poskytnuté SHMÚ (obr. 4).

Podľa výpočtov v testovanom dátovom súbore mesačných a ročných zrážkových úhrnov z tejto stanice nebol preukázaný štatisticky významný trend na hladine významnosti $\alpha = 0{,}05$. Prezentované údaje majú teda charakter nezávislých a náhodných údajov.

Ďalšou skupinou testovaných údajov sú periodické mesačné merania výšky hladiny podzemnej vody (HPV) na 11 pozorovacích vrtoch, zhromažďované od roku 2003. Tieto údaje predstavujú z každého vrtu súbor údajov v rozsahu do 162 meraní, dostatočný na celkové zhodnotenie dlhodobého trendu (tab. 5). Ako je evidentné, trend na štatisticky významnej úrovni (pokles HPV) sa potvrdil v 10 z 11 prípadov. Z týchto dátových súborov bol následne Senovou metódou vypočítaný sklon trendu $\beta$ – smernica regresnej priamky (tab. 6).

Poslednou skupinou testovaných údajov je štatistický súbor údajov zo zariadení na podpovrchové odvodňovanie územia. Súbor zahŕňa údaje za obdobie od konca roka 2001 do začiatku roka 2019. Údaje sa kvôli zjednodušeniu vzťahujú na 5 stanovíšť – V-1 až V-5, na ktoré sa sústreďuje voda odvádzaná z územia subhorizontálnymi odvodňovacími vrtmi (SHV), a to v počte 3 – 5 vrtov na stanovište. Pri testovaní hypotézy $H_0$ bola pri všetkých 5 prípadoch táto hypotéza zamietnutá a potvrdil sa štatisticky významný trend – pokles výdatnosti (tab. 7). Senovou metódou bola za každé stanovište vypočítaná smernica regresnej priamky trendu (tab. 8).

## Diskusia

Napriek tomu, že predpokladáme závislosť HPV od množstva zrážok a dátový súbor úhrnov zrážok nevykazuje žiaden trend, v súbore meraní hladín podzemnej vody sa štatisticky významný trend potvrdil v prevažujúcej väčšine hodnotených vrtov. Vypočítaním Senovho koeficientu $\beta$ (smernice trendovej priamky) bol kvantifikovaný priemerný štatistický pokles hladiny podzemnej vody – jeho priemerná hodnota za celé merané obdobie je približne 1,0 m, pričom v rámci intervalu spoľahlivosti 95 % môže nadobudnúť hodnotu z intervalu od 0,5 až do 1,5 m.

Pokles množstva vody odvádzanej odvodňovacími opatreniami z monitorovanej oblasti je badateľný z trendovej analýzy výdatnosti odvodňovacích vrtov. MK-test preukázal pri všetkých skupinách odvodňovacích vrtov štatisticky významný klesajúci trend. To znamená, že množstvo vody odvádzanej z horninového prostredia postupom času klesá. Použitím Senovho výpočtu sme sa pokúsili tento pokles kvantifikovať. Po prepočítaní na celé obdobie zberu údajov došlo k štatistickému poklesu výdatnosti v priemere o 37 %.

Keďže sa nepotvrdil klesajúci trend množstva zrážok, klesajúce trendy HPV a výdatnosti SHV sú v rozpore s predpokladom závislosti hydrogeologických parametrov od množstva zrážok. Tento jav môže mať viacero vysvetlení:

- podzemná voda v skúmanom území mala z veľkej časti charakter statických zásob a sanačnými opatreniami bola postupne odvedená,
- hladina podzemnej vody vplyvom hĺbkovej drenáže poklesla v okolí odvodňovacích vrtov pod úroveň, z ktorej odvodňovacie vrty vodu drénujú,
- vplyvom povrchových odvodňovacích zariadení (navrhovaných spolu s hĺbkovým odvedením podzemnej vody – ich účinnosť sa v rámci režimových pozorovaní nehodnotila) sa významne znižuje prestup zrážkovej vody do horninového prostredia,
- zmena charakteru zrážok – čoraz častejšie sa vyskytujú krátko trvajúce prívalové dažde, keď zrážková voda vo významnejšej miere odteká po povrchu (za výrazného prispenia povrchových sanačných opatrení) a menej dotuje horninové prostredie.

Napriek tomu, že dlhodobé trendy indikujú priaznivý stav vo vývoji hydrogeologickej situácie zosuvného územia, havarijné stavy vznikajú častejšie pri extrémnych výkyvoch počasia. Je nevyhnutné udržiavať kapacitu odvodňovacích zariadení a ak je to možné, aj ju zvyšovať, aby zvládli náporové situácie a rýchlo odviedli aj extrémne množstvo zrážok preč zo zosuvného územia.

Doručené / Received: 4. 5. 2020
Prijaté na publikovanie / Accepted: 11. 8. 2020

*Mineralia Slovaca, Web ISSN 1338-3523, ISSN 0369-2086*
*52, 1 (2020), 57 – 62,* 

# Calculating minor constituents in synthetic corundum abrasives

IVAN TURNOVEC[1] and ĽUDMILA ILLÁŠOVÁ[2]

[1] Drahokam Turnov, Turnov, Czech Republic
[2] Constantine the Philosopher University in Nitra, Slovak Republic

**Abstract:** Electromelted corundum and SiC are the most frequently used industrial abrasives. The final products of electromelting of $Al_2O_3$ and bauxites contain contaminants. Their content and present glass phases adversely affect the functional properties of the abrasives. It is shown that the content of the contaminants can be calculated from chemical analysis. The calculation is similar to that used to determine the theoretical analysis of clay and other raw materials for the manufacture of ceramics (e.g. calculation by Kollauner-Matejka). An example of such calculation is shown in the case of the brown i.e. the most common corundum and the results are compared with those, obtained by microscope analysis as a reference. These calculations can be used for quality control during production and also for monitoring of quality changes during research and development of new types of electro corundum. The computed compositions are in good agreement with those found by the microscope analysis. The content of the contaminants was also monitored as a function of particle size of the abrasives. A certain correlation was observed between the crystal size and the classification method of the particle size. The content of the deleterious contaminants decreased with decreasing size of the crystals from large to medium whilst it increased as the crystals further decreased from medium to fine particles; it could reach up to 20 % in the worst case.

**Key words:** synthetic corundum abrasives, cracking grinding wheels, brown corundum, mineral composition, calculating

**Graphical abstract**

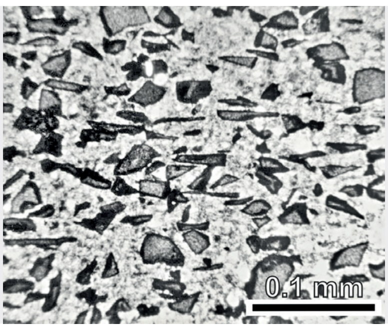


**Highlights**

- Electromelting of $Al_2O_3$ and bauxites at production of corundum and SiC, as the most frequent industrial abrasives, produces contaminants.
- The content of the contaminants can be calculated from chemical analysis (e.g. Kollauner-Matejka calculation method), which results are in good agreement with those from microscope analysis.

## Introduction

Each abrasive tool consists of abrasive grains, their bond and pores, i.e. components of a solid and gasiform nature. Abrasive grains represent a special mineral phase and the bond is either anorganic, for example the synthetic resin, or the rubber-based materials. The variability of individual components is great. Their properties and distribution in the abrasive tool directly affect also its physical-mechanical properties. Petrological and mineralogical procedures have made it possible to solve some technological problems of many years and to integrate the control methods for verifying the quality of abrasive grains.

### Definition of abrasive materials and abrasive tools

The abrasive can only be a material with higher hardness than the material we want to work with and which is rigid enough to withstand the mechanical destruction. The abrasive tool can also be described as the abrasive grains connected with a metal, ceramic, glass or organic bond. These grains are connected in a defined geometric shape, most frequently as an abrasive wheel. The parameters that define the quality of abrasive tool at present are as follows: (a) type of abrasive; (b) type of bond; (c) abrasive grain size; (d) shape of abrasive grains; (e) hardness of the tool (which means the resistance of abrasive grain to mechanical break out of the wheel); (f) structure of the tool determined by pore volume or volume of abrasive grains used.

### Type of abrasive

An abrasive is a material that indicates the same or greater hardness than the workpiece and is resistant to temperature and chemical reactions. In the past, silicious sand, garnet and emery (a natural rock made of corundum) were used as abrasives, later joined by the diamond dust.

During the industrial revolution in the 18th and 19th centuries, following the requirements of the evolving technologies, the synthesis of hard substances was achieved (Baumann, 1962; Kamencev, 1950; Polubelova et al., 1968; Novotný & Turnovec, 1967; Turnovec, 1971; Hořínek & Turnovec, 1970; Turnovec & Illášová, 2009, 2011).

An overview of the main natural and synthetic types of abrasives can be seen in Chart 1. The hardest abrasive is diamond, the softest one is quartz. The methodology of studying abrasive materials when it comes to preparation and making cuts is a rather complex. Therefore, a methodology of studying the cuts was developed. The first researchers who studied the cuts in the reflected light were Filonenko and Lavrov (1958). In the following text we focus on silicon carbide and corundum abrasives as well as on abrasive tools.

**Silicon carbide (SiC, carborundum)** was independently synthesized by Acheson (1892) and Schützenberger (1892). Acheson´s technology is still in use today (Turnovec & Kleander, 1970; Kleander, 1971). It is produced in the electric resistance furnaces bearing the Acheson´s name and it is made of silicious sand and carbon raw material, which is a petroleum coke (Fig. 1). It has been experimentally demonstrated that the initial temperature for SiC formation is 1200–1400 °C. The main reactions and formation of α-SiC occur in the range of 1700–2300 °C.

**The electro-melted corundum**, as an essential raw material for the production of abrasive grains, contains, in addition to the corundum phase, also other accompanying minerals and their total content may exceed 10 %. The basic types of corundum abrasive materials are:

a) monocorundum (named as Alucryst special);
b) brown corundum (also known as Normalcorundum) and its microcrystalline modification;
c) white corundum (named as Elektrit, Alundum, etc.);
d) red corundum (called Rubin);
e) alloyed corundum (also known as zirconium, vanadium, manganese-titanium corundum, etc.).

Monocorundum is made by crystallization of $Al_2O_3$ dissolved in a sulphide melt by melting a mixture of bauxite or industrial aluminum oxide with a suitable sulphide (most often pyrite) in an electric furnace. This production was patented by Hagelund in 1922 and the technology is still used today. Unlike other corundum materials, monocorundum is chemically the cleanest material with the best cutting properties. The main raw material for brown corundum is bauxite. The white corundum is produced without any additives, while adding $Cr_2O_3$ produces the red corundum and adding other additives participate in producing other alloyed corundums.

For corundums produced by melting an industrial alumina, the main pollutant is β-corundum and the glass phase. The influence of other accompanying components is negligible. During the crystallization process in alloyed corundums, adulterants (e.g. baddeleyte in Zr-corundum) often appear as the catalyzers that favorably influence the resulting structure and increase the toughness of the resulting abrasive. For brown corundum made from bauxites, the detrimental accompanying components are carbides and titanium nitrides, formed during over-reduction of the bauxite melt. These components, although only in the trace content, significantly increase their volume C in the critical temperature range of 500–600 ºC and cause their destruction. The formation of accompanying components can be quantified from the chemical composition. An indicator is that, in addition to nitrides and carbides, the greater quantities of anorthite or mullite glass phase are formed. On the contrary, the presence of titanium in the structural lattice of corundum crystals is a benefit because during the burning, the toughness of the abrasive grains is increasing.

## Mineral composition and properties of abrasive grains

The functional properties of corundum abrasive grains are influenced both by the composition and structure of the melting products and by the technology of their production. In general, the quality of all abrasive grains is determined by their size and granularity, mechanical strength, shape, mineral composition and structure, and by the content of inclusions (metal and magnetic particles). Standard ČSN 224012 defines an abrasive grain as a crystal or abrasive material particles whose width do not exceed 5 mm and the ratio of the largest dimension to the smallest does not exceed 90 % of the grains.

The influence of the mineral composition of abrasive grains was studied for addressing the causes of cracking the abrasive tools (with ceramic bonding) already during the burning. During the burning, not only a ceramic bonding mass is formed, but also mutual reactions between the abrasive grains and the liquid phase of the bond can be noticed. The gradual heating results in the diffusion of $Al_2O_3$, which is caused by the aggressiveness of the alkali oxides of bond, especially by $Na_2O$, represented in congruently forming liquid phase (Turnovec, 1984).

## Cracking of ceramically bonded brown corundum grinding wheels

On cracked wheels, the boundaries between grains and bond were observed – first under binoculars, later on polished sections in the reflected light. It has been shown that the cracks are present in the grain-bond interface as well as within the grains themselves. In the wheels around the cracks already formed during burning, kidney-like formations, later identified as anosovite and rutile, were found on the grain surface and at the points of cracking. These are impurities (oxygen-free titanium compounds), which, during oxidation burning between 500–600 ºC, extremely increase their volume and cause anomalous expansion of the abrasive grains. This is the evidence that the bauxite used was over-reduced during melting of brown corundum (which was a fatal mistake; water infiltrating the bauxite was up to 11 %, which caused the over-reduction with the same total amount of bauxite and reducing agent).

The functional properties of the abrasive depend on the content of the accompanying components (mainly β-corundum in white and hexaaluminate in brown corundum or glass phases). Similar to the rational analyses of ceramic raw materials (e.g. Kollauner-Matějka calculations), the mineral composition of corundums can be calculated. As an example, calculations for brown corundum are given. Its melting conditions are close to equilibrium. They take place in the liquid phase and the subsequent crystallization is sufficiently slow. Crystallization occurs in the CaO – $Al_2O_3$ – $SiO_2$ system, near the $Al_2O_3$ peak (Fig. 1). According to the Rankin's diagram (Filonenko & Lavrov, 1958), three final crystallization products are possible:

I. corundum; mullite; anorthite;

II. corundum; anorthite;

III. corundum, calcium hexaaluminate; anorthite.

This is a simplification that does not take into account the other accompanying components, which are the MgO and $TiO_2$ compounds, mostly the spinellides and taosite. The proportion of spinellides is only trace to negligible, but, most importantly, it does not affect functional properties. The situation is different for titanium compounds (Turnovec, 1969, 1971, 1982a). A crystallization diagram is shown in Fig. 2.

From the simple ratio of oxides bound to individual components, it is clear that the most preferred melting product is the one in which, in addition to corundum, only anorthite is present. The least preferred is a melt allowing the formation of hexaluminate. Based on the steichiometric ratios of the individual oxides, the proportions of the main components can be calculated from the analytical data. Chemical analysis is a part of quality control and one of the basic quality parameters and is listed in the Czechoslovak Standard ČSN 22 4044. Material conforming to ČSN standard can have a very variable mineral composition thus relating to its functional properties.

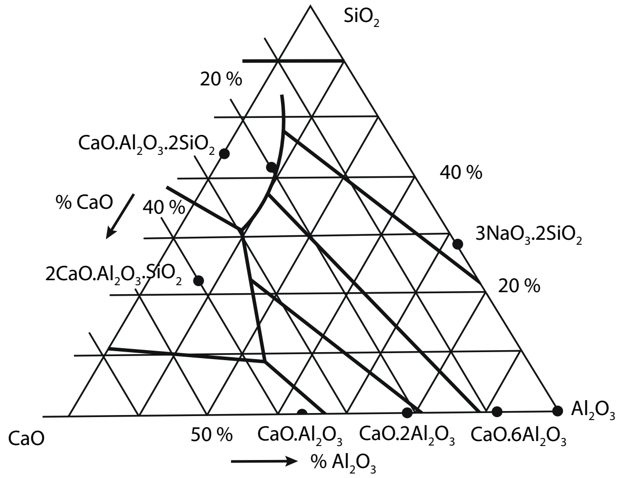


**Fig. 1.** Three phase diagram CaO – $Al_2O_3$ – $SiO_2$, near the top of the $Al_2O$ (Filonenko & Lavrov, 1958).

The originally proposed calculation method (Turnovec, 1970) was quite demanding. During practical use it was simplified and made more effective (Turnovec, 1982b). *Denoting variables and auxiliary variables:*

A. $Al_2O_3$ content determined by analysis;

B. $SiO_2$ content determined by analysis;

C. $TiO_2$ content determined by analysis;

D. CaO content determined by analysis.

H1 – content of $Al_2O_3$ in anorthite; H2 – content of $Al_2O_3$ in calcium hexaaluminate; H3 – content of $Al_2O_3$ in mullite; H4 – content of $Al_2O_3$ in taosite.
*Resulting variables:*
AN = anorthite content in %; MUL = mullite content in %; HXL = hexaaluminate content in %; TA = taosite

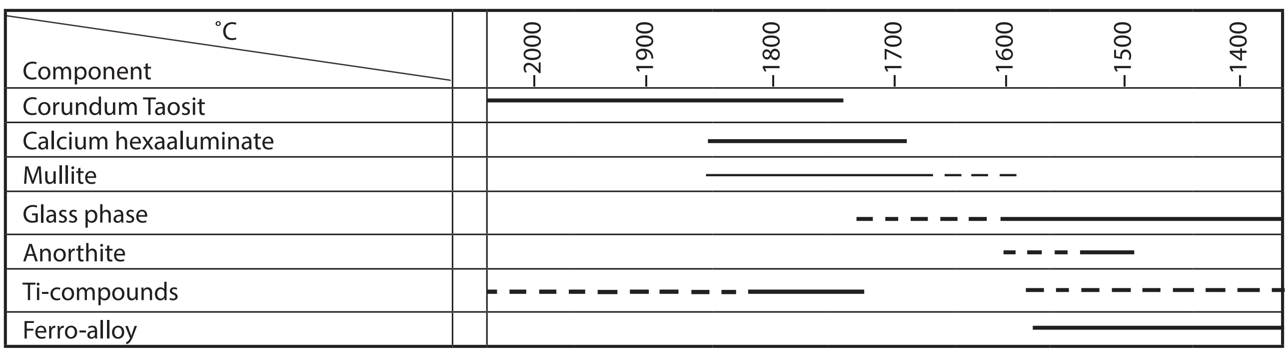


**Fig. 2.** The situation is different in the presence of compounds containing titanium (Turnovec, 1969, 1971, 1982a).

content in %; KC = corundum content in %; KF = physical corundum content, i.e. with taosite in %; KM = corundum module, i.e. ratio of $Al_2O_3$ content in corundum phase to $Al_2O_3$ content in accompanying components.

### Method for calculating mineral composition

**The first step** – deciding the ratio D : B (CaO : $SiO_2$).

There are three possibilities:

a) the ratio is greater,

b) the ratio is 0.467,

c) the ratio is smaller.

**The second step**

possibility a)

AN = 1.58 × B × 1.467;

H 1 = AN – B × 1.467;

HXL = 11.91 × (D – 0.467 × B);

H 2 = HXL – (D + 0.467 × B).

Possibility b)

AN = 1.58 × (B + D);

H 1 = AN – B × 1.467.

Possibility c)

AN = 1.58 × D × 3.142;

H 1 = AN – 3.142 × D;

MUL = 3.546 × (B – 2.141 × D);

H 3 = MUL – (B + 2.141 × D).

**The third step – a futher calculation common to all three**

TA = 2,276 × C;

H 4 = TA – C;

KC = A – (H 1 + H 2 + H 4);

KF = KC + TA.

**The fourth step** – a calculation of the corundum module

KM = (KF – C) : (H 1 + H 2 + H 3)

Key to the variables and auxiliary variables used:

A. $Al_2O_3$ content from the analysis;

B. $SiO_2$ content from the analysis;

C. $TiO_2$ content from the analysis;

D. CaO content from the analysis.

H 1 – $Al_2O_3$ content in anorthite;

H 2 – $Al_2O_3$ conte nt in calcium hexaaluminate;

H 3 – $Al_2O_3$ content in mullite;

H 4 – $Al_2O_3$ content in taosite.

**The resulting variables:**

AN = content of anorthite in %;

MUL = content of mullite in %;

HXL = content of hexaaluminate in %;

TA = content of taosite in %; KO = content of corundum in %;

KF = content of physical corundum (total $Al_2O_3$ incl. taosite) in %;

KM = corundum modulus i.e. a ratio between $Al_2O_3$ in the corundum phase and $Al_2O_3$ in the remaining constituents.

**Tab. 1**
Mineral composition of brown corundum calculated from analytical data and determined microscopically.

| Mineral composition of brown corundum calculated from analytical data and determined microscopically | | | | | | | | | | | | | | |
|---|---|---|---|---|---|---|---|---|---|---|---|---|---|---|
| | Chemical composition | | | | Calculation of mineral composition | | | | | | | Microscopic analysis | | |
| sample | $Al_2O_3$ | $SiO_2$ | $TiO_2$ | CaO | AN % | MUL % | HXL % | TA % | KC % | KF % | KM | Corundum % | Calcium hexaaluminate | Glass phase* |
| 1 | 96.88 | 0.94 | 1.09 | 0.64 | 2.18 | - | 2.39 | 2.48 | 93.37 | 95.86 | 27.03 | 93.5 | 2.6 | 3.9 |
| 2 | 95.63 | 0.64 | 2.00 | 1.35 | 1.48 | - | 12.52 | 4.55 | 81.64 | 86.19 | 7.38 | 86.2 | 12.3 | 1.5 |
| 3 | 93.79 | 1.82 | 2.90 | 0.84 | 4.17 | - | - | 6.60 | 88.56 | 95.16 | 59.29 | 95.0 | - | 5.0 |
| 4 | 96.79 | 1.06 | 1.35 | 0.55 | 2.46 | - | 0.65 | 3.07 | | 96.64 | | 95.0 | st | 5.0 |
| 5 | 95.06 | 2.50 | 1.80 | 0.17 | 0.84 | 7.57 | - | 4.10 | 87.74 | 91.84 | 17.95 | 90.4 | - | 9.6 |
| 6 | 95.17 | 2.54 | 1.20 | 0.53 | 2.63 | 4.98 | - | 2.73 | 91.37 | 94.10 | 24.45 | 90.5 | - | 9.5 |
| 7 | 94.56 | 0.71 | 2.10 | 1.35 | 1.65 | - | 12.13 | 4.78 | 80.82 | 85.60 | 7.55 | 86.0 | 12.1 | 1.9 |

Notes: The designation of the components of the calculation is kept as for the calculation formulas AN = anortite, MUL = mullite, TA = content of taosite, HXL = calcium hexaaluminium, KC = physical corundum, taosite, KF = content of physical corundum (total $Al_2O_3$ incl. taoiste), KM = corundum modulus i.e. a ratio between $Al_2O_3$ in the corundum phase and $Al_2O_3$ in the remaining constituents.

* The glass phase represents all translucent components filling the spaces between microscopic analyses of corundum crystals, no distinction is made when the main constituents are anortite or mullite about the glass phase.

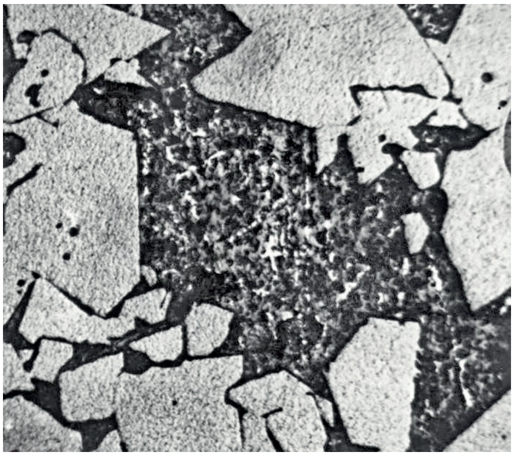

**Fig. 3.** Anorthite glass phase surrounded by corundum (Turnovec, 1982b). Width of view 80 µm.

## Conclusion

The methods and approach of petrologists and mineralogists can significantly help in assessing the properties of abrasives and abrasive tools and many other technical materials, especially in their development. At the end, we summarize some examples where petrology contributed to solving technological problems in the field of abrasives: determination of mineral phases resulting from the production of abrasive materials; determining the structures and size of the crystals formed; solving the technological problem in the production of brown corundum (over-reduction); quantification of mineral composition from analytical data; evaluation of thermal expansion and its elimination by annealing; evaluation of abrasive grain shapes.

Comparison of calculations with microscopic analysis and basic chemical composition is shown in the attached table. As the table shows, the difference between the quantified and microscopically determined composition is only small. Conversions can be used to monitor quality during research work, but also for statistical evaluation of technical production control (Tab. 1). The agreement between the calculated and microscopically determined composition is relatively high.

The contents of the accompanying components were also monitored depending on the size of the abrasive grains. It has also been shown that there is a certain regularity depending on the size of the crystals and the size sorting method. From the largest to the medium grains, the pollutants content decreases, from the medium to the fine grains, pollutants again increase and can reach up to 20 % in the unfavorable case. The study of the polished sections has proved to be very effective in identifying individual mineral phases, but also in the study of the internal construction of abrasive tools and structures as described for natural rocks.

Calculation methods of the rational, i.e. mineral compositions from the chemical composition are quite accurate. The ability to determine the crystallization type by the calculation method (i.e. the presence of anorthite or mullite glass phase as indicators of the presence of other compounds) becomes a useful advantage in evaluating the properties of corundum abrasives and abrasive tools. The quantification of the mineral phases in electro-melted corundum enables to solve not only the abrasive or refractory phases but also technological problems (especially the over-reduction of the melting), which cannot be detected solely by analytical data. Through the computer algorithm, the results are available parallel with the analytical data, which allows technological interventions, increasing or decreasing the reducing agent content in the melt. It is advisable to ensure the formation of the anorthite glass, as the mullite phase increases, a danger of over-reduction of blocks becomes real. Timely quantification and adjustment of the batch brings a significant saving of funds, because the thermal adjustment (modification) of the over-reduced materials is very expensive and unnecessary, if the reduction is managed properly.

**Acknowledgment.**

Authors express their thanks to reviewers Ľ. Tuček and P. Bačík for their valuable comments and suggestions, upgrading the quality of primary manuscript.

## References

Baumann, H. N., 1962: Petrology of fused alumina abrasives. *Amer. ceram. Soc. Bull., 35, 387–390.*

Filonenko, N. Ye. & Lavrov, I. V., 1958: Petrography of artificial abrasives. *Leningrad, Mashgiz.*

Hořínek, V. & Turnovec, I., 1970: Rozvoj výroby základních brusných materiálů. Sb. Konference. Brusiva a jejich použití v čs. průmyslu, *Benátky n. Jizerou, 2, 1–13 (in Czech).*

Kamencev, M. V., 1950: Isskustvennyje abrazivnyje materijaly. *Leningrad, Mašgiz (in Russian).*

Kleandr, V., 1971: Výroba karbidu křemíku pro brusné a žárovzdorné účely. Sb. konf. Elektrotermické procesy. *Žilina, Dom techniky SVTS, 22–38 (in Czech).*

Novotný, P. & Turnovec, I., 1967: Izomerie brusných zrn. Brusivo a broušení. *Benátky nad Jizerou, 3, 17–21 (in Czech).*

Polubelova et al., 1968: Proizvodstvo abrazivnych materialov. *Mašinostrojenije (Leningrad) (in Russian).*

Turnovec, I., 1969: Tepelná roztažnost brusných zrn. Elektrik A 96. *Sklář keramik (Praha), 19, 14–16 (in Czech).*

Turnovec, I., 1970: Fyzikálně mechanické a chemické vlastnosti brusných zrn. Brusivo a broušení. *Benátky nad Jizerou, 1, 4–9 (in Czech).*

Turnovec, I., 1982a: Mineralogicko-petrologická charakteristika umělého hnědého korundu vyráběného redukčním tavením bauxitů. *Acta Univ. Carol., Geol. (Praha), 1–2, 151–171 (in Czech).*

Turnovec, I., 1982b: Výpočet minerálního složení umělého hnědého korundu. *Sklář keramik (Praha), 32, 255–257 (in Czech).*

Turnovec, I., 1984: Reakce korundových brusných zrn a pojiva během výpalu. *Sklář keramik (Praha), 34, 298–299 (in Czech).*

Turnovec, I. & Illášová, Ľ., 2009: Brúsenie šperkových a ozdobných kameňov, 1 časť. *Nitra, Univ. Konšt. Filozofa (in Slovak).*

Turnovec, I. & Illášová, Ľ., 2011: Brúsenie šperkových a ozdobných kameňov, 2. časť. *Nitra, Univ. Konšt. Filozofa (in Slovak).*

Turnovec, I. & Kleandr, V., 1970: Karbid křemíku pro brusné a žárovzdorné účely. *Sklář keramik (Praha), 20, 11, 285–289 (in Czech).*

# Výpočet zastúpenia sprievodných zložiek v umelom korundovom brúsive

Elektrónovaný korund a SiC sú najčastejšie používané priemyselné brúsivá. Konečné produkty elektrolytického spracovania $Al_2O_3$ a bauxitov obsahujú kontaminanty. Ich obsah a obsah sklených fáz nepriaznivo ovplyvňuje funkčné vlastnosti brúsiv. Ukázalo sa, že obsah kontaminantov možno vypočítať chemickou analýzou. Výpočet je podobný výpočtu, ktorý sa použil na stanovenie teoretickej analýzy hliny a iných surovín na výrobu keramiky (napr. výpočty podľa Kollaunera--Matejku). Príklad takéhoto výpočtu je uvedený na zistenie obsahu hnedého, najbežnejšieho korundu a výsledky sa porovnávajú s výsledkami získanými mikroskopickou analýzou ako referencie. Tieto výpočty sa môžu použiť na kontrolu kvality počas výroby a tiež na sledovanie zmien kvality počas výskumu a vývoja nových typov elektrokorundu.

Každý brúsny nástroj sa skladá z brúsnych zŕn, spojiva a pórov, teda zo zložiek pevnej a plynnej povahy. Brúsne zrná sú špeciálnou minerálnou fázou a spojivo je buď anorganické, môže to byť syntetická živica, alebo materiály na báze kaučuku. Pestrosť jednotlivých zložiek je veľká. Od ich vlastností a rozloženia v brúsnom nástroji priamo závisia aj fyzikálno-mechanické vlastnosti. Petrologické a mineralogické postupy umožnili vyriešiť niektoré mnohoročné technologické problémy a doplniť kontrolné metódy na overovanie kvality brúsnych zŕn. Od obsahu sprievodných zložiek (hlavne β-korundu v bielom a hexahlinitanu v hnedom korunde, prípadne sklených fáz) závisia funkčné vlastnosti brúsiva. Podobne, ako sa vyčísľujú racionálne analýzy keramických surovín, možno vyčísliť minerálne zloženie korundov. Ako príklad uvádzame výpočty v prípade hnedého korundu. Podmienky jeho tavenia sa približujú rovnovážnym. Prebiehajú v tekutej fáze a následná kryštalizácia je dostatočne pomalá. Kryštalizácia nastáva v systéme CaO – $Al_2O_3$ – $SiO_2$, v oblasti blízkej vrcholu $Al_2O_3$. Poznáme tri konečné produkty kryštalizácie: 1. korund, mullit, anortit; 2. korund, anortit; 3. korund, hexahlinitan vápenatý, anortit.

Ide o zjednodušenie, ktoré neberie do úvahy ďalšie sprievodné zložky. Tými sú zlúčeniny MgO a $TiO_2$, teda prevažne spinelidy a taosit. Zastúpenie spinelidov je iba stopové až bezvýznamné a neovplyvňuje funkčné vlastnosti. Iná situácia je v prípade zlúčenín titánu. Z jednoduchého pomeru oxidov viazaných na jednotlivé zložky je zrejmé, že najvýhodnejší je taký produkt tavby, v ktorom sa okrem korundu bude vyskytovať iba anortit. Najmenej výhodná je tavba umožňujúca vznik hexahlinitanu. Na základe stechiometrických pomerov jednotlivých oxidov možno z analytických údajov vypočítať zastúpenie hlavných zložiek. Chemická analýza je súčasťou kontroly kvality a patrí medzi základné kvalitatívne parametre. Je uvedená v ČSN 22 4044. Materiál zodpovedajúci ČSN môže mať veľmi variabilné minerálne zloženie a s tým súvisia aj jeho funkčné vlastnosti.

Metódy aj prístup petrológov a mineralógov môžu významne napomôcť pri posudzovaní vlastností brúsiva a brúsnych nástrojov, ale aj mnohých ďalších technických hmôt, najmä pri ich vývoji. V závere zrekapitulujeme niektoré príklady, keď k riešeniu technologických problémov v odbore brúsiv prispela práve petrológia: stanovenie minerálnych fáz vznikajúcich pri výrobe brúsnych materiálov, stanovenie štruktúr a veľkosti vznikajúcich kryštálov, vyriešenie technologického problému pri výrobe hnedého korundu (preredukovanie), vyčíslenie minerálneho zloženia z analytických údajov, hodnotenie tepelnej rozťažnosti a jej odstránenia žíhaním, hodnotenie tvarov brúsnych zŕn. Porovnanie výpočtov s mikroskopickou analýzou a základné chemické zloženie je v pripojených tabuľkách. Ako vyplýva z tabuliek, rozdiel medzi vyčísleným a mikroskopicky stanoveným zložením je iba malý, nepatrný. Prepočty možno využiť pri sledovaní kvality počas výskumných prác, ale aj na štatistické hodnotenie technickej kontroly výroby. Zhoda medzi vypočítaným a mikroskopicky zisteným zložením je pomerne vysoká. Obsah sprievodných zložiek sa sledoval aj v závislosti od veľkosti brúsnych zŕn. Ukázalo sa, že aj tu existuje istá zákonitosť, podmienená veľkosťou kryštálov a spôsobom veľkostného triedenia. Od najväčších zŕn k stredným obsah prímesí klesá, od stredných k jemným opäť škodlivín pribúda a ich obsah môže v nepriaznivom prípade dosiahnuť až 20 %. Štúdium nábrusov sa ukázalo ako veľmi efektívne pri identifikácii jednotlivých minerálnych fáz, ale aj pri štúdiu vnútornej stavby brúsnych nástrojov.

Doručené / Received: 4. 3. 2020
Prijaté na publikovanie / Accepted: 11. 8. 2020

# Inštrukcie autorom

## Etika publikovania, záväzná pri publikovaní v časopise Mineralia Slovaca: *www.geology.sk/mineralia* *položka* *Publikačná etika*

**1. Geovedný časopis Mineralia Slovaca publikuje scientometricky hodnotné recenzované pôvodné vedecké články s vysokým citačným potenciálom. V úvode príspevku musí autor jasne deklarovať, čím konkrétnym je jeho príspevok prínosný pre rozvoj geovied. Rešeršné štúdie sa publikujú len ojedinele.**

**2.** Články na publikovanie (manuskripty) sa do redakcie zasielajú poštou (dva vytlačené exempláre a CD so všetkými súbormi v editovateľnej podobe) alebo e-mailom (editovateľné súbory a kompletná verzia vo formáte PDF).

**3. Súčasne s článkom je potrebné redakcii poslať autorské vyhlásenie o originalite textu a obrázkov. Kópie obrázkov z iných publikácií musia byť legalizované získaním práva na publikovanie. Vyhlásenie musí obsahovať meno autora (autorov), akademický titul a trvalé bydlisko.**

**4.** Rozsah manuskriptu na publikovanie je najviac 25 rukopisných strán (MS Word, Times New Roman, veľkosť písmen 12 bodov, riadkovanie 1,5) vrátane literatúry, obrázkov a vysvetliviek. V prípade veľkého odborného prínosu sú v ojedinelých prípadoch povolené aj dlhšie články.

**5.** Články sú publikované v angličtine alebo v slovenčine. Články v slovenčine musia obsahovať anglický preklad názvu, abstraktu, kľúčových slov, resumé a popisov k obrázkom a tabuľkám. Články písané v angličtine musia obsahovať slovenské resumé.

### Text

**1.** Abstrakt stručne sumarizuje článok. Môže mať najviac 200 slov a nemá obsahovať citácie. Počet kľúčových slov je maximálne 6. Text má mať úvod, charakteristiku (stav) skúmaného problému, použitú metodiku, nové zistenia, ich interpretáciu, diskusiu, záver a zoznam literatúry. Východiskové údaje musia byť zreteľne odlíšené od interpretácií. V texte musia byť odvolávky na všetky použité obrázky a tabuľky.

**2.** Hierarchiu nadpisov v texte je potrebné vyznačiť ceruzkou na ľavom okraji strany manuskriptu: 1 – najvyššia, 2 – nižšia, 3 – najnižšia.

**3.** V texte sa uprednostňuje citácia v zátvorke, napr. (Dubčák, 1987; Hrubý et al., 1988), pred formou ... podľa Dubčáka (1987).

**4.** Pozícia obrázkov a tabuliek v texte sa označí. Nie je vhodné, aby text v editore MS Word obsahoval vložené obrázky, ale náhľadová verzia v pdf ich má obsahovať.

**5.** Grécke písmená treba identifikovať na ľavom okraji slovom (napr. sigma). Potrebné je odlišovať pomlčku od spojovníka. Symboly, matematické značky, názvy skamenelín a pod., ktoré sa majú vysádzať kurzívou, autor v rukopise podčiarkne vlnovkou.

### Obrázky a tabuľky

**1.** Ilustrácie a tabuľky vysokej kvality bývajú publikované buď **na šírku stĺpca (81 mm), alebo strany (170 mm).** Optimálna veľkosť písma a čísiel v publikovaných obrázkoch je 2 mm. Články v slovenčine musia mať popisy v obrázkoch a tabuľkách v slovenčine, záhlavie tabuliek a texty pod obrázkami a tabuľkami sú v slovenčine a angličtine. Články v angličtine majú všetky texty v angličtine. **Maximálny rozmer ilustrácie a tabuľky vytlačený v časopise je 170 x 230 mm.** Väčšie (skladané) ilustrácie sú publikované len v ojedinelých prípadoch.

**2. Pri počítačovej tvorbe obrázkov odporúčame používať programy s vektorovým zobrazením (Corel Draw, Adobe Illustrator a pod.). Čiary tzv. vlasovej hrúbky, softvérová alebo rastrová výplň plôch (napr. v Corel Draw) nie sú prípustné.** Výplne v obrázkoch musia pozostávať zo samostatne vysádzaných objektov.

**3.** Ilustrácie vrátane fotografií musia obsahovať **grafickú mierku** v centimetrovej či metrovej škále, prípadne sa rozmer zobrazených objektov vyjadrí v popise obrázka. Mapy a profily musia mať aj **azimutálnu orientáciu** a jednotné vysvetlivky, ktoré sa uvedú pri prvom obrázku. Zoskupené obrázky, napr. fotografie a diagramy, sa uvádzajú ako jeden obrázok s jednotlivými časťami označenými písmenami (a, b, c atď.).

**4. Pri zasielaní fotografií vo forme počítačových súborov (formáty JPG alebo TIF) sa požaduje rozlíšenie minimálne 600 DPI. Publikovanie farebných ilustrácií môže byť spoplatnené.**

### Literatúra

**1. Minimálne 50 % citácií musí reprezentovať publikácie od roku 2000.** V zozname literatúry sa v abecednom poradí uvádza len literatúra citovaná v danom článku.

**2. Spôsob uvádzania literatúry v zozname literatúry**

***Knižná publikácia:*** Gazda, L. & Čech, M., 1988: Paleozoikum medzevského príkrovu. *Bratislava, Alfa, 155 s.*

***Časopis:*** Vrba, P., 1989: Strižné zóny v metapelitoch. *Miner. Slov., 21, 135 – 142.*

***Zborník:*** Návesný, D., 1987: Vysokodraselné ryolity. *In: Romanov, V. (ed.): Stratiformné ložiská gemerika. Špec. publ. Košice, Slov. geol. spol., 203 – 215.*

***Manuskript:*** Radvanský, F., Slivka, B., Viktor, J. & Srnka, T., 1985: Žilné ložiská jedľoveckého príkrovu gemerika. Záverečná správa z úlohy SGR--geofyzika. *Manuskript. Spišská Nová Ves, archív Št. Geol. Úst. D. Štúra, 28 s.*

**3.** Pri článku viac ako dvoch autorov sa v texte cituje iba prvý autor s dodatkom et al., ale v zozname literatúry sa uvádzajú všetci.

# Instructions to authors

## Publication ethics, being obligatory for publishing in the journal Mineralia Slovaca: *www.geology.sk/mineralia* *item* *Publication ethics*

**1. Geoscientific journal Mineralia Slovaca publishes scientometrically valuable original peer-reviewed scientific articles with a high citation potential. In the introduction of each article the author(s) must clearly declare, which innovative data the paper brings for the development of geosciences. The retrieval studies are published only exceptionally.**

**2.** The articles for publishing (manuscripts) must be sent to Editorial Office by post (two printed copies and CD with editable files), or by e-mail (editable files plus complete preview version in PDF format).

**3. Simultaneously with the article the Editorial Office must receive the author´s proclamation that no part of the manuscript was already published and figures and tables are original as well. Copied illustrations from other publications must contain a copyright.**

**4.** The extent of the manuscript for publishing is limited to 25 manuscript pages (MS Word, 12 points Times New Roman, line spacing 1.5) including figures, tables, explanations and references. In the case of contribution with a high scientific value, the longer manuscripts for publishing are exceptionally permitted.

**5.** Articles can be published in Slovak or English languages. The title, abstract, key words, shortened text (resumé), as well as description to figures and tables in Slovak articles are published also in English. Articles published in English contain Slovak resumé.

### Text

**1.** Abstract briefly summarizing the article is limited to 200 words, no references are allowed. The maximum number of key words is 6. Text of the article has to contain the introduction, characterization (state) of investigated problem, applied methodology, obtained new data, discussion, conclusion and references. The obtained data must be distinctly separated from interpretations. All applied figures and tables must be referred in the text.

**2.** The hierarchy of headings in the manuscript must be indicated by a pencil note: 1 – highest level, 2 – lower, 3 – lowermost level.

**3.** The references in the text prefer parentheses, e.g. (Dubčák, 1987; Hrubý et al., 1988). The form "according to Dubčák (1987)" should be used only exceptionally.

**4.** Position of figures and tables must be indicated in the manuscript. Editable text of manuscript sent to editorial office must be without figures and tables, though the preview PDF has to contain them in a correct position.

**5.** Greek letter in the text must be identified at the left margin of the text (e.g. sigma). The text should strictly distinguish the dash from hyphen. Symbols, mathematic signs, names of fossils, etc., which should be printed in italics, must be underlined by the wavy line in the manuscript.

### Figures and tables

**1.** The high quality figures and tables can be published either in **maximum width of column (81 mm) or page (170 mm).** The optimum size of letters and numbers in the camera-ready figure is 2 mm. Articles published in Slovak contain the Slovak descriptions in figures and tables, the tables headings and descriptions beneath figures and tables are in Slovak and English. English articles contain all texts in English. **Maximum dimension of figures and tables in the journal is 170 x 230 mm. Larger (fanfolded)** illustrations are published only exceptionally.

**2. For figures drawing the editorial office recommends the vector graphics editors (Corel Draw, Adobe Illustrator, etc.). The very thin lines (hair lines), the pre-defined software or raster fillings of polygons (e.g. in Corel Draw) are not allowed.** The filling must consist from separately set objects.

**3.** Each illustration including photographs must contain graphic (metric) scale, eventually the dimensions of visualized objects have to be stated in the describing text to figure. Maps and profiles must contain also the azimuth orientation, their detail explanations are stated at the first figure. Grouped figures, e.g. photographs and diagrams, are compiled as one figure with separate parts designated by letters (a, b, c, etc.).

**4. The photographs sent as JPG of TIF files are required for having minimum 600 DPI resolution.** Publishing of colour illustrations can be charged by a fee.

### References

**1. Minimum 50 % of referred works must represent contemporary publications after 2000.** The references in alphanumeric order encompass only literature cited in the article.

**2. Examples of referring:**

***Book:*** Gazda, L. & Čech, M., 1988: Paleozoic of the Medzev nappe. *Bratislava, Alfa, 155 p.*

***Journal:*** Vrba, P., 1989: Shear zones in the metapelite complexes. *Miner. Slov., 21, 135–142.*

***Anniversary volume:*** Návesný, D., 1987: High-potassium rhyolites. *In: Romanov, V. (ed.): Stratiform deposits of Gemericum. Spec. publ. Košice, Slov. geol. soc., 203–215.*

***Manuscript:*** Radvanský, F., Slivka, B., Viktor, J. & Srnka, T., 1985: Vein deposits of the Jedlovec nappe of Gemericum. Final report from the project SGR-geophysics. *Manuscript. Spišská Nová Ves, Archive Št. Geol. Úst. D. Štúra, 28 p.*

**3.** The article with more than two authors is referred by the name of the first author with the amendment et al., but the list of references contains names of all authors.

**Ďalšie informácie/Further information:** mineralia.slovaca@geology.sk; zoltan.nemeth@geology.sk

## OBSAH – CONTENT

### PÔVODNÉ ČLÁNKY – ORIGINAL PAPERS


*Pelech, O., Žecová, K., Jamrich, M., Littva, J., Demko, R., Zlinská, A. & Olšavský, M.*
**Trenčianska kotlina and Ilavská kotlina basins – Remnants of an inverted Early Miocene wedge top basin (Western Carpathians, Slovakia)**
Trenčianska a Ilavská kotlina – zvyšky invertovanej nesenej spodnomiocénnej panvy

*Quintana, J. R., Melgar, G. A. O., Peña A. C. & Cambra, K. E. N.*
**Main geological and mineralogical characteristics of the Cajálbana lateritic deposit, Pinar del Río, Cuba**
Hlavné geologické a mineralogické charakteristiky lateritického ložiska Cajálbana v provincii Pinar del Río, Kuba

*Ščerbáková, B., Gawlick, H.-J. & Németh, Z.*
**Differential stresses estimated from calcite veins in HP-LT Triassic Hallstatt Limestones (Northern Calcareous Alps, Austria)**
Diferenciálne napätia z deformovaných kalcitových žíl vo vysokotlakovo-nízkoteplotne deformovaných triasových hallstattských vápencoch (Severné Vápencové Alpy, Rakúsko)

*Stercz, D. Grega, K. Pačajová & Ľ. Petro*
**Hydrogeological parameters trend analysis in the the Slanec village landslide area (Slovakia), crossed by transit gas pipeline of European imporance**
Trendová analýza hydrogeologických parametrov zosuvného územia v trase tranzitného plynovodu európskeho významu pri obci Slanec

*Turnovec, I. & Illášová, Ľ.*
**Calculating minor constituents in synthetic corundum abrasives**
Výpočet zastúpenia sprievodných zložiek v umelom korundovom brúsive



**Indexed / Abstracted / Accessed by SCOPUS and EBSCO**
Indexované / abstraktované / sprístupňované databázami SCOPUS a EBSCO

**www.geology.sk/mineralia**